Vacuum system and photoelectron distributions in the collider

R. Kersevan, FCCIS 2023 WP2 Workshop

Angelicum Centro Congressi, Rome, Nov 13-15, 2023

CERN

Technology Department TE Vacuum Surfaces & Coatings

OUTLINE

- FCC study program (2013-today)
- FCC-ee: relevant machine and vacuum parameters
- Vacuum chamber cross section
- Synchrotron radiation spectrum, flux, power
- SR absorbers: yes or no?
- Pumping solutions
- The MDI region
- Synchrotron radiation ray-tracing
- Pressure profiles
- Future work and conclusions
- Acknowledgments

Vacuum chamber cross-section; Prototyping of vacuum components

- The vacuum chamber cross section in the arcs is

CDR version, 115 mm wide, 70 mm ID
Now looking at 105 mm wide, 60 mm ID

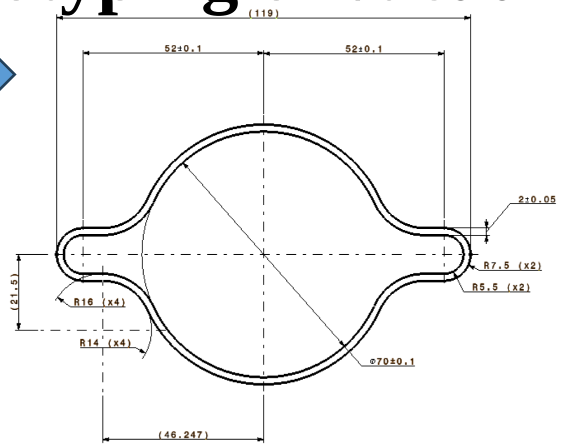

- It is made out of **extruded copper alloy**; it will be NEG-coated and every 5~6 m there will be a **SR PHOTON ABSORBER** (**SRA**) which will intercept the SR generated along the preceding dipole magnets.
- The design of the SRAs is **very demanding**, because each of them will receive a highly collimated SR fan, with **very high surface power density (especially for the ttbar)**
- In addition, the SRAs must satisfy some **geometrical criteria** which make their design challenging: we are prototyping some innovative design implementing **ADDITIVE MANUFACTURING** (3D printing) and **STIR-WELDING** technology, with **SHAPE-MEMORY ALLOY** rings for joining the different vacuum chamber segments (and BPM button electrodes) and bulk **COLD-SPRAY DEPOSITION** for selected components
- **Upon selection of the most suitable technology, we will look for INDUSTRIAL PARTNERS capable to deliver large quantities of these components in a TIMELY FASHION, following STRICT QUALITY CONTROL procedures**

Plasma-sprayed "bosses" for machining the BPM button electrodes
Friction stir welding of elliptical flanges to vacuum chamber extrusion

Chamber: 2mm layer sprayed all around

Chamber prototype with x4 bosses for direct BPM buttons machining and SMA rings

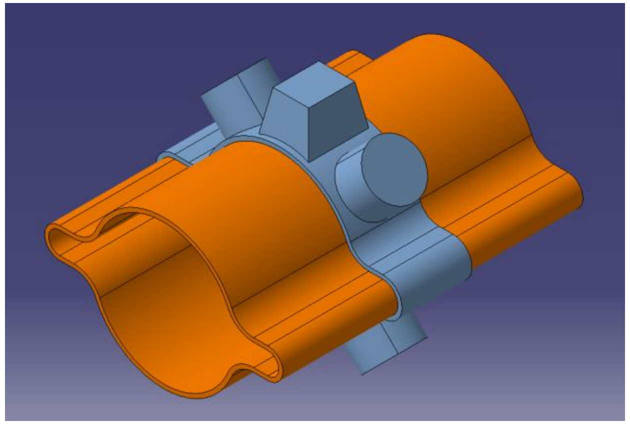

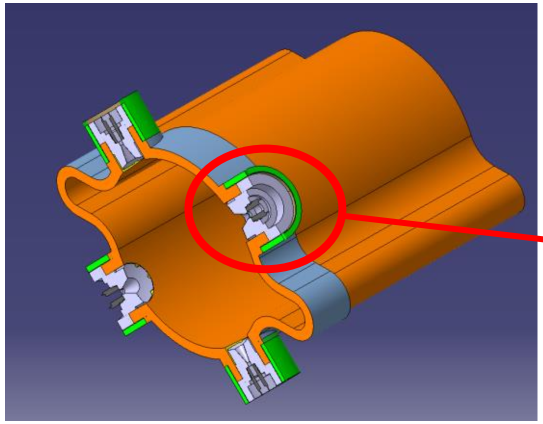

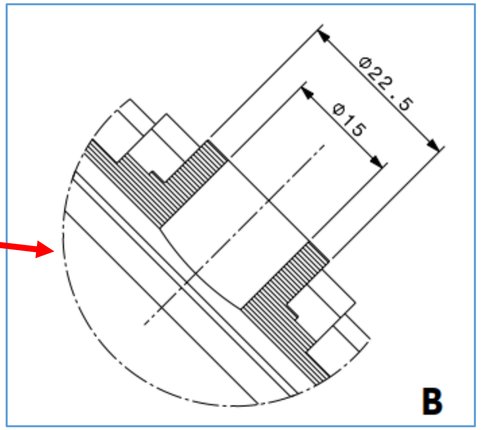

FRICTION STIR WELDING →

- Flange is redesigned as per Phase 1 results

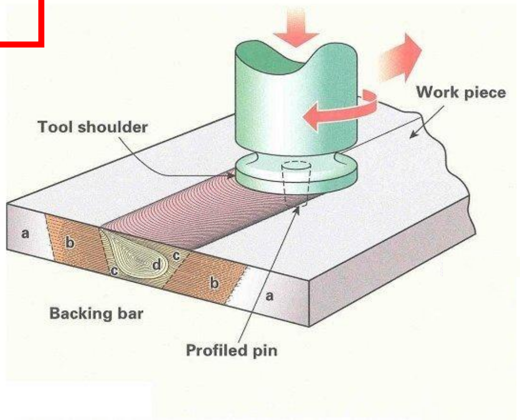

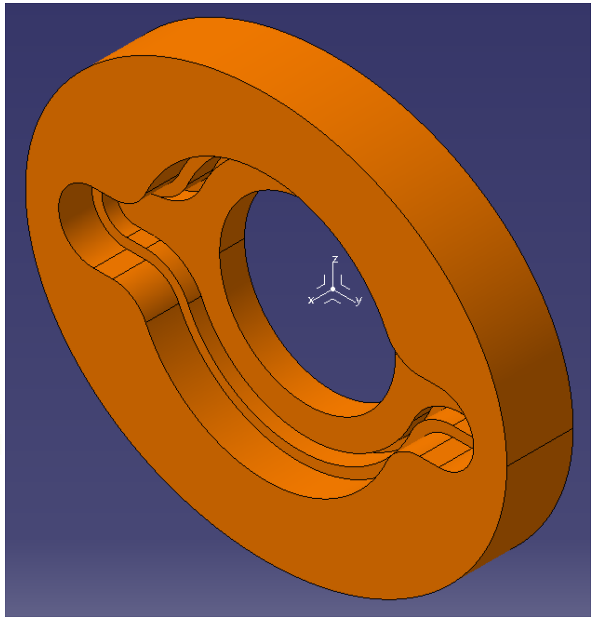

Initial geometry of the SR photon absorber, now superseded by 3D-printed one (next slide)

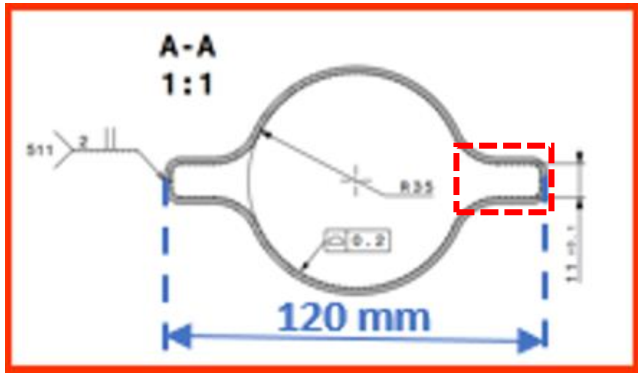

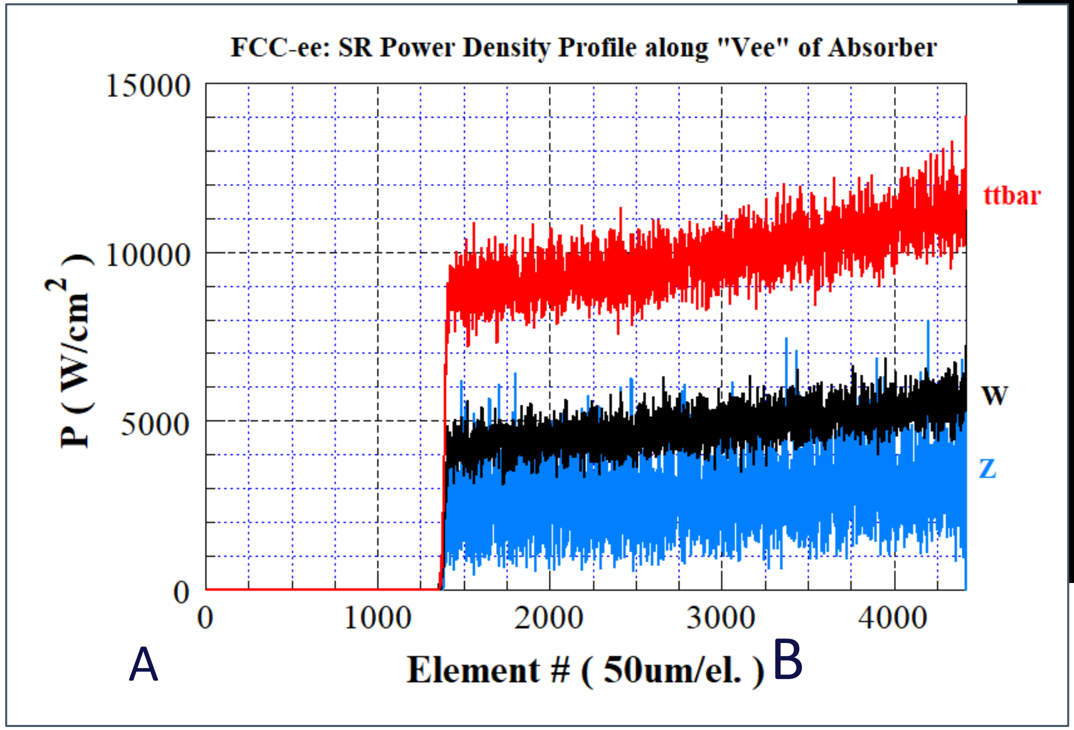

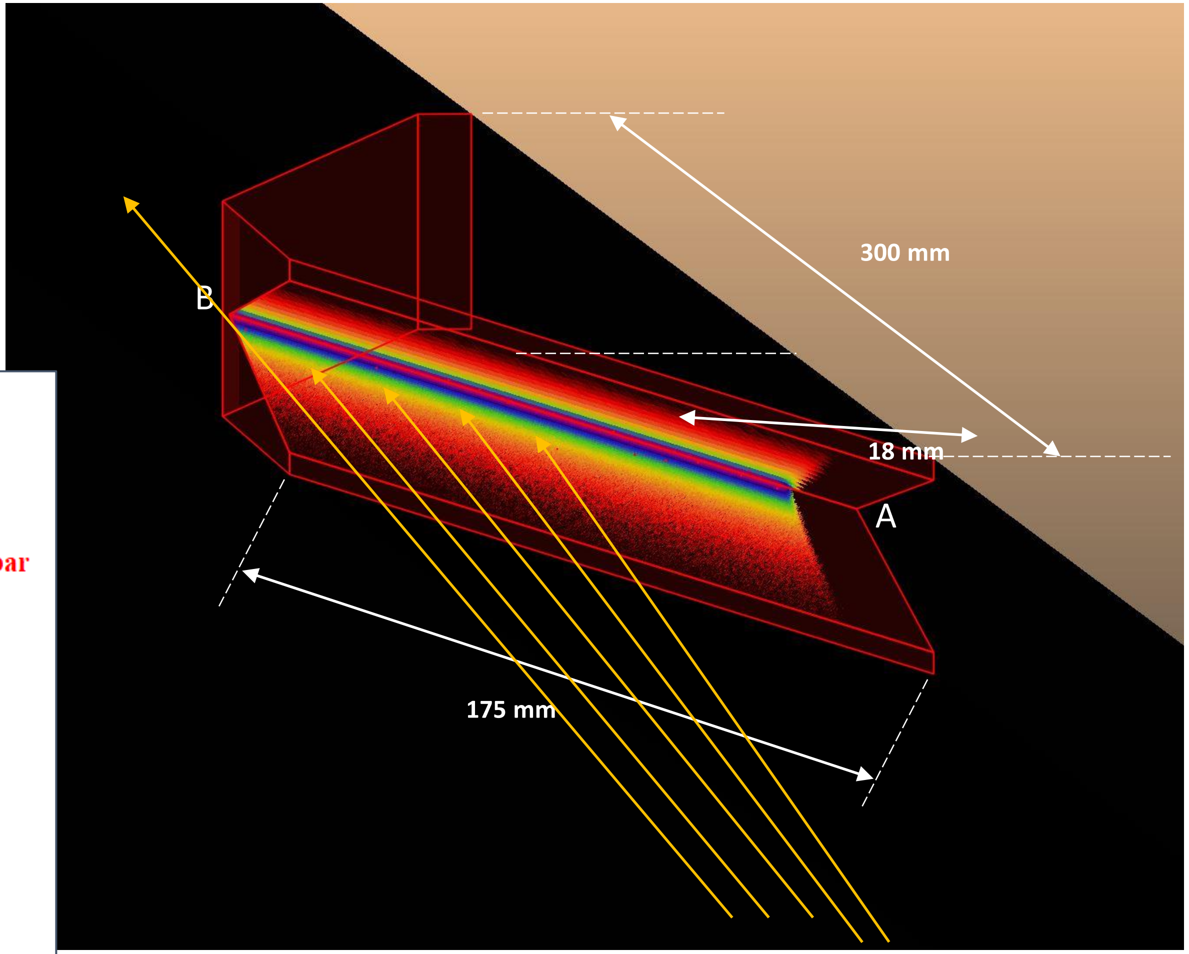

Another example: 3D-PRINTED SR ABSORBER, with INTEGRATED COOLING CIRCUIT AND SWIRL TAPE TO IMPROVE HEAT EXCHANGE

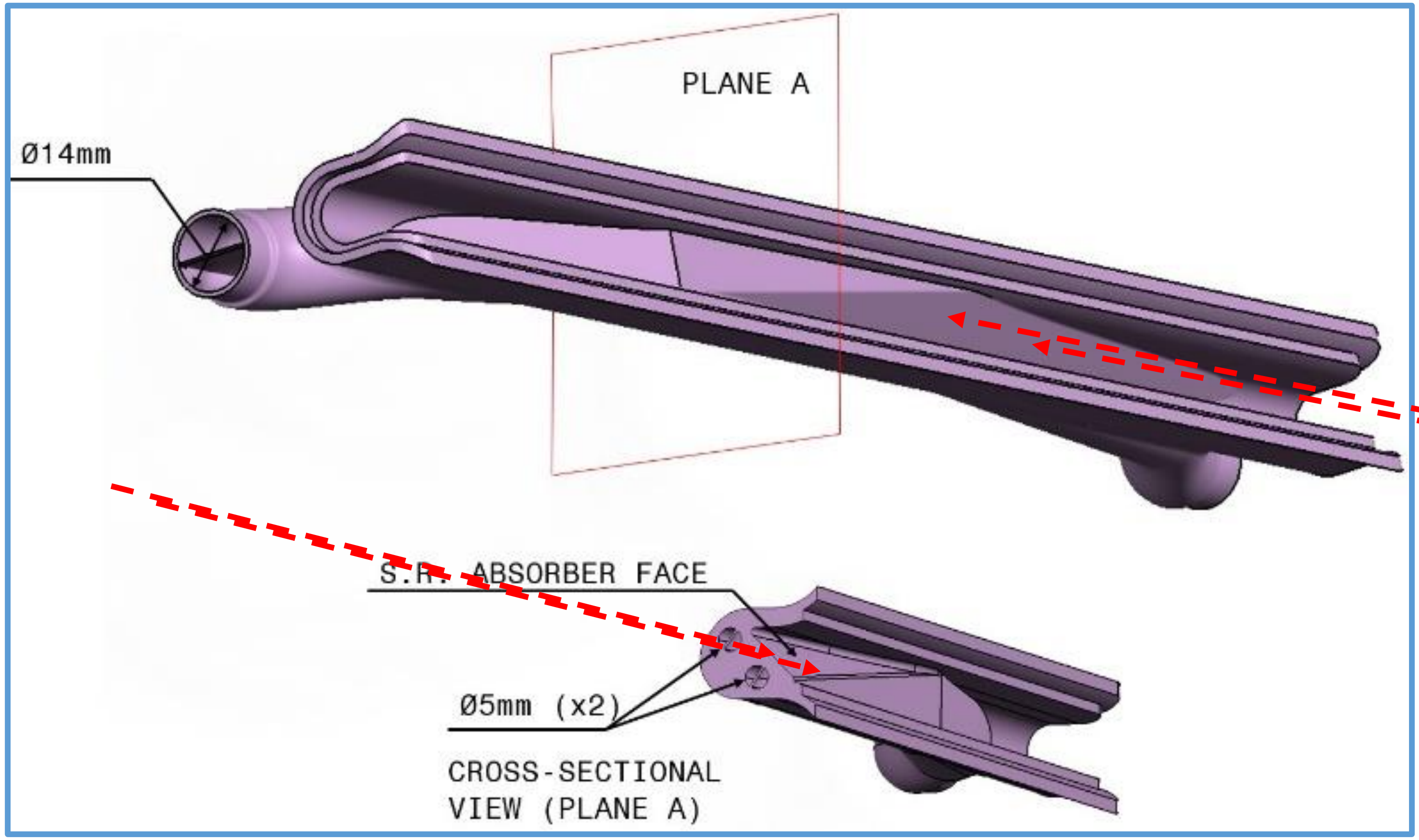

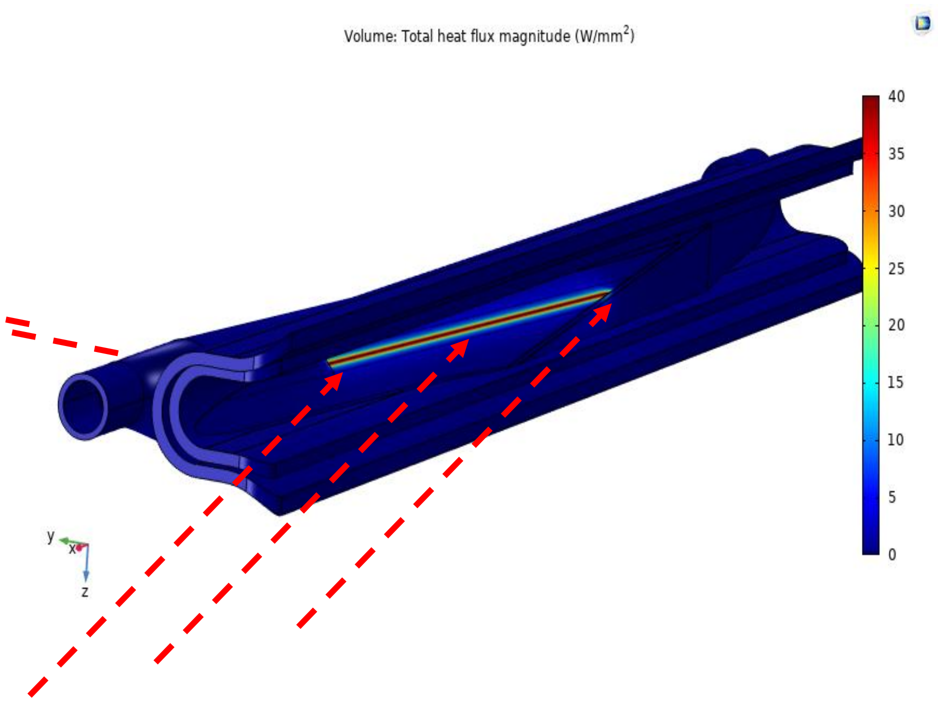

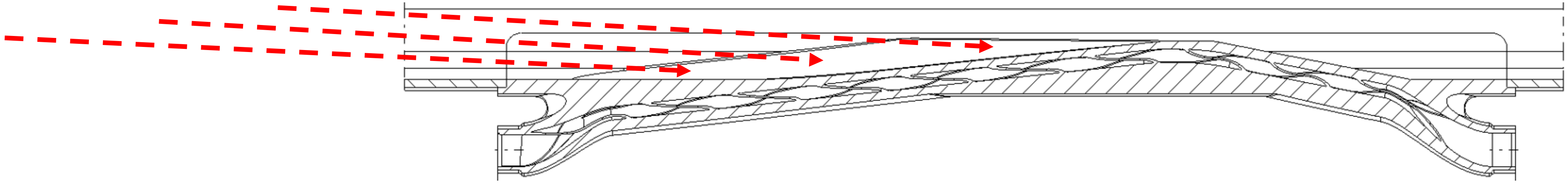

Comparison of LEP extruded cross-section (dipole chambers) with FCC-ee's

LEP:
ellipse 131x70 mm^2

FCC-ee:
115 mm wide, 70 mm ID

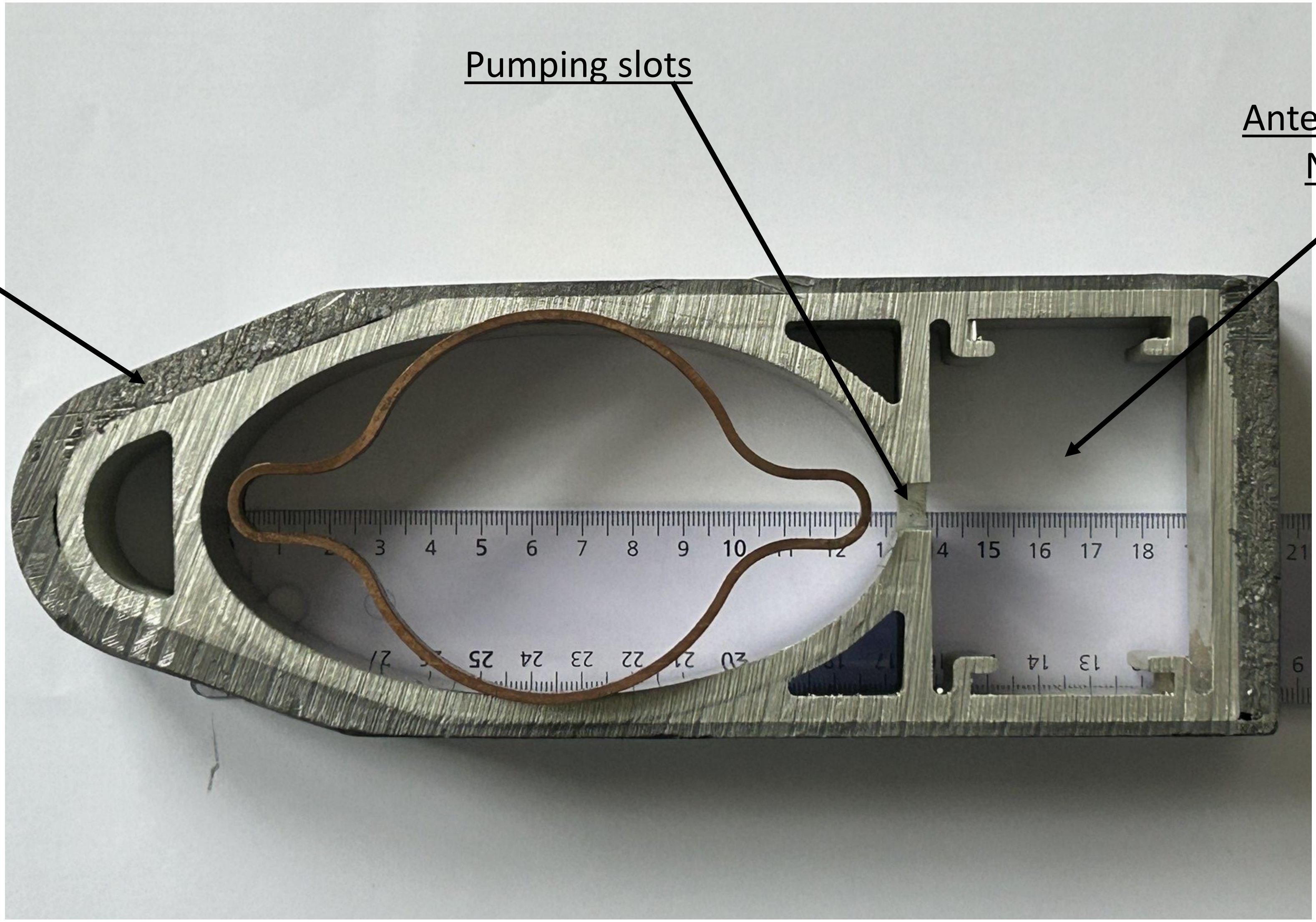

The specific conductance of FCC-ee is ~1/2 that of LEP, ~100:50 l·m/s
The proposed 60 mm ID version for FCC-ee would have a 37% conductance decrease, i.e. only ~1/3 that of LEP

View of the VACUUM CHAMBERS with PUMPING DOMES (right) and inside (old) QUADRUPOLE and (old) DIPOLE MAGNET (left)

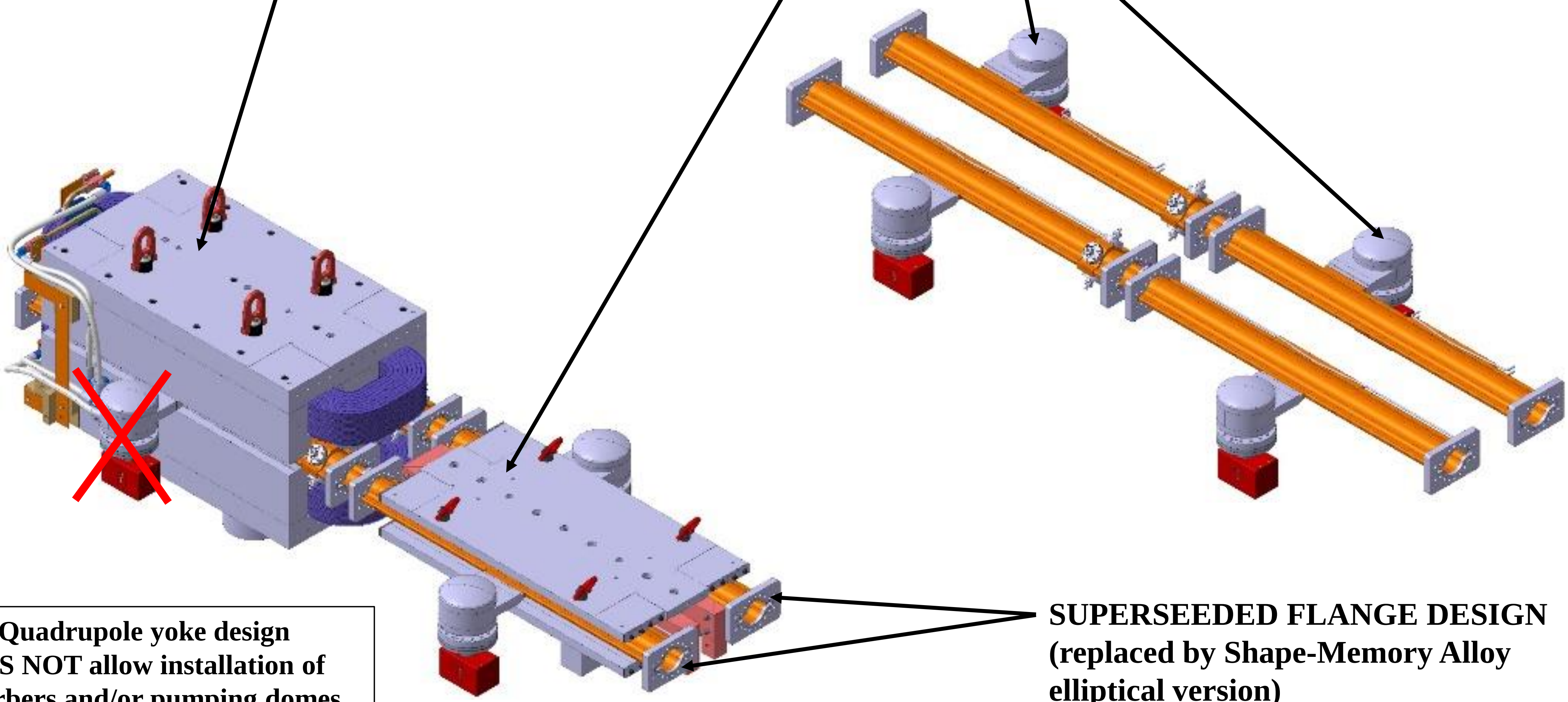

New Quadrupole yoke design DOES NOT allow installation of absorbers and/or pumping domes along it

SUPERSEEDED FLANGE DESIGN (replaced by Shape-Memory Alloy elliptical version)

FCC-hh beam screen and FCC-ee vacuum chamber prototype testing

BESTEX at KARA light source (Peter Lindquist Henriksen, formerly L.A. Gonzalez)

Karlsruher Institut für Technologie

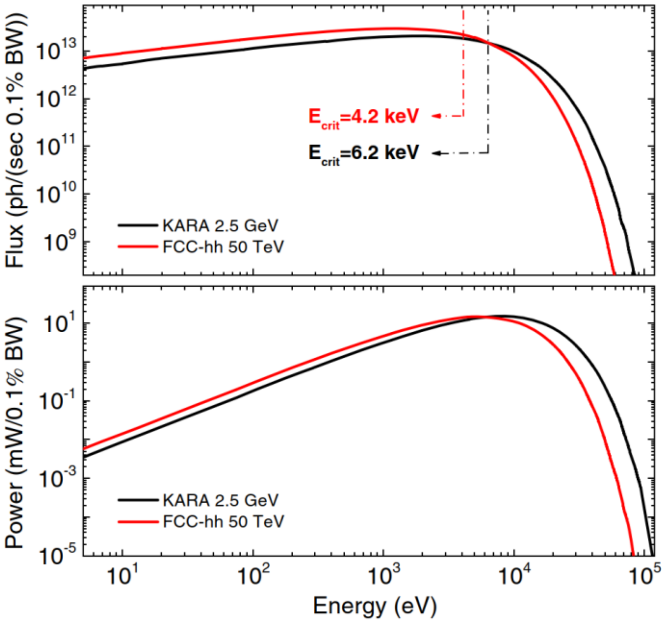

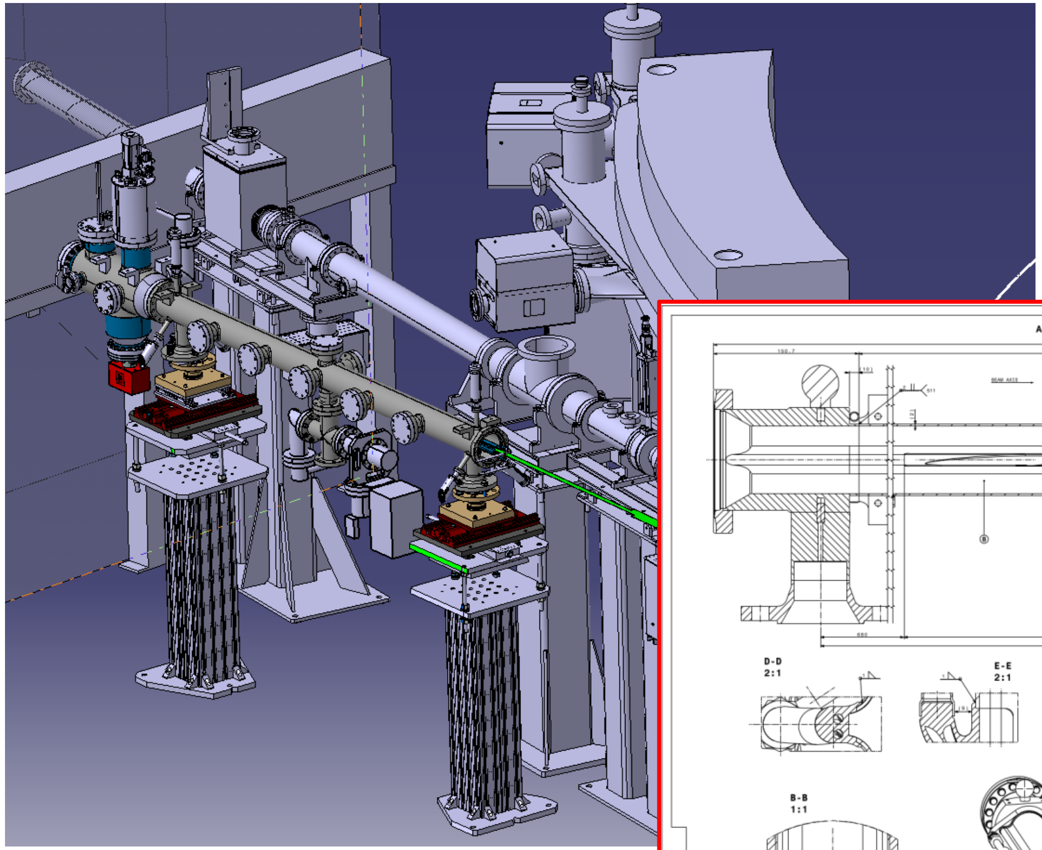

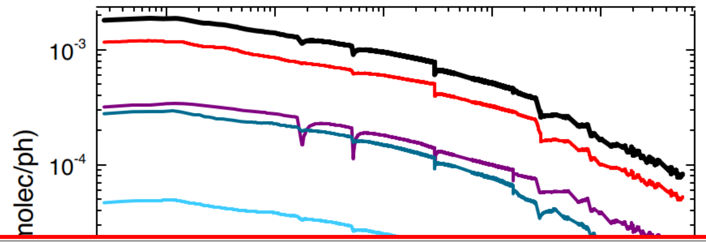

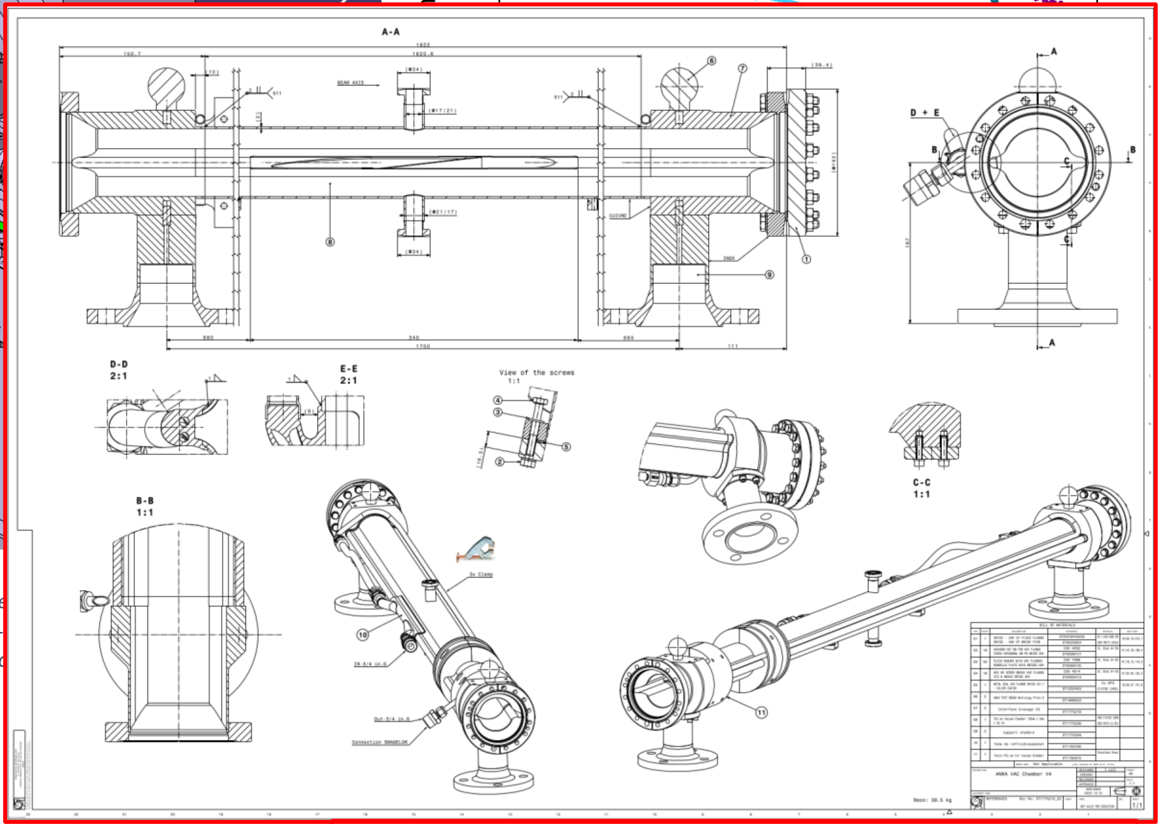

TABLE I. Comparison of the BESTEX (for the configuration of this specific work) and the FCC-hh relevant baseline parameters.

	BESTEX	FCC-hh
Critical energy [keV]	6.2	4.3
SR flux [ph/s/m]	4.84×10^{16}	1.7×10^{17}
SR power [W/m][a]	32	32[b]
Glancing angle [mrad]	18	1.35

[a]Power received at the BS.
[b]Average value. Power ranges between 21 and 42 W/m.

L. A. Gonzalez, et al. *Commissioning of a beam screen test be... hadron collider type synchrotron radiation beam.* DOI: 10.11...

L. A. Gonzalez, et al. *Photostimulated desorption performanc... beam screen.* DOI: 10.1103/PhysRevAccelBeams.24.113201

This project has received funding from the European Union's Horizon Europe Research and Innovation programme under Grant Agreement No 101057511.

PRELIMINARY; Court. F. Luiz, CERN

Schematics of BESTEX at KARA/KIT

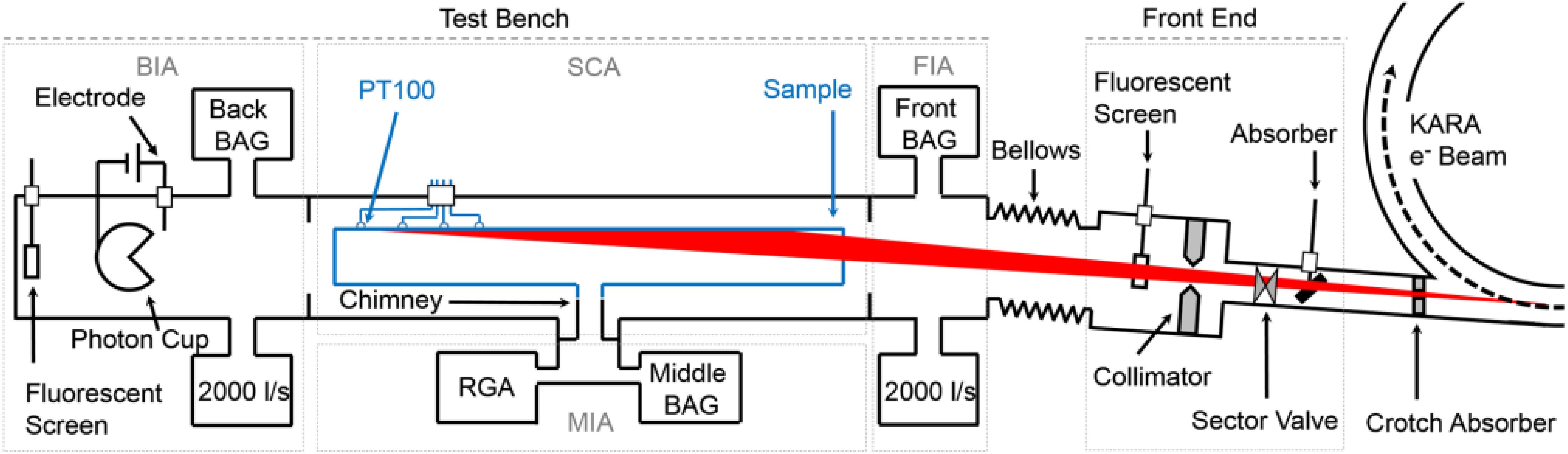

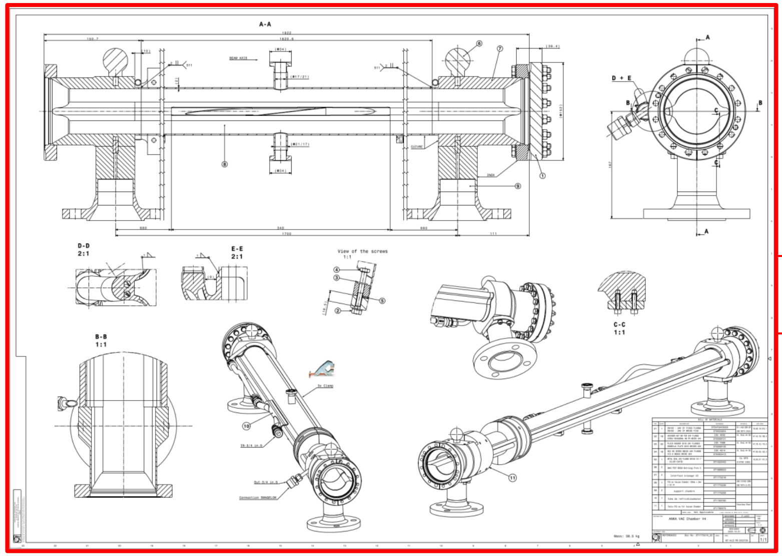

PRELIMINARY; Court. F. Luiz, CERN

- **Machine parameters from official web page http://tlep.web.cern.ch/content/machine-parameters**
- **Very small vertical emittance for all energies**
- **High current (B-factory level) for Z-pole**
- **Luminosity lifetime t_{lum} dominates beam current decay, but vacuum lifetime must be at least several times longer than t_{lum}: good vacuum is a must**

Consequence of 50 MW/beam MAX

$$P\,(W) = 88.46 \cdot E^4(GeV) \cdot I(mA) / \rho(m)$$

$$F\,(ph/s) = 8.08 \cdot 10^{17} \cdot E(GeV) \cdot I(mA)$$

The beam currents at the various energies scale as the reciprocal of the 4th power of the beam energy:

The beam current at ttbar is only $(45.6/182.5)^4$ = $1/4^4$=1/256 that of the Z-pole

Old parameter table (97 km rings)

parameter	Z	W	H (ZH)	ttbar
beam energy [GeV]	45.6	80	120	182.5
arc cell optics	60/60	90/90	90/90	90/90
momentum compaction [10^{-5}]	1.48	0.73	0.73	0.73
horizontal emittance [nm]	0.27	0.28	0.63	1.45
vertical emittance [pm]	1.0	1.0	1.3	2.7
horizontal beta* [m]	0.15	0.2	0.3	1
vertical beta* [mm]	0.8	1	1	2
length of interaction area [mm]	0.42	0.5	0.9	1.99
tunes, half-ring (x, y, s)	(0.569, 0.61, 0.0125)	(0.577, 0.61, 0.0115)	(0.565, 0.60, 0.0180)	(0.553, 0.59, 0.0350)
longitudinal damping time [ms]	414	77	23	6.6
SR energy loss / turn [GeV]	0.036	0.34	1.72	9.21
total RF voltage [GV]	0.10	0.44	2.0	10.93
RF acceptance [%]	1.9	1.9	2.3	4.9
energy acceptance [%]	1.3	1.3	1.5	2.5
energy spread (SR / BS) [%]	0.038 / 0.132	0.066 / 0.153	0.099 / 0.151	0.15 / 0.20
bunch length (SR / BS) [mm]	3.5 / 12.1	3.3 / 7.65	3.15 / 4.9	2.5 / 3.3
Piwinski angle (SR / BS)	8.2 / 28.5	6.6 / 15.3	3.4 / 5.3	1.39 / 1.60
bunch intensity [10^{11}]	1.7	1.5	1.5	2.8
no. of bunches / beam	16640	2000	393	39
beam current [mA]	1390	147	29	5.4
luminosity [10^{34} $cm^{-2}s^{-1}$]	230	32	8	1.5
beam-beam parameter (x / y)	0.004 / 0.133	0.0065 / 0.118	0.016 / 0.108	0.094 / 0.150
luminosity lifetime [min]	70	50	42	44
time between injections [sec]	122	44	31	32
allowable asymmetry [%]	±5	±3	±3	±3
required lifetime by BS [min]	29	16	11	10
actual lifetime by BS ("weak") [min]	> 200	20	20	25

New parameter table (90.7 km rings)

Parameters

FCC-ee collider parameters as of June 3, 2023.

Beam energy	[GeV]	45.6	80	120	182.5
Layout		PA31-3.0			
# of IPs		4			
Circumference	[km]	90.658816			
Bend. radius of arc dipole	[km]	9.936			
Energy loss / turn	[GeV]	0.0394	0.374	1.89	10.42
SR power / beam	[MW]	50			
Beam current	[mA]	1270	137	26.7	4.9
Colliding bunches / beam		15880	1780	440	60
Colliding bunch population	[10^{11}]	1.51	1.45	1.15	1.55
Hor. emittance at collision ε_x	[nm]	0.71	2.17	0.71	1.59
Ver. emittance at collision ε_y	[pm]	1.4	2.2	1.4	1.6
Lattice ver. emittance $\varepsilon_{y,\mathrm{lattice}}$	[pm]	0.75	1.25	0.85	0.9
Arc cell		Long 90/90		90/90	
Momentum compaction α_p	[10^{-6}]	28.6		7.4	
Arc sext families		75		146	
$\beta^*_{x/y}$	[mm]	110 / 0.7	220 / 1	240 / 1	1000 / 1.6
Transverse tunes $Q_{x/y}$		218.158 / 222.200	218.186 / 222.220	398.192 / 398.358	398.148 / 398.182
Chromaticities $Q'_{x/y}$		0 / +5	0 / +2	0 / 0	0 / 0
Energy spread (SR/BS) σ_δ	[%]	0.039 / 0.089	0.070 / 0.109	0.104 / 0.143	0.160 / 0.192
Bunch length (SR/BS) σ_z	[mm]	5.60 / 12.7	3.47 / 5.41	3.40 / 4.70	1.81 / 2.17
RF voltage 400/800 MHz	[GV]	0.079 / 0	1.00 / 0	2.08 / 0	2.1 / 9.38
Harm. number for 400 MHz		121200			
RF freqeuncy (400 MHz)	MHz	400.786684			
Synchrotron tune Q_s		0.0288	0.081	0.032	0.091
Long. damping time	[turns]	1158	219	64	18.3
RF acceptance	[%]	1.05	1.15	1.8	2.9
Energy acceptance (DA)	[%]	±1.0	±1.0	±1.6	-2.8/+2.5
Beam crossing angle at IP $\pm\theta_x$	[mrad]	±15			
Piwinski angle $(\theta_x \sigma_{z,\mathrm{BS}})/\sigma^*_x$		21.7	3.7	5.4	0.82
Crab waist ratio	[%]	70	55	50	40
Beam-beam ξ_x/ξ_y[a]		0.0023 / 0.096	0.013 / 0.128	0.010 / 0.088	0.073 / 0.134
Lifetime (q + BS + lattice)	[sec]	15000	4000	6000	6000
Lifetime (lum)[b]	[sec]	1340	970	840	730
Luminosity / IP	[10^{34}/cm^{2}s]	140	20	5.0	1.25
Luminosity / IP (CDR, 2 IP)	[10^{34}/cm^{2}s]	230	28	8.5	1.8

Synchrotron Radiation Spectra

- Z-Pole: very high photon flux (→ large outgassing load);
- Z-pole: compliance with scheduled operation (~~integrated luminosity first 2 years~~), requires quick commissioning to I_{NOM}=~~1.390 A~~ 1270 mA;
- T-pole (182.5): extremely large and penetrating radiation, critical energy ~~1.25 MeV~~ 1.36 MeV;
- T-pole (and also W and H): need design which minimizes activation of tunnel and machine components (→ FLUKA);
- W, H-pole: intermediate between Z and T; still E_{crit} > Compton edge (~100 keV (Al), ~200 keV (Cu))

Critical energy: $\varepsilon_c = 2218 \cdot E^3$ (GeV) / ρ(m)

90.7 km machine

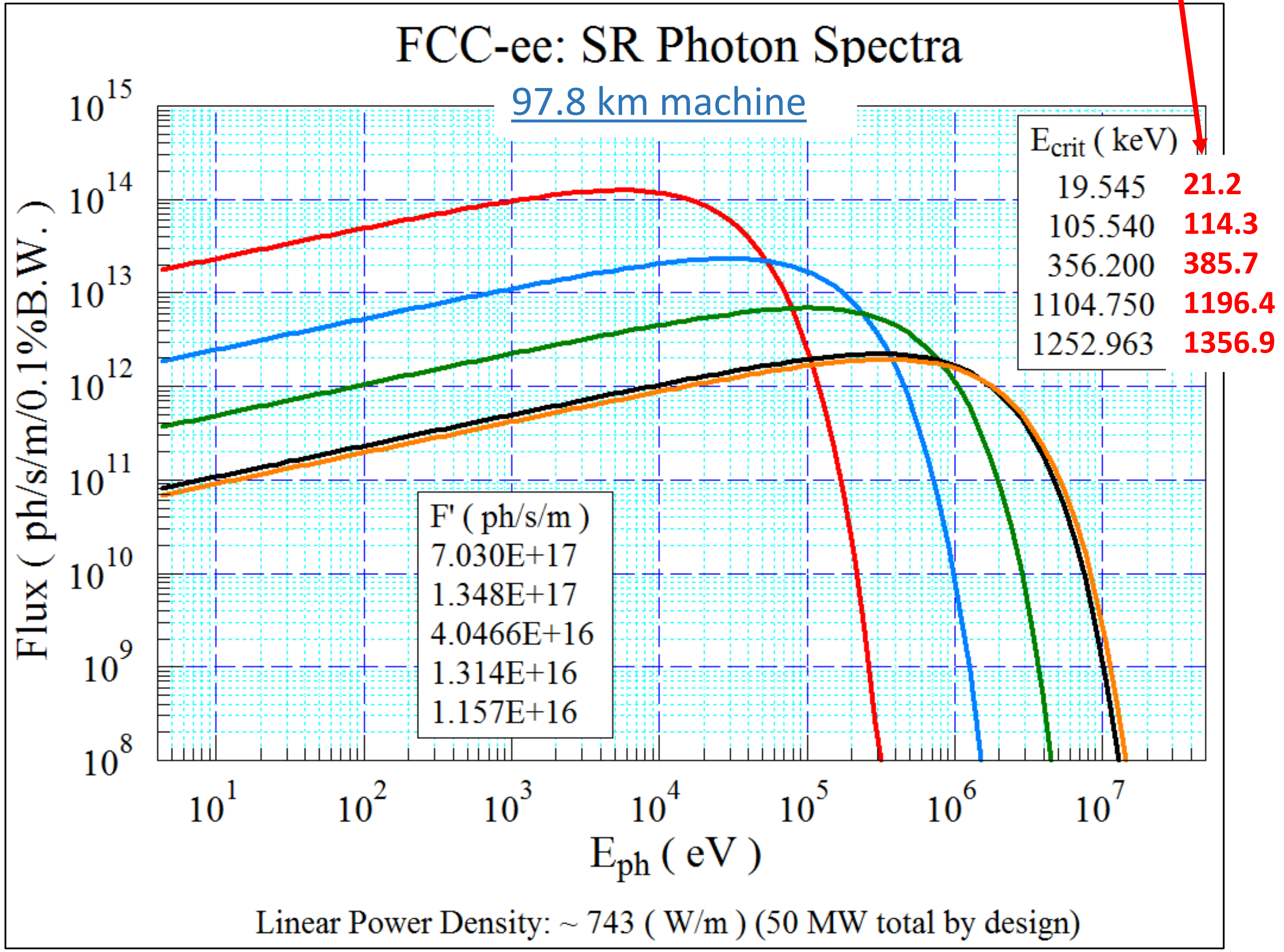

Synchrotron radiation spectrum, flux, power

Typical vertical opening angle SR: $1/\gamma$; γ(ttbar)=357,143; $1/\gamma$=2.8 µrad → @50 m = 0.14 mm

SR Spectra computed with SYNRAD+

- Radiation projected onto five 14x6 cm^2 screens;
- 1 cm-long dipole arc trajectories;
- Flux distribution shown here,
- Logarithmic scale for textures,
- 6 orders of magnitude displayed;

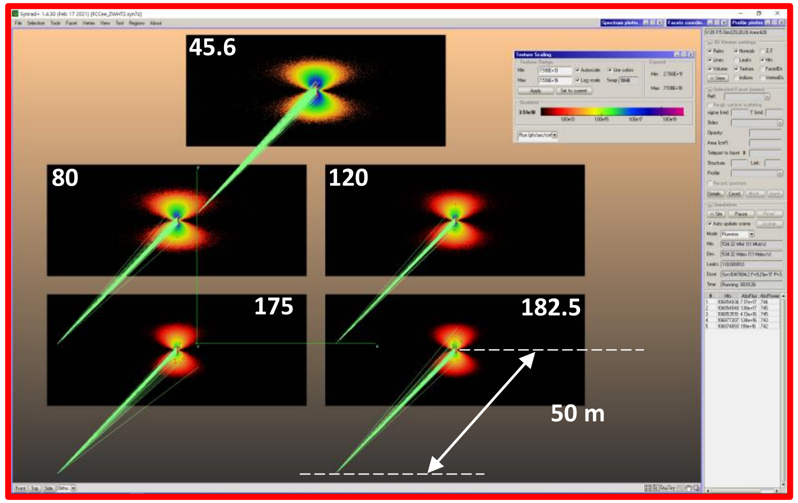

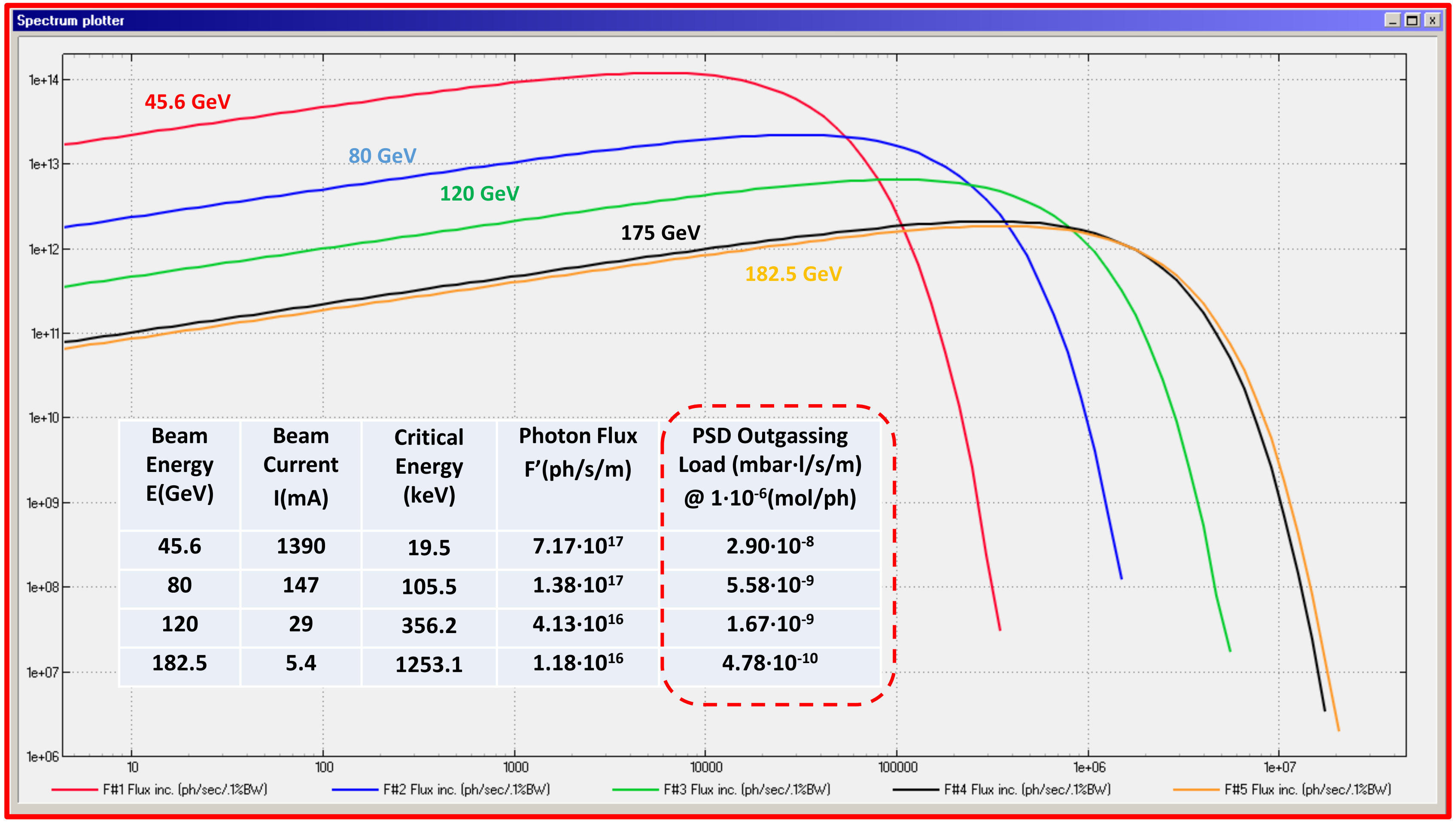

Beam Energy E(GeV)	Beam Current I(mA)	Critical Energy (keV)	Photon Flux F'(ph/s/m)	PSD Outgassing Load (mbar·l/s/m) @ $1\cdot10^{-6}$(mol/ph)
45.6	1390	19.5	$7.17\cdot10^{17}$	$2.90\cdot10^{-8}$
80	147	105.5	$1.38\cdot10^{17}$	$5.58\cdot10^{-9}$
120	29	356.2	$4.13\cdot10^{16}$	$1.67\cdot10^{-9}$
182.5	5.4	1253.1	$1.18\cdot10^{16}$	$4.78\cdot10^{-10}$

Units: Vertical: photons/s/(0.1% bandwidth)/m; Range [10^6 - $2\cdot10^{14}$]
Horizontal eV; Range [4 - $5\cdot10^7$]

- Gas Load for W-, H-, T-poles will have a significant contribution proportional to SR power, due to <u>Compton photons</u> (as per LEP operation, ref. "*The pressure and gas composition evolution during the operation of the LEP accelerator at 100 GeV*", M. J. Jimenez et al., Vacuum 60 (2001) p183-189);

F (FCC-ee)>100 keV (%)	
Z	0.0639
W	9.220
H	28.852
T(175)	47.810
T(182.5)	49.717

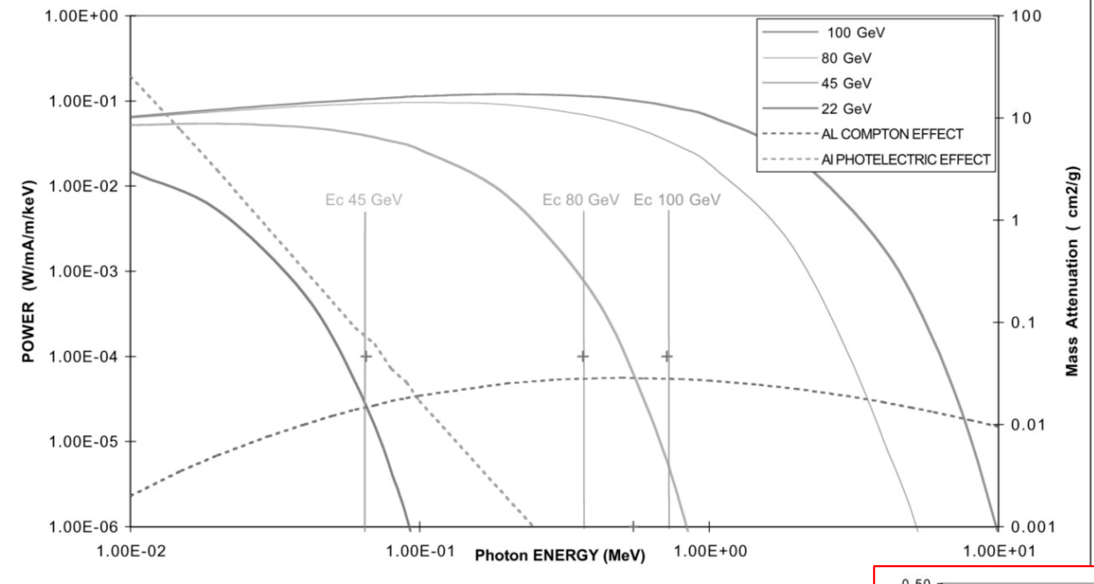

Fig. 2. The LEP synchrotron radiation spectrum.

A.S. Wilhelm and I. Jovanovic

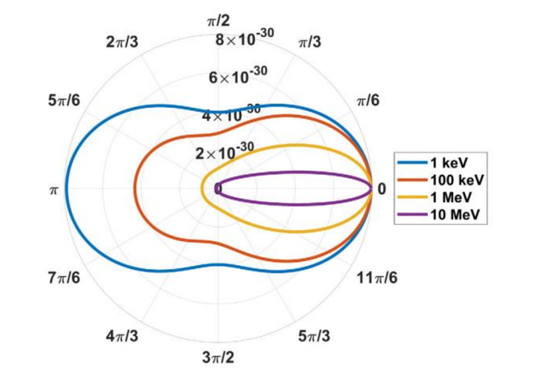

Fig. 1. The Klein–Nishina differential cross-section shapes for photons of various energies scattered off a hydrogen atom. The photon is incident at $\theta = 0$ and cross-section is measured in m^2. For heavier atoms, the magnitude of the KNDCS changes, but the shape is invariant for a given photon energy. Higher energy photons are much less likely to undergo a high-angle scattering than lower energy photons.

NIM A 1031 2022 166502

- If copper alloy is chosen as the material for the vacuum chamber, then a smaller fraction goes into Compton, and shielding improves;

- In addition, copper has a lower photon-stimulated desorption yield;

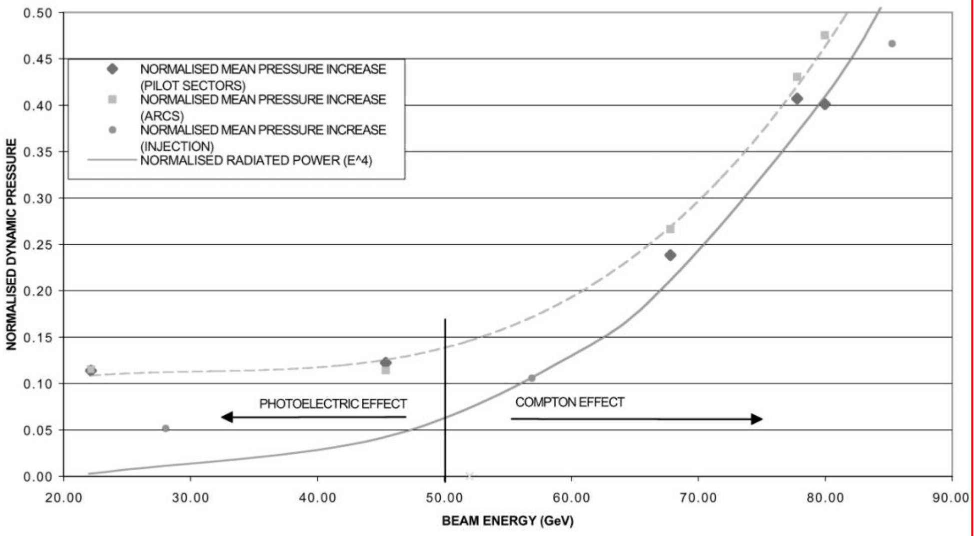

Fig. 5. Normalised pressure increase (low beam energy, measured in LEP arcs, 1999).

As soon as the Compton component will become dominant there will be a (large?) amount of secondary radiation coming back into the vacuum and generating also photoelectrons

Material: OFC copper; Specific Cond.: 48.2 l·m/s (CO, 20 °C)

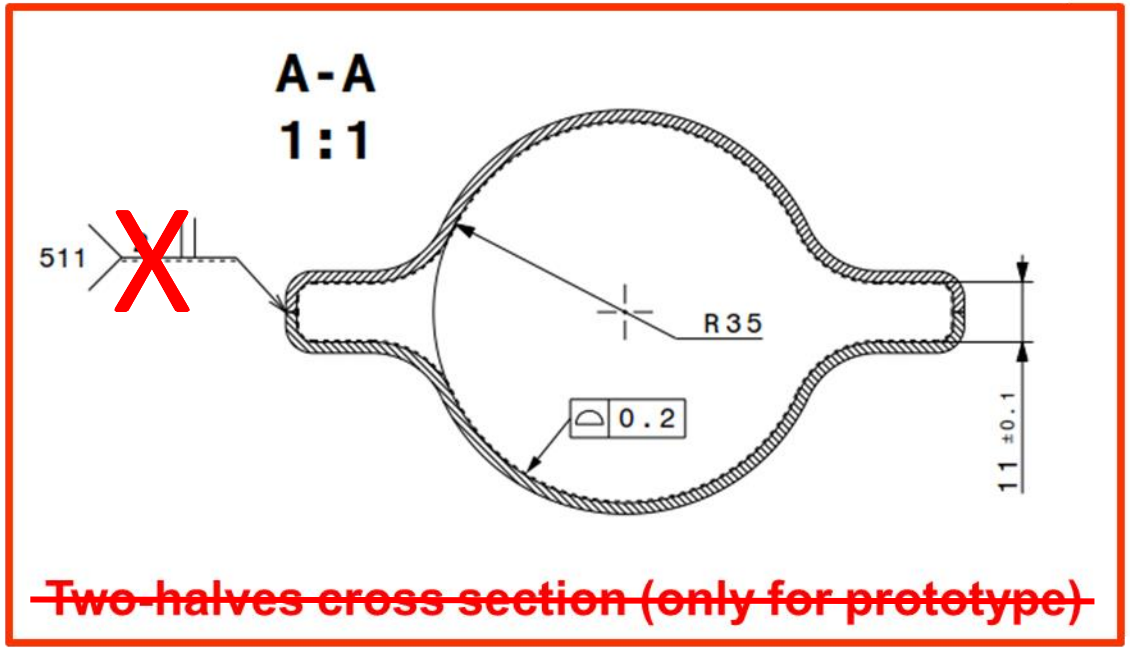

Lumped absorbers (1 every ~ 6 m, covering the entire horizontal SR photon fan)

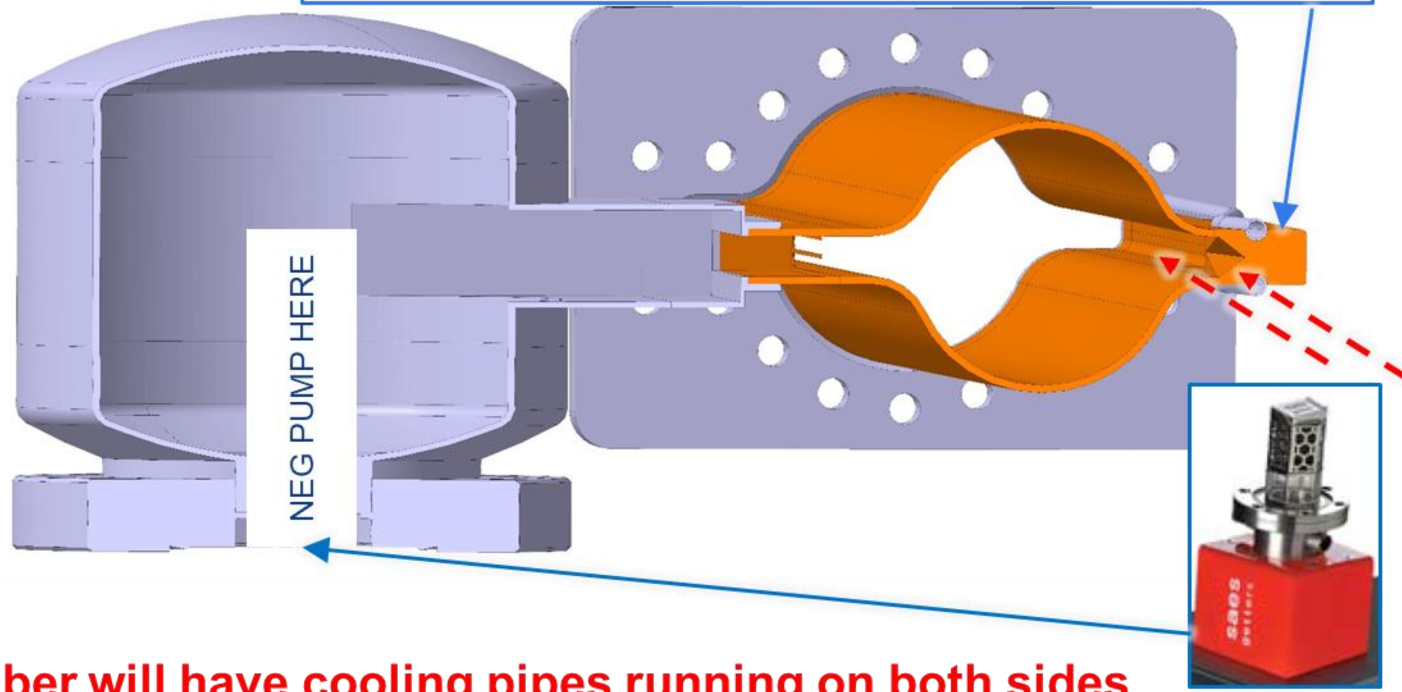

- Left: Cross-section of the prototype (real chamber will have cooling pipes running on both sides of winglets;
- Right: Cross-section at pumping dome/absorber location; The connection to the beam chamber is via a slotted grid; The SR absorber is placed in front of the pumping dome (for external beam only); The conductance of the pumping dome and tapered transition is ~ 110 l/s (CO, 20 C);

We have been asked to look at the possibility to use a smaller vacuum chamber, with internal radius of 30 mm instead of 35: under study now, seems feasible, although the specific conductance decreases to ~30 l·m/s

Pumping solutions: NEG-coating everywhere + lumped NEG pumps

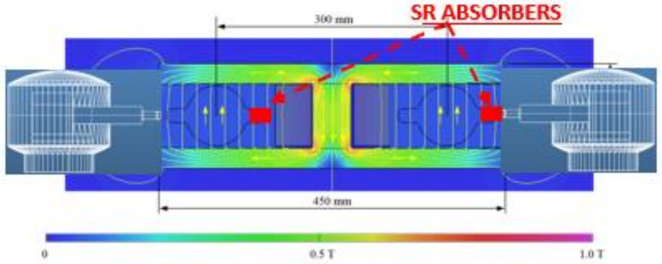

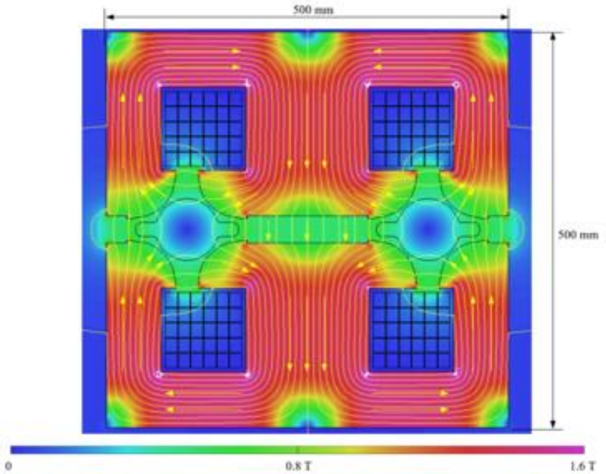

Material: OFC copper;
Specific Cond.: ~47 l·m/s (CO, 20 ºC)

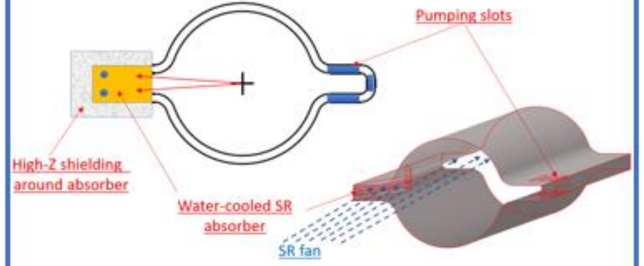

Schematics of SR absorbers and pumping slots (internal beam)

FCC-ee CAD Models

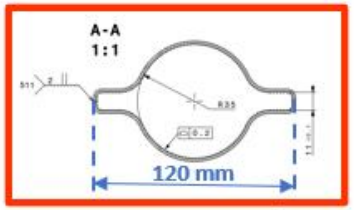

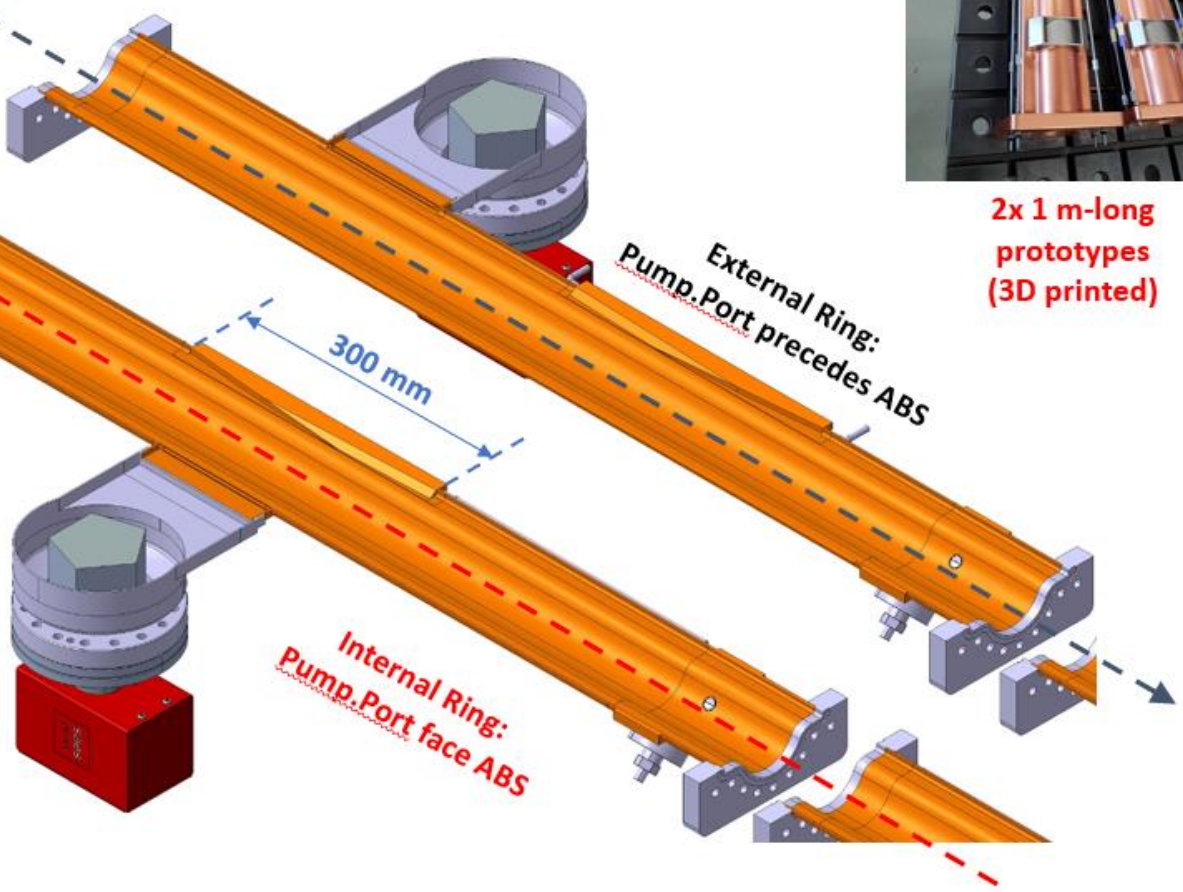

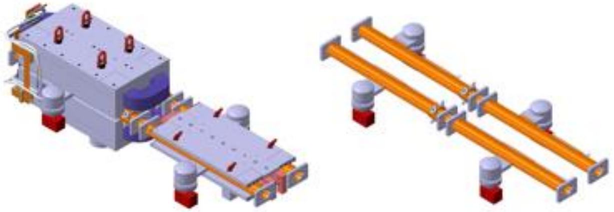

2x 1 m-long prototypes (3D printed)

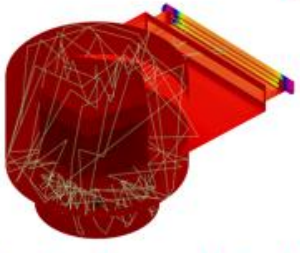

Pumping dome optimized via Molflow+ simulation: NEXTorr 1000

Pressure profiles (with baseline 70 mm ID chamber)

- These 2 models represent a section of the arcs (~140 m long)
- We have used Molflow+ to calculate the PSD pressure rise at different beam doses, using the photon irradiation maps calculated by SYNRAD+
- A sample 140.7 m-long section of an arc has been considered, with the two beams side by side: 5 dipoles and 5 quadrupoles as sources of SR
- The orbits along 5 dipoles interleaved with 5 quadrupoles are simulated, importing the lattice files from MADX into SYNRAD+
- The 3D model for B1 has 25 absorbers placed at ~ 5.6 m average spacing (avoiding quadrupoles and sextupoles which have tight coils), while B2 has no absorbers, and the SR fan is let impinge onto the bottom of the external winglet (see also B. Humann, FCC Week)
- The MDI region adopts the same philosophy: **lumped absorbers covering ~100% of the primary SR photon fans**

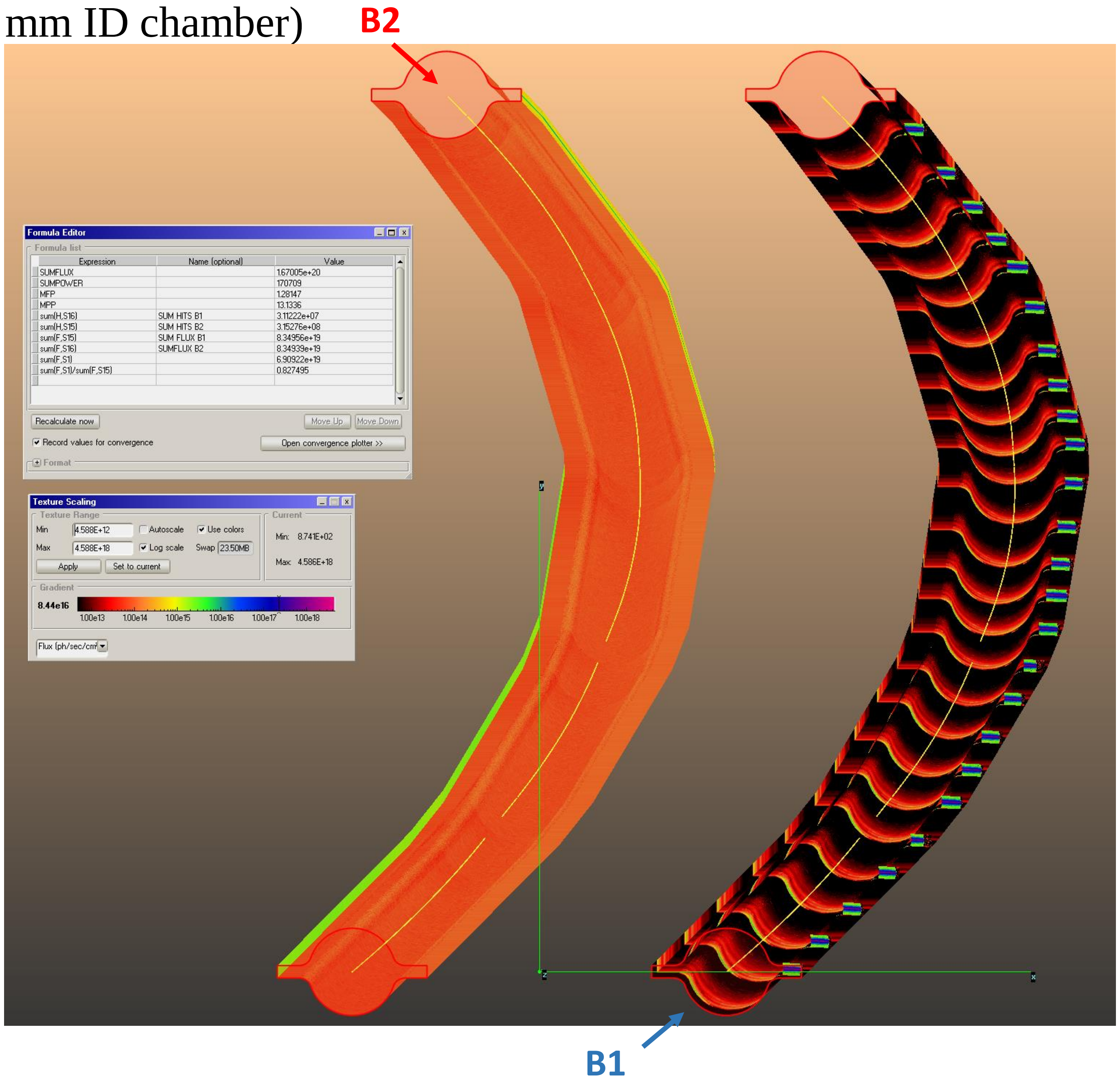

Pressure profiles (now for 60 mm ID chamber)

- These 2 models represent a section of the arcs (132.4 m long)
- We have used Molflow+ to calculate the PSD pressure rise at different beam doses, using the photon irradiation maps calculated by SYNRAD+
- A sample 132.4 m-long section of an arc has been considered, with the two beams side by side: 4 dipoles and 4 quadrupoles as sources of SR
- The orbits along 4 dipoles interleaved with 4 quadrupoles are simulated, importing the lattice files from MADX into SYNRAD+
- The 3D model for B2 has 26 absorbers placed at ~ 5.0 m average spacing (avoiding quadrupoles and sextupoles which have tight coils), while B1 has no absorbers, and the SR fan is let impinge onto the bottom of the external winglet
- The MDI region adopts the same philosophy: **lumped absorbers covering ~100% of the primary SR photon fans**
- **~12% MORE ABSORBERS as compared to the 70 mm ID chamber and different lattice!**

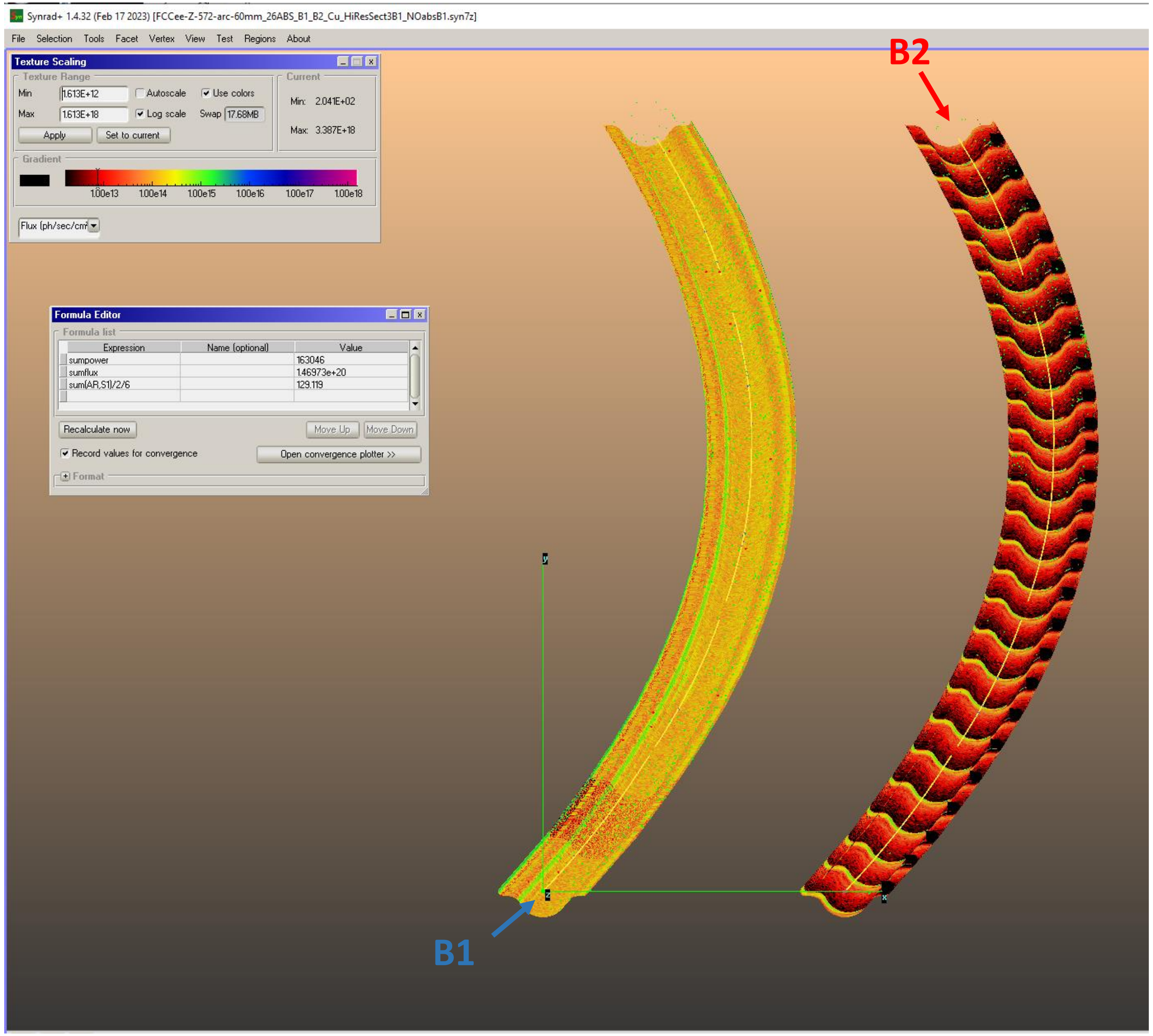

Pressure profiles

- We have calculated the PSD pressure profiles for 4 different beam doses, corresponding to times of 1 h, 10 h, 100 h, 1000 h at nominal current (1270 mA); Simulated gas: CO
- On the left the case with 3x 100 (l/s) lumped pumps/beam, and no NEG-coating
- On the right, the case with NEG-coating with some residual sticking (*s*=0.001) for 1h case

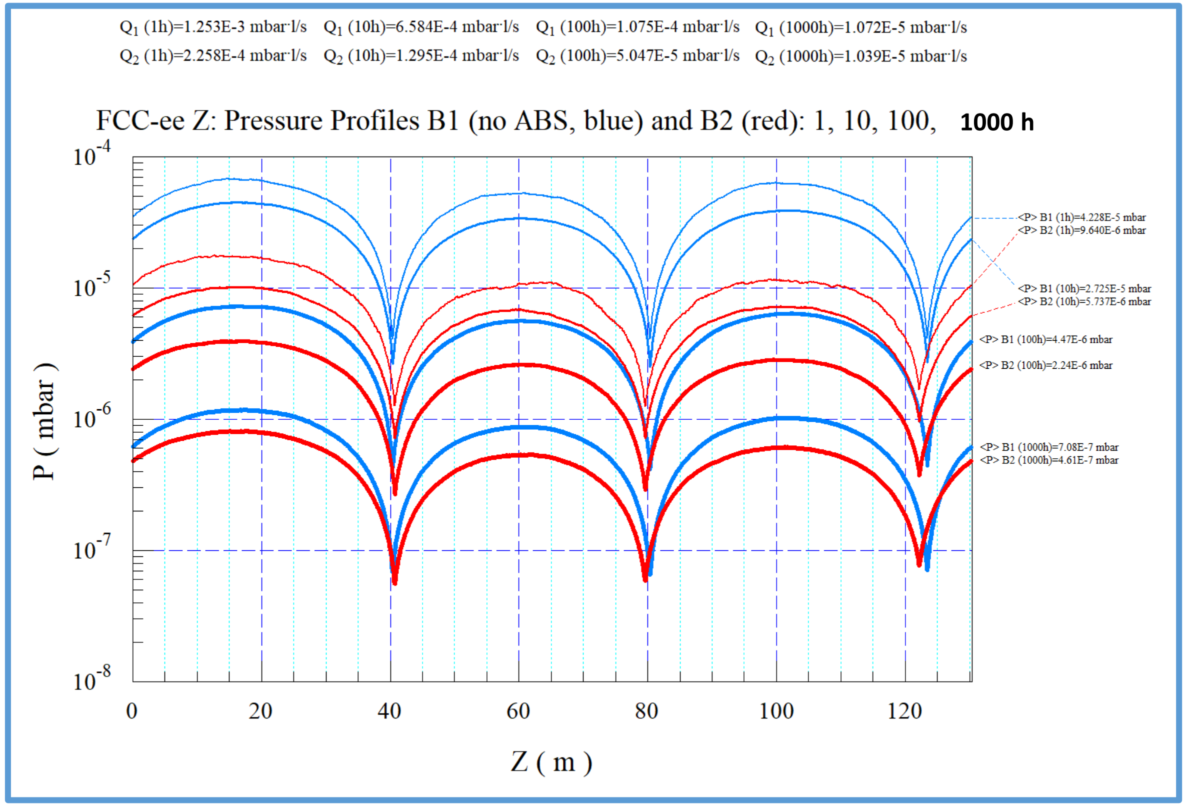

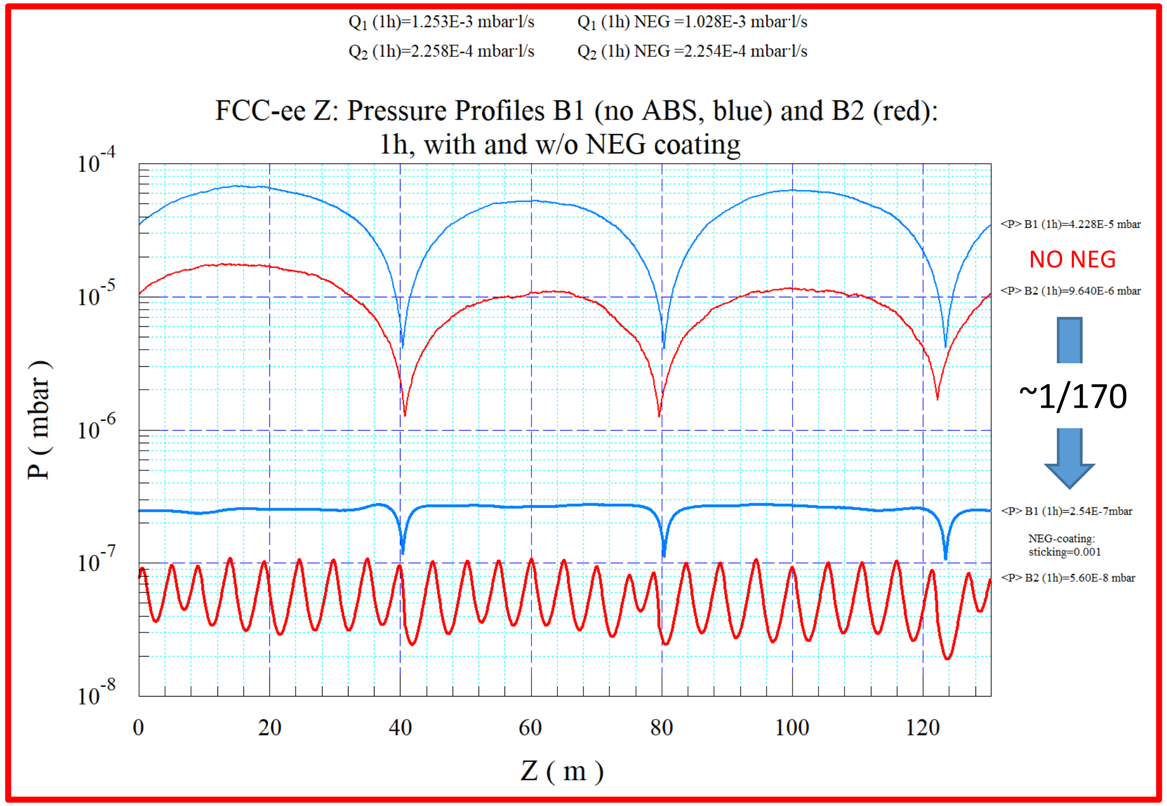

FCC-ee Z: SR photon irradiation maps

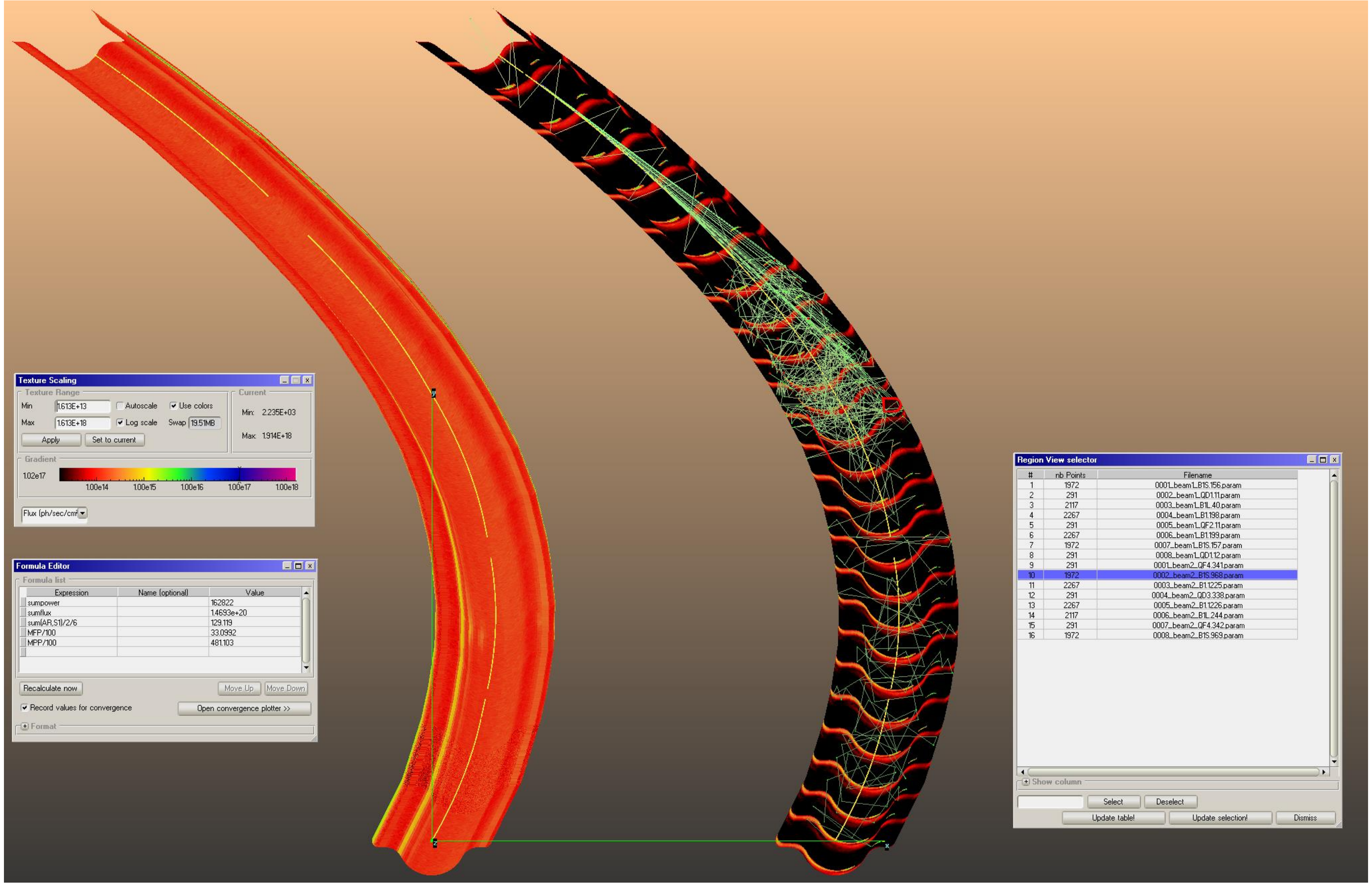

FCC-ee Z: SR photon irradiation maps: closer look at the SR spots: increased resolution along 755 cm section of the ring

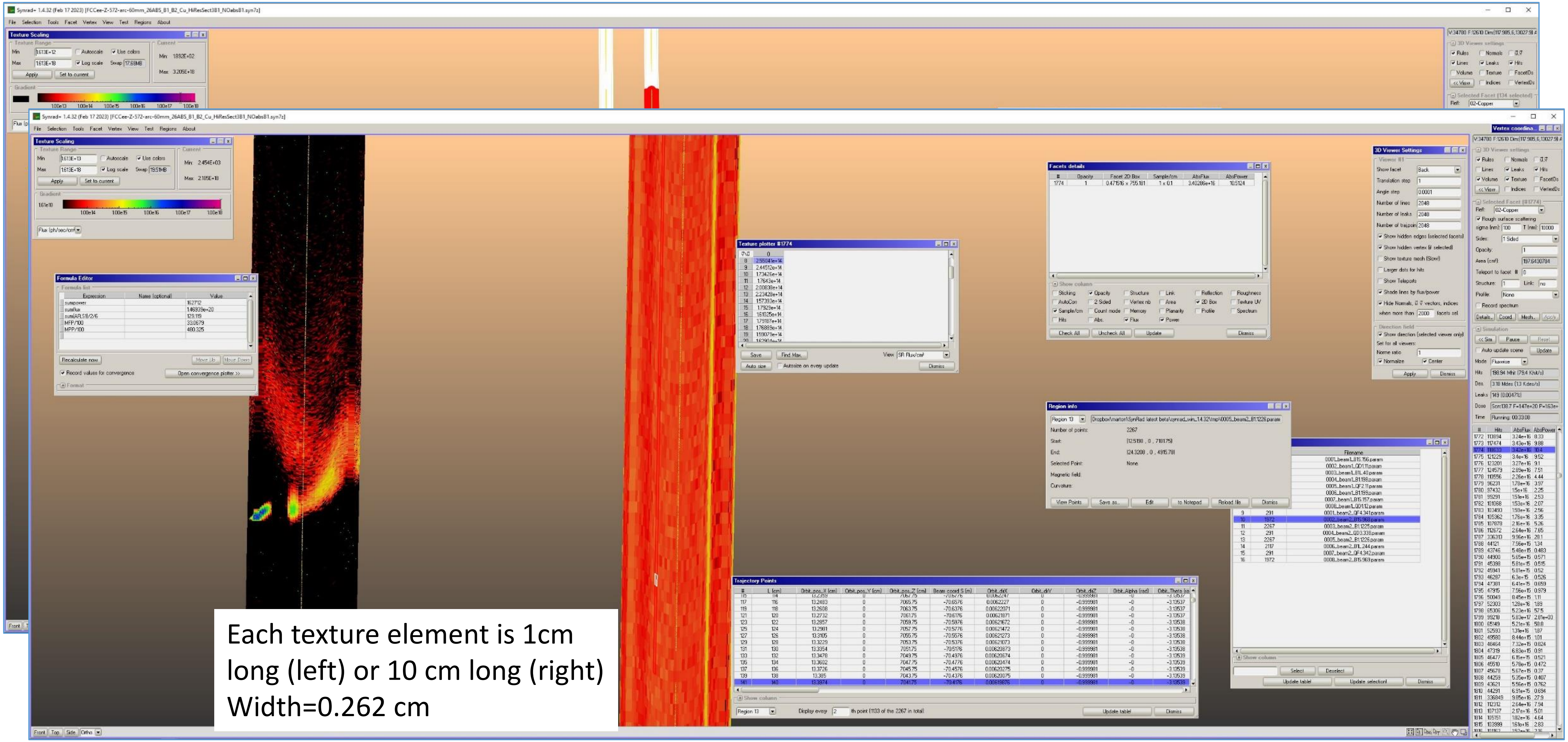

Each texture element is 1cm long (left) or 10 cm long (right)
Width=0.262 cm

FCC-ee Z: SR photon irradiation maps: closer look at the SR spots: increased resolution along 755 cm section of the ring

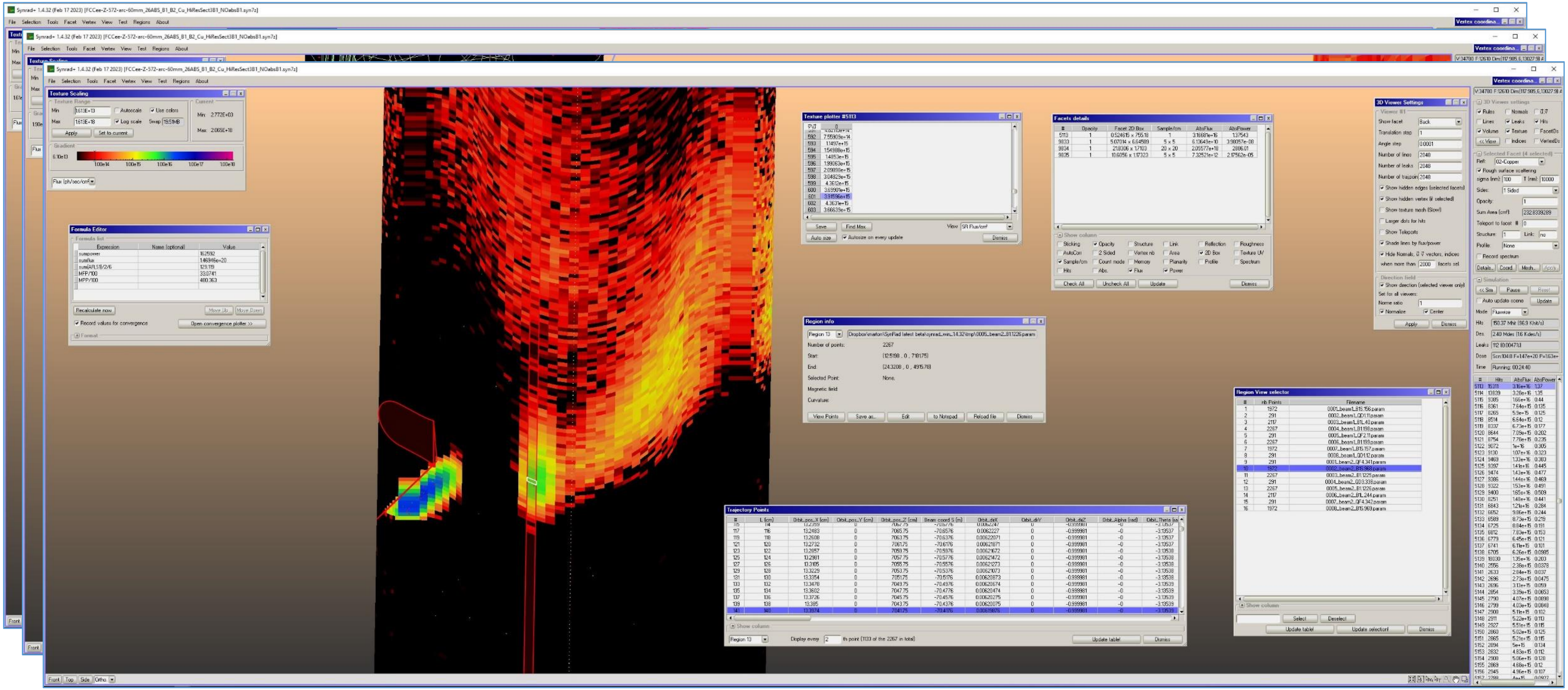

FCC-ee Z: SR photon irradiation maps: closer look at the SR spots: increased resolution along 755 cm section of the ring

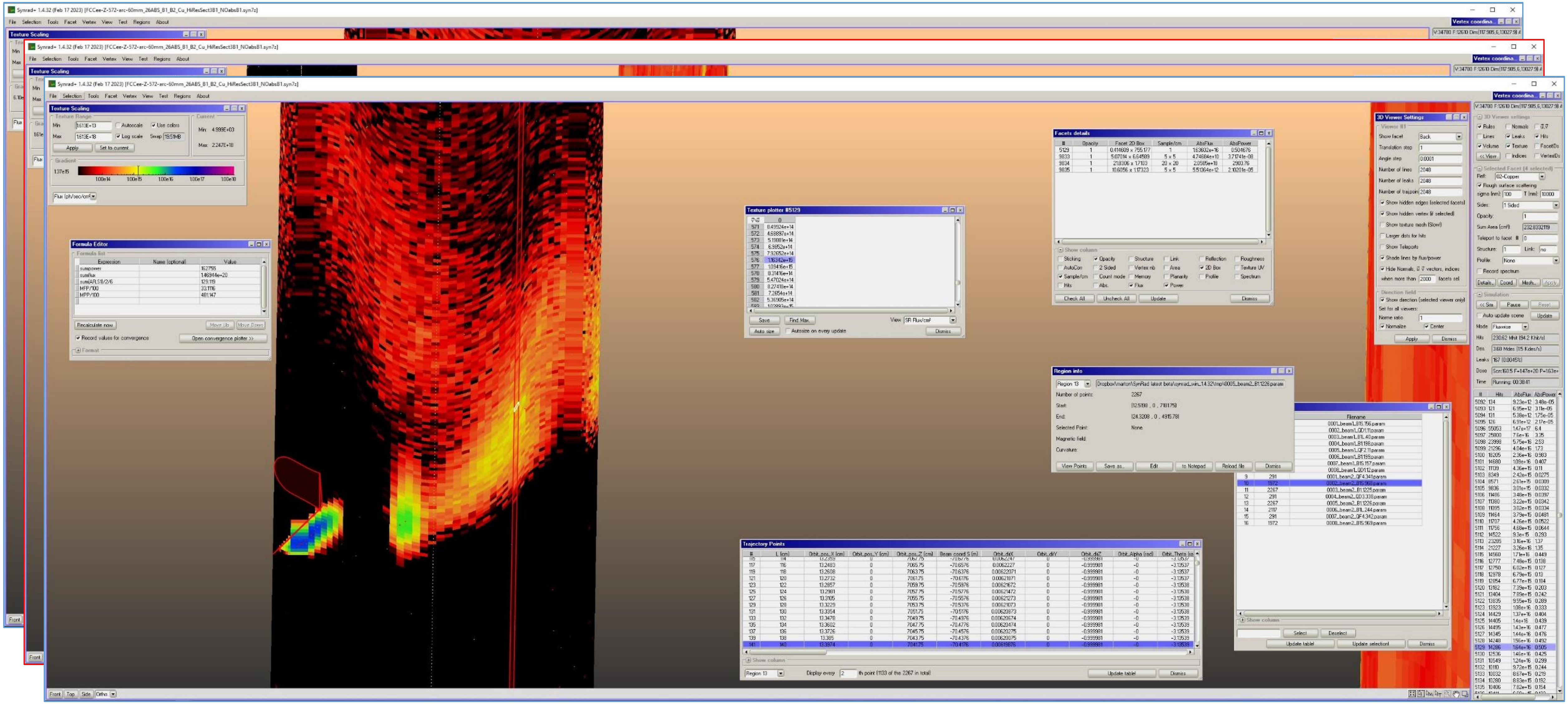

IMPORTANT:

FCC-ee Z: SR photon irradiation maps:

The 26 absorber on B2 intercept 77.6% of the SR primary fan, with only 22.4% ending up on the vacuum chamber (VC) walls

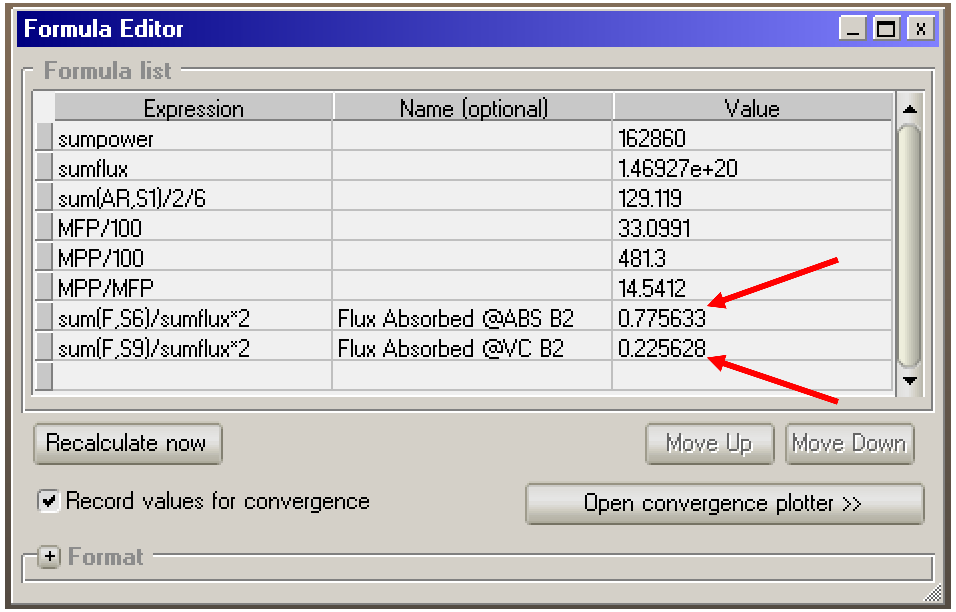

Expression	Name (optional)	Value
sumpower		162860
sumflux		1.46927e+20
sum(AR,S1)/2/6		129.119
MFP/100		33.0991
MPP/100		481.3
MPP/MFP		14.5412
sum(F,S6)/sumflux*2	Flux Absorbed @ABS B2	0.775633
sum(F,S9)/sumflux*2	Flux Absorbed @VC B2	0.225628

FCC-ee Z: SR photon irradiation maps:

For B1, with NO Absorbers, ~50% of the SR flux is absorbed on the “circular”part of the chamber (shown here for one segment only)…

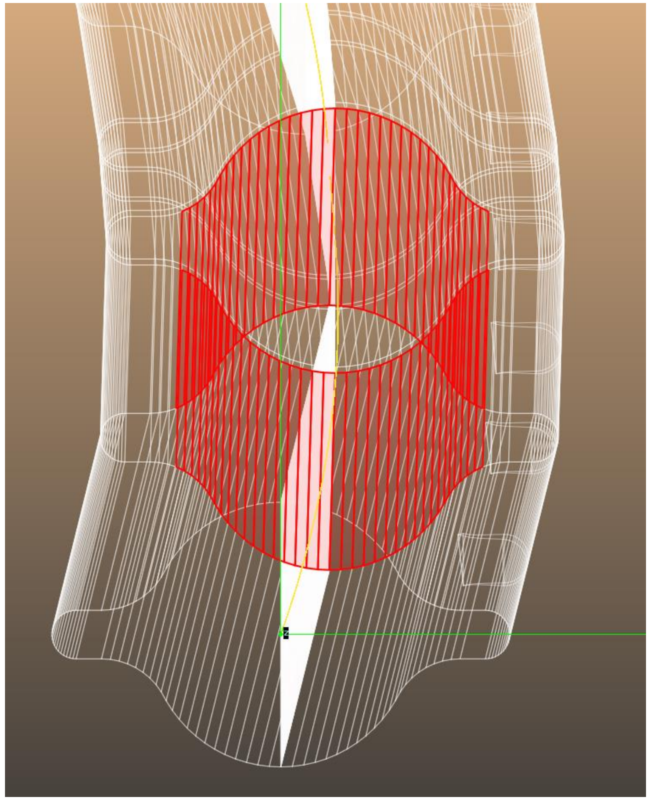

FCC-ee Z: from SR photon irradiation maps to Photo-Electron production and SEY/EC

EUROPEAN ORGANIZATION FOR NUCLEAR RESEARCH
European Laboratory for Particle Physics

Large Hadron Collider Project

LHC Project Report 206

Photoelectron Yield and Photon Reflectivity from Candidate LHC Vacuum Chamber with Implications to the Vacuum Chamber Design

V. Baglin, I.R. Collins, O. Gröbner

Abstract

Studies of the photoelectron yield and photon reflectivity at grazing incidence (11 mrad) from candidate LHC vacuum chamber materials have been made on a dedicated beam line on the Electron–Positron Accumulator (EPA) ring at CERN. These measurements provide realistic input toward a better understanding of the electron cloud phenomena expected in the LHC. The measurements were made using synchrotron radiation with critical photon energies of 194 eV and 45 eV; the latter corresponding to that of the LHC at the design energy of 7 TeV. The test materials are mainly copper, either, i) coated by co-lamination or by electroplating onto stainless steel, or ii) bulk copper prepared by special machining. The key parameters explored were the effect of surface roughness on the reflectivity and the photoelectron yield at grazing photon incidence, and the effect of magnetic field direction on the yields measured at normal photon incidence. The implications of the results on the electron cloud phenomena, and thus the LHC vacuum chamber design, is discussed.

conditions: as-received, baked at 150°C for 9 hours and baked at 150°C for 24 hours.

3 RESULTS

3.1 Photon reflection

With the test chamber aligned in the 'straight through position', *i.e.* photons impinging directly onto the collector, a current, I_{ST}, proportional to the photon flux is recorded for a sufficiently large negative bias (space charge is overcome above ~ 20V) as shown in Figure 2. The test chamber is then aligned to a mean incidence angle of 11Êmrad and irradiated whilst the photoelectron current is measured at the collector. Under the assumption that the photon spectrum is unchanged on reflection, then this collector current, I_{11}, with the same negative bias is proportional to the forward scattered reflected photon flux. The ratio of I_{11} to I_{ST} then defines the forward scattering photon reflection, R. For positive bias of the collector the small recorded current can be attributed to photoelectrons produced on the test chamber by back-scattered light from the collector.

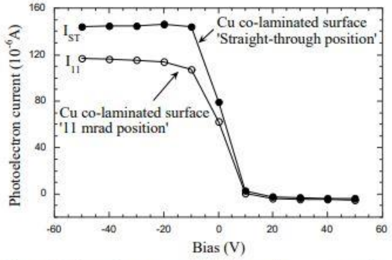

Figure 2. Photoelectron currents, I_{ST} and I_{11}, measured at the collector for the Cu co-laminated test chamber irradiated by 45 eV critical energy synchrotron radiation in straight through and 11 mrad positions respectively.

3.2 Photoelectron yields

The photoelectron yield is measured at the mean angle of incidence of 11 mrad using a positively biased (up to 1kV) 200 mm long stainless steel wire electrode. The measured photocurrent, I_Y, on this electrode converges for increasing voltage but never completely saturates since this measurement is local, *i.e.* the collection length increases with increasing bias. From the measurement of the photoyield of sawtooth chamber with the light at quasi-normal incidence, normalised to the measured photoyield of the end collector at normal incidence, the collection length was determined to be 500 mm.

The electron yield per incident photon, Y, is derived from the photon flux, $\dot{\Gamma}$, into the test chamber making appropriate allowance for the attenuation due to the collimator, F: 46% and 65% of the photons from the beam line enter the set-up at 45 eV and 194 eV critical energies respectively. A correction due to the effective collection length, L_{coll} with respect to the length irradiated, L_{Ir} (3.4 m), is applied. The photoelectron yield is given by: $Y = \frac{I_Y}{q\dot{\Gamma}F}\frac{L_{Ir}}{L_{Coll}}$

For the simulations of the electron-cloud and the beam induced multipacting effects, the electron yield per absorbed photon, Y*, is a more appropriate parameter which is given by: $Y^* = \frac{Y}{1-R}$. A summary of the results for R and Y* for all materials studied so far is given in Table 1.

Table 1. Forward scattering photon reflection R and photoelectron yields per absorbed photon, Y^*, of the studied materials under different surface conditioning, irradiated by 45 eV and 194 eV critical energy synchrotron radiation.

Surface	Status	45 eV R (%)	45 eV Y* (e/ph)	194 eV R (%)	194 eV Y* (e/ph)
Cu co-lam.	as-received	80.9	0.114	77.0	0.318
	air baked	21.7	0.096	18.2	0.180
Cu elect.	as-received	5.0	0.084	6.9	0.078
Cu sawtooth	as-received	1.8	0.053	-	-
	150°C, 9h	1.3	0.053	1.2	0.052
	150°C, 24h	1.3	0.040	1.2	0.040

3.3 Effect of magnetic fields on the photoelectron yields

The vacuum system in the arcs of the LHC will be mainly located in strong magnetic fields arising from dipoles, quadrupoles and corrector magnets. In the presence of a magnetic field any emitted electron will be subject to a Lorentz force that can deviate its motion.

For a dipole field (0.08-0.1 T) aligned parallel to the irradiated collector to within < 0.8°, a strong suppression, by a factor larger than 50, of the photoelectron yield is observed. The degree of suppression is related to the alignment of the field relative to the emitting surface indicating that the photoelectron emission is non-isotropic; a misalignment of 1.5° results in a suppression factor of 25. The strong suppression is attributed to low energy electrons being turned back into the surface by the external applied field. On the other hand a solenoid field (0.2 T) aligned perpendicular to the surface has no significant effect on the measured photoelectron current, again indicative of a non-isotropic electron emission.

4 DISCUSSION

For a given surface the forward scattered photon reflectivity is slightly higher at 45 eV critical energy than at 194 eV. This observation is in line with the increase of the reflectivity for low photon energies. On the other hand the photoelectron yield seems to increase slightly for increasing critical energy.

The Cu co-laminated material exhibits both the highest forward scattering photon reflection and

FCC-ee Z: from SR photon irradiation maps to Photo-Electron production and SEY/EC

Available online at www.sciencedirect.com

SCIENCE DIRECT®

ELSEVIER

Nuclear Instruments and Methods in Physics Research A 554 (2005) 92–113

NUCLEAR INSTRUMENTS & METHODS IN PHYSICS RESEARCH Section A

www.elsevier.com/locate/nima

First experimental and simulation study on the secondary electron and photoelectron yield of NEG materials (Ti–Zr–V) coating under intense photon irradiation

Y. Suetsugu[a,*], K. Kanazawa[a], K. Shibata[a], H. Hisamatsu[a], K. Oide[a], F. Takasaki[a], R.V. Dostovalov[b], A.A. Krasnov[b], K.V. Zolotarev[b], E.S. Konstantinov[b], V.A. Chernov[b], A.E. Bondar[b], A.N. Shmakov[c]

[a] *Accelerator Laboratory, High Energy Accelerator Research Organization (KEK), 1-1 Oho, Tsukuba, Ibaraki 305-0801, Japan*
[b] *Budker Institute of Nuclear Physics (BINP), Novosibirsk 630090, Russia*
[c] *Boreskov Institute of Catalysis SD RAS, Novosibirsk 630090, Russia*

Received 13 June 2005; received in revised form 10 August 2005; accepted 11 August 2005
Available online 1 September 2005

Abstract

A beam duct coated with NEG materials (Ti, Zr, V), which had been known to have a low secondary electron yield (SEY), was studied for the first time under intense photon irradiation using a positron beam at the KEK B-Factory (KEKB) to investigate a way to suppress the electron cloud instability (ECI). A 2.56 m test copper chamber was coated with the NEG materials (we call it NEG coating here) by magnetron sputtering. It was installed at an arc section of the KEKB positron ring, where the chamber was irradiated by direct photons with a line density of 6.5×10^{14} photons $m^{-1} s^{-1} mA^{-1}$. The vacuum pressure around the test chamber during a usual beam operation was lower than the case of non-coated copper chambers by a factor of 4–5. The number of electrons around positron bunches was measured by a special electron monitor up to a stored beam current of 1600 mA. The measured electron current, however, was almost the same as a non-coated copper chamber, especially at low-beam currents, and the effect of the NEG coating was smaller than expected. A simulation explained the result that abundant photoelectrons in the positron ring reduce the effect of the low SEY. The maximum SEYs of the NEG coating and non-coated copper were evaluated using a simulation as about 0.9–1.0 and 1.1–1.3, respectively, which were consistent with the values after a sufficient electron bombardment. Their photoelectron yields were also estimated as 0.22–0.28 and 0.26–0.34, respectively, and were in good agreement with the previous experimental results. The study indicates that the suppression of photoelectrons, by a

Table 3
Photoelectron yield (η_e), reflectivity (R) and effective photoelectron yield (η_e^*) from the NEG-coated chamber prepared at KEK

	η_e (electrons photon^{-1})	R (%)	η_e^* (electrons photon^{-1})
Cu (smooth, Ra = 0.02)	0.29	33.2	0.434
NEG (before activation)	0.32	19.5	0.39
NEG (after activation)	0.19	14.8	0.23

chamber. The effective yield (η_e^*) was calculated using η_e and R by $\eta_e^* = \eta_e/(1 - R)$. The η_e of the NEG-coated surface before the activation was larger, or almost the same, as that of smooth copper (about 0.3). After activation, η_e decreased to about 70% of that of smooth copper (about 0.2). The NEG coating was found to have a photoelectron yield of the same order, but slightly smaller than that of the un-coated copper at the present critical energy and the angle of incidence. The obtained η_e^* is slightly larger, and R is smaller than those measured at CERN [12,50], where $\eta_e^* \sim 0.1$ and $R \sim 80\%$. The difference may be understood by that of the critical energies of the SR.

FCC-ee Z: from SR photon irradiation maps to Photo-Electron production and SEY/EC

Available online at www.sciencedirect.com
ScienceDirect
ELSEVIER
Nuclear Instruments and Methods in Physics Research A 578 (2007) 470–479
NUCLEAR INSTRUMENTS & METHODS IN PHYSICS RESEARCH Section A
www.elsevier.com/locate/nima

Recent studies on photoelectron and secondary electron yields of TiN and NEG coatings using the KEKB positron ring

Y. Suetsugu*, K. Kanazawa, K. Shibata, H. Hisamatsu

Accelerator Laboratory, High Energy Accelerator Research Organization (KEK), 1-1 Oho, Tsukuba, Ibaraki 305-0801, Japan

Received 28 May 2007; received in revised form 14 June 2007; accepted 14 June 2007
Available online 20 June 2007

Abstract

In order to obtain a method to suppress electron-cloud instability (ECI), the photoelectron and the secondary electron yields (PEY and SEY) of a TiN coating and an NEG (Ti–Zr–V) coating on copper have been studied so far by using the KEK B-factory (KEKB) positron ring. Recently, test chambers with these coatings were installed at a straight section of the ring where the irradiated photon density was considerably smaller than that at the arc section of a previous experiment. The number of electrons around beams was measured by an electron current monitor; this measurement was performed up to a stored beam current of approximately 1700 mA (1389 bunches). For the entire range of the beam current, the electron currents of the NEG-coated and the TiN-coated chambers were clearly smaller as compared to those of the uncoated copper chamber by the factors of 2–3 and 3–4, respectively. The small photon density, that is, the weak effect of photoelectrons, elucidated the differences in the SEYs of these coatings when compared to the measurements at the arc section. By assuming almost the same PEY (η_e) values obtained in the previous study, the maximum SEY (δ_{max}) for the TiN and NEG coatings and the copper chamber was again estimated based on a previously developed simulation. The evaluated δ_{max} values for these three surfaces were in the ranges of 0.8–1.0, 1.0–1.15, and 1.1–1.25, respectively. These values were consistent with the values obtained so far. As an application of the simulation, the effective η_e, η_{e-eff} (which included the geometrical effect of the antechamber) and δ_{max} values were also estimated for copper chambers with one or two antechambers. These chambers were installed in an arc section and a wiggler section, respectively. The evaluated η_{e-eff} and δ_{max} values were approximately 0.008 and 1.2, and 0.04 and 1.2, respectively, where $\eta_e = 0.28$ was assumed on the side wall. As expected, the η_{e-eff} values were considerably smaller than those obtained in the case of a simple circular chamber ($\eta_e = 0.28$–0.3). Further, the δ_{max} values were consistent with those obtained so far. With regard to the uncertainty in the simulation, the effect of the SEY spectrum on the estimation of δ_{max} values is briefly discussed. As the next step in our study, we plan to combine beam ducts with antechambers and TiN coatings; this combination is the most promising solution to ECI at present.

© 2007 Elsevier B.V. All rights reserved.

PACS: 29.20.Dh; 29.27.Bd

Keywords: Electron-cloud instability; Secondary electron yield; Photoelectron yield; NEG coating; TiN coating; Antechamber

1. Introduction

One of the most critical problems in current and future high-luminosity colliders is the electron-cloud instability (ECI) in various positron and proton rings [1–11]. One promising method to suppress the ECI is to apply a surface coating with a low secondary electron yield (SEY) to the inner surface of the beam duct [9–31]. We have been focusing on a TiN coating and an NEG (Ti–Zr–V) coating and on investigating the effect of their SEYs on the electron cloud formation by using the KEK B-factory (KEKB) positron ring, that is, the low energy ring (LER) [32]. In the previous reports, the test chambers with these surfaces were installed at an arc section in the LER; around this section, the photons of the synchrotron radiation (SR) were directly irradiated with a line density of approximately 6.5×10^{14} photons $m^{-1} s^{-1} mA^{-1}$ [30,31]. The number of electrons around the beams was measured using an electron current monitor [30] and the measured values were

*Corresponding author. Tel.: +81 298 64 5227; fax: +81 298 64 3182.
E-mail address: yusuke.suetsugu@kek.jp (Y. Suetsugu).

0168-9002/$ - see front matter © 2007 Elsevier B.V. All rights reserved.
doi:10.1016/j.nima.2007.06.015

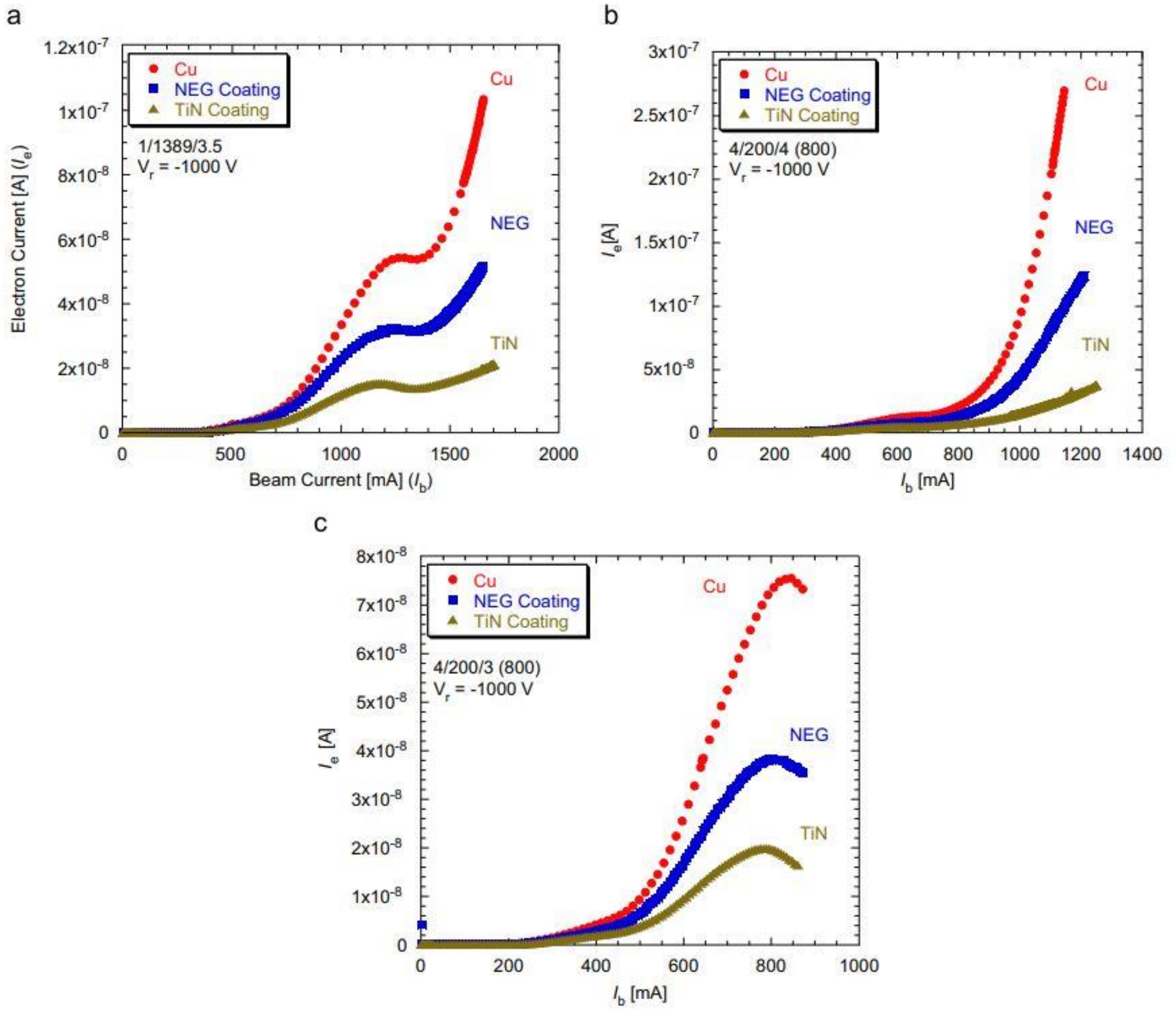

Fig. 2. Behaviors of measured electron current (I_e) with respect to beam current (I_b) of the uncoated copper, NEG-coated, and TiN-coated chambers for the bunch filling patterns: (a) 1/1389/3.5 (1389 bunches), (b) 4/200/4 (800 bunches), and (c) 4/200/3 (800 bunches), where the repeller voltage (V_r) is −1000 V. The bunch filling pattern 1/1389/3.5, for example, means one train of 1389 bunches filled by an average of 3.5 RF-bucket spacings.

MDI Interaction Point: sources of radiation and radiation dump

SOURCE	POWER	CRITICAL ENERGY
• SR EM-fields of colliding bunches (Beamstrahlung)	~ 400 kW	~ 2 MeV
• SR solenoid (2T) + anti-solenoid	~ 40 kW	~ 0.02 MeV
• SR IR quadrupoles	~ 7 kW	~ 0.02 MeV
• radiative Bhabha (beam-beam Bremsstrahlung)	~ 0.7 kW	~ 5000 MeV

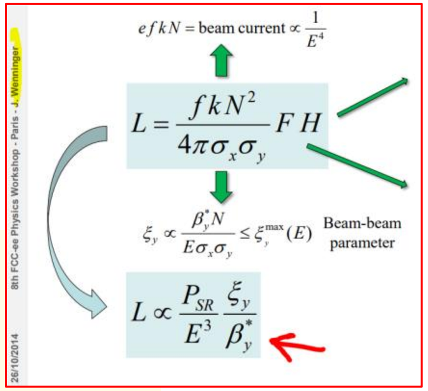

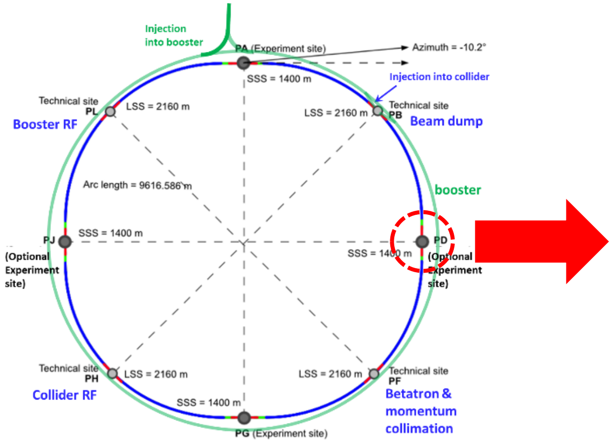

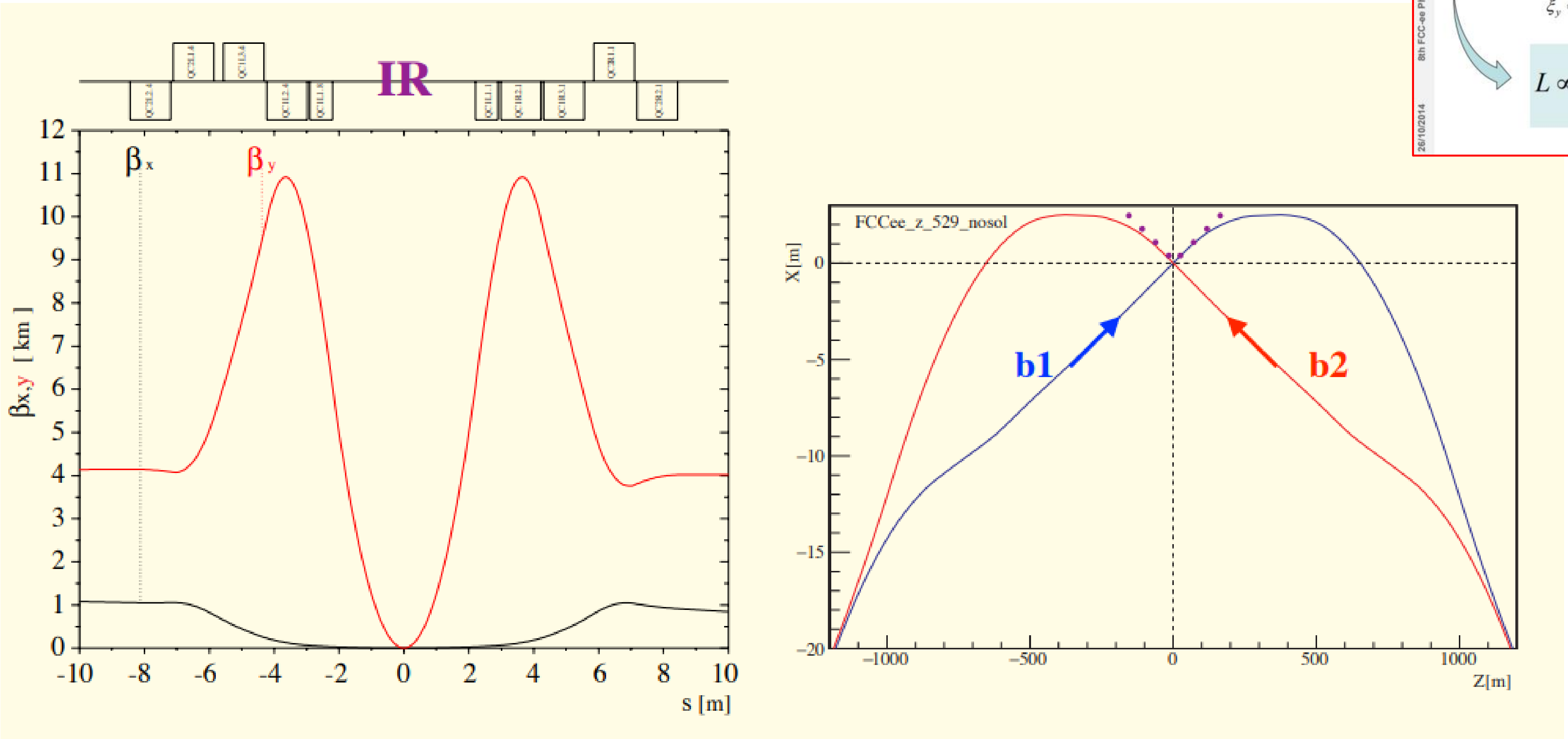

Beta functions and geometry of the IP region; crossing angle is 30 mrad

MDI Interaction Point: sources of radiation and radiation dump

- **Main goal**: reduce/eliminate the radiation background reaching the detector
- Five main effects (excluding hot-spots and heating due to impedance issues)

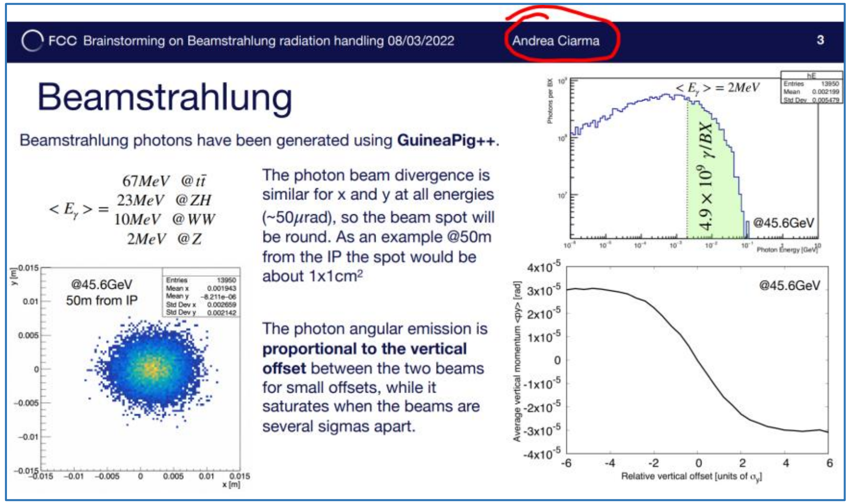

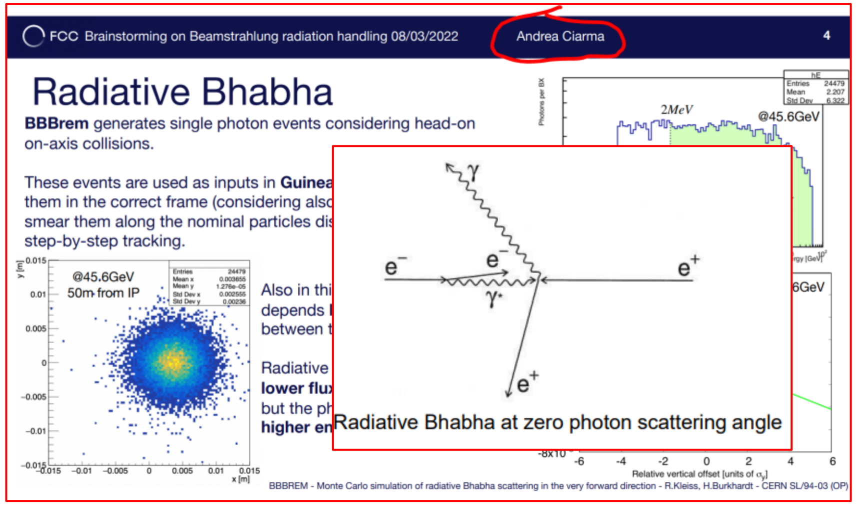

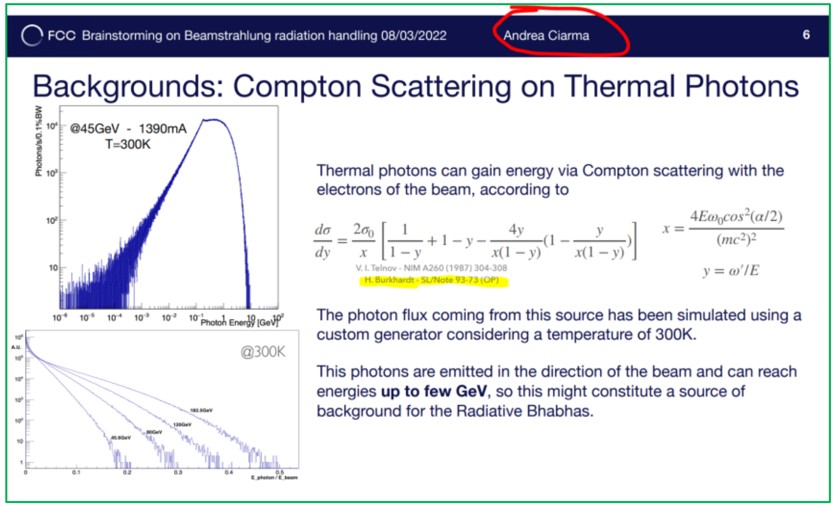

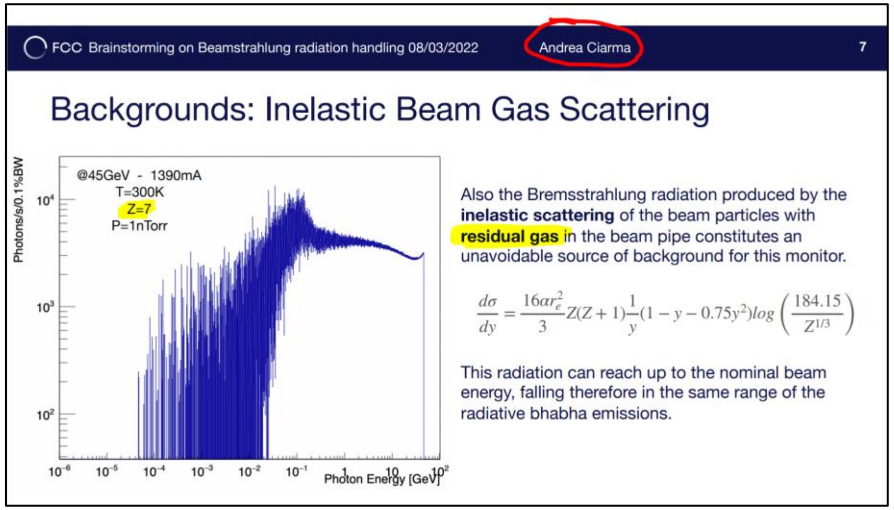

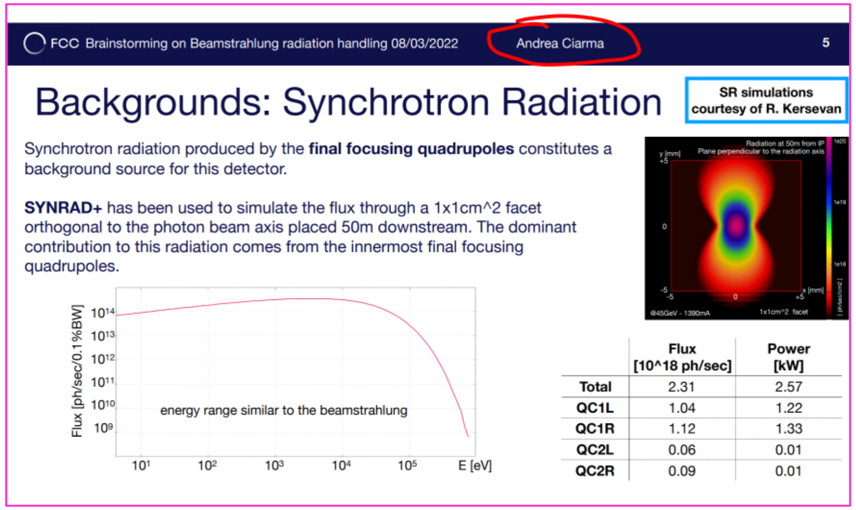

MDI Interaction Point: sources of radiation and radiation dump

- Solenoid/anti-solenoid fields (K.D.J. André); Strong effect on SR
- 2T @15 mrad

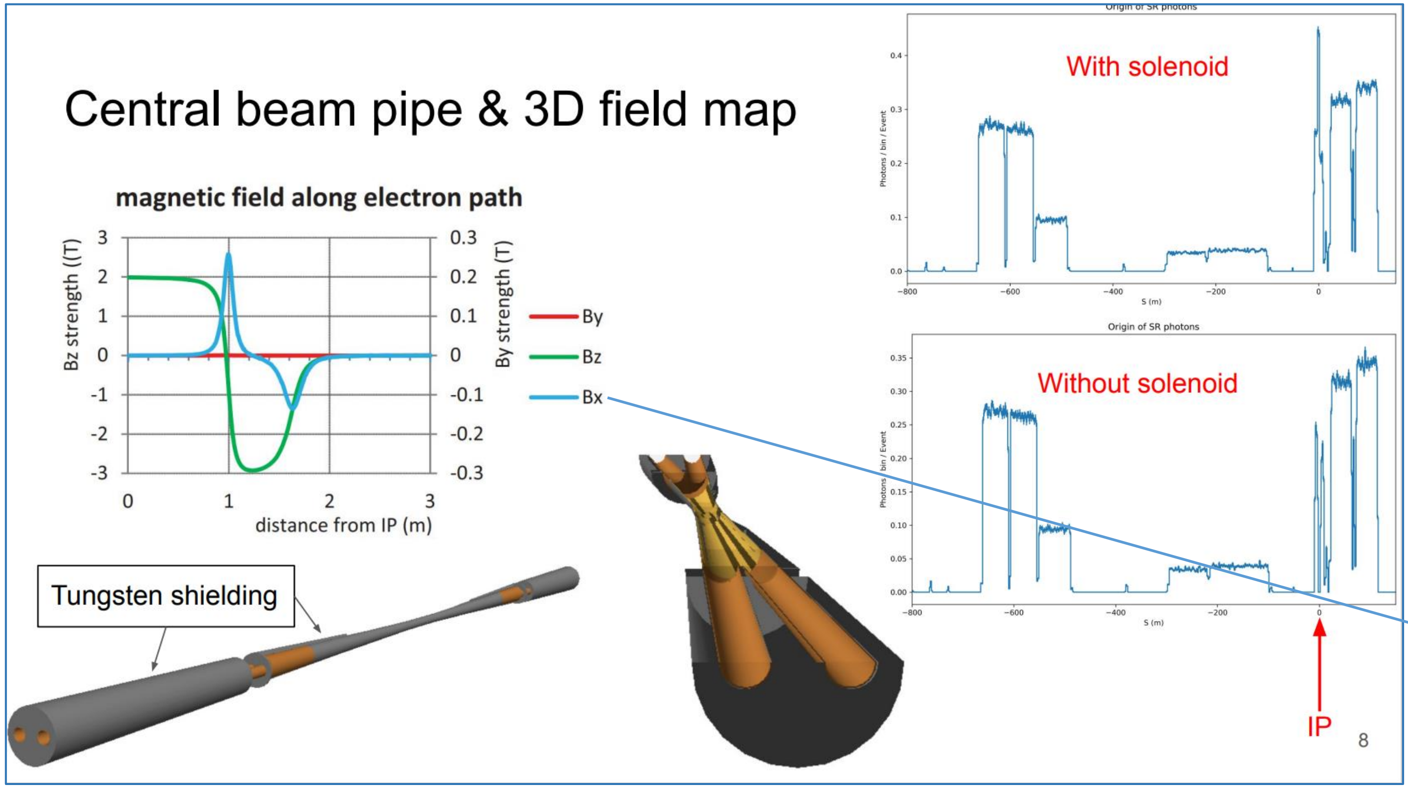

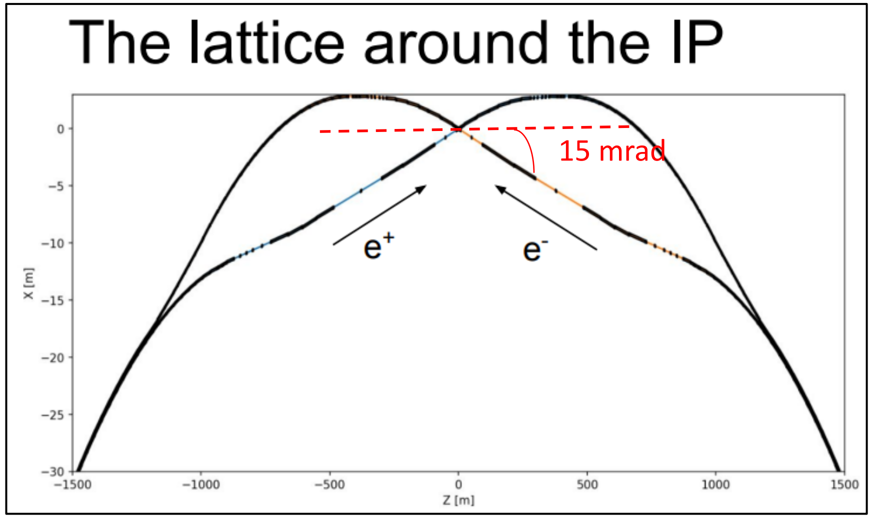

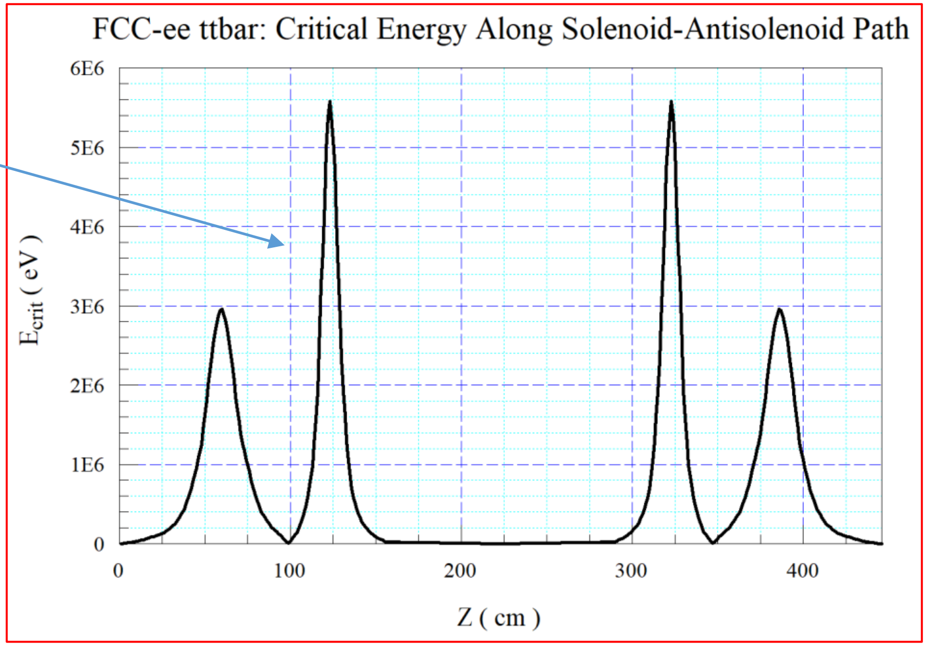

MDI Interaction Point: sources of radiation and radiation dump

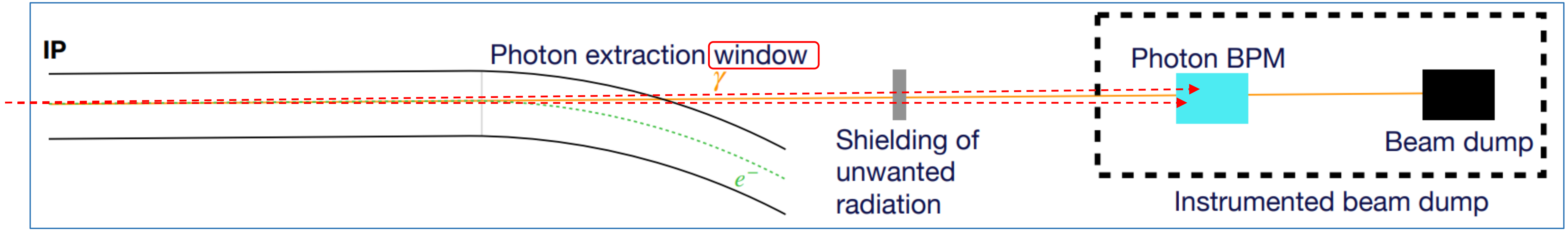

- Where applicable, develop shielding solutions for sensitive equipment in the tunnel (electronics, etc).

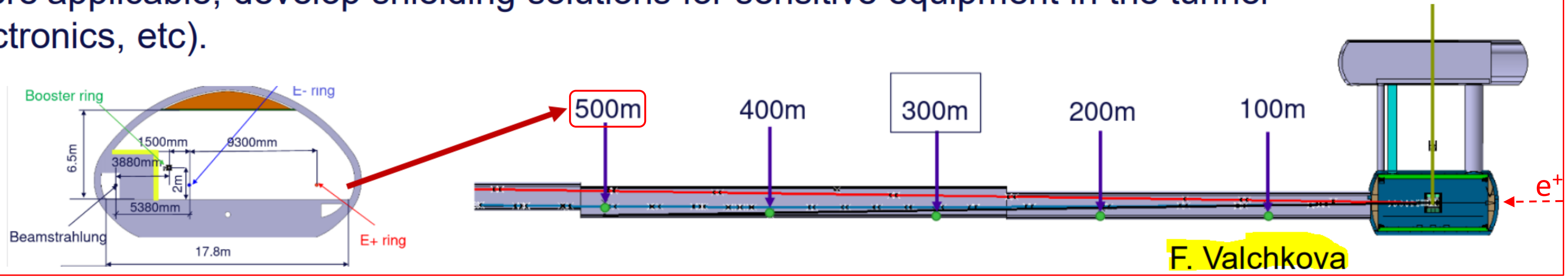

MDI modeling with SYNRAD+ and Molflow+:

Model created automatically from the lattice files (M. Ady, via OpticsBuilder)
Crossing angle is 30 mrad = 1.72°

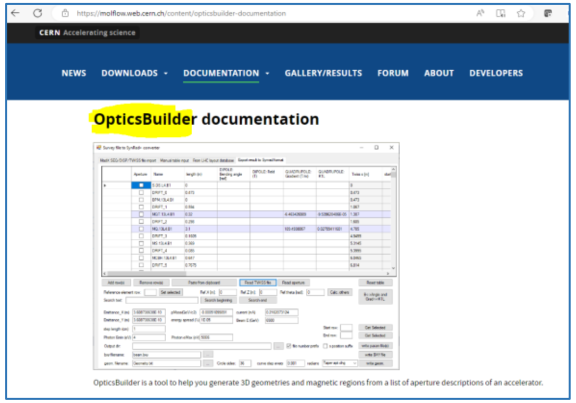

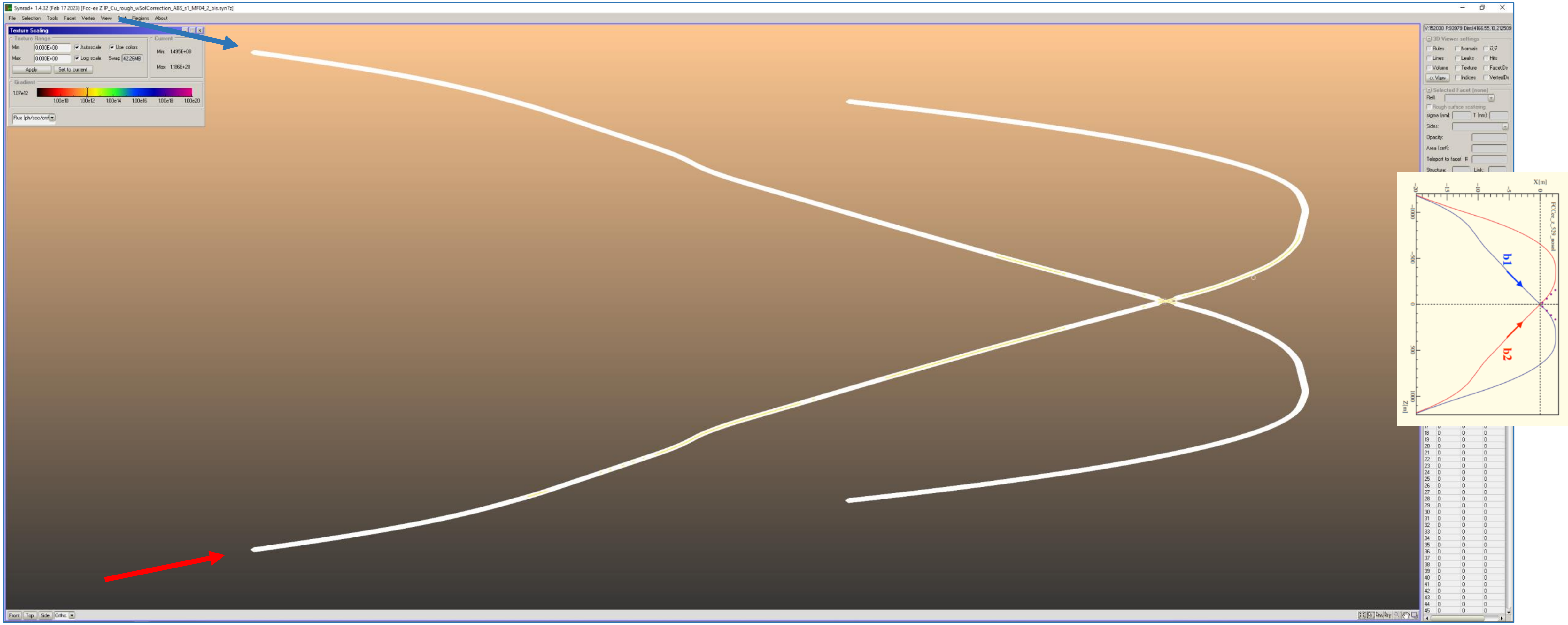

Full length of the model is 2x 1902 m; only the part in red has been modeled, 923 m long (incoming beam, left to right)

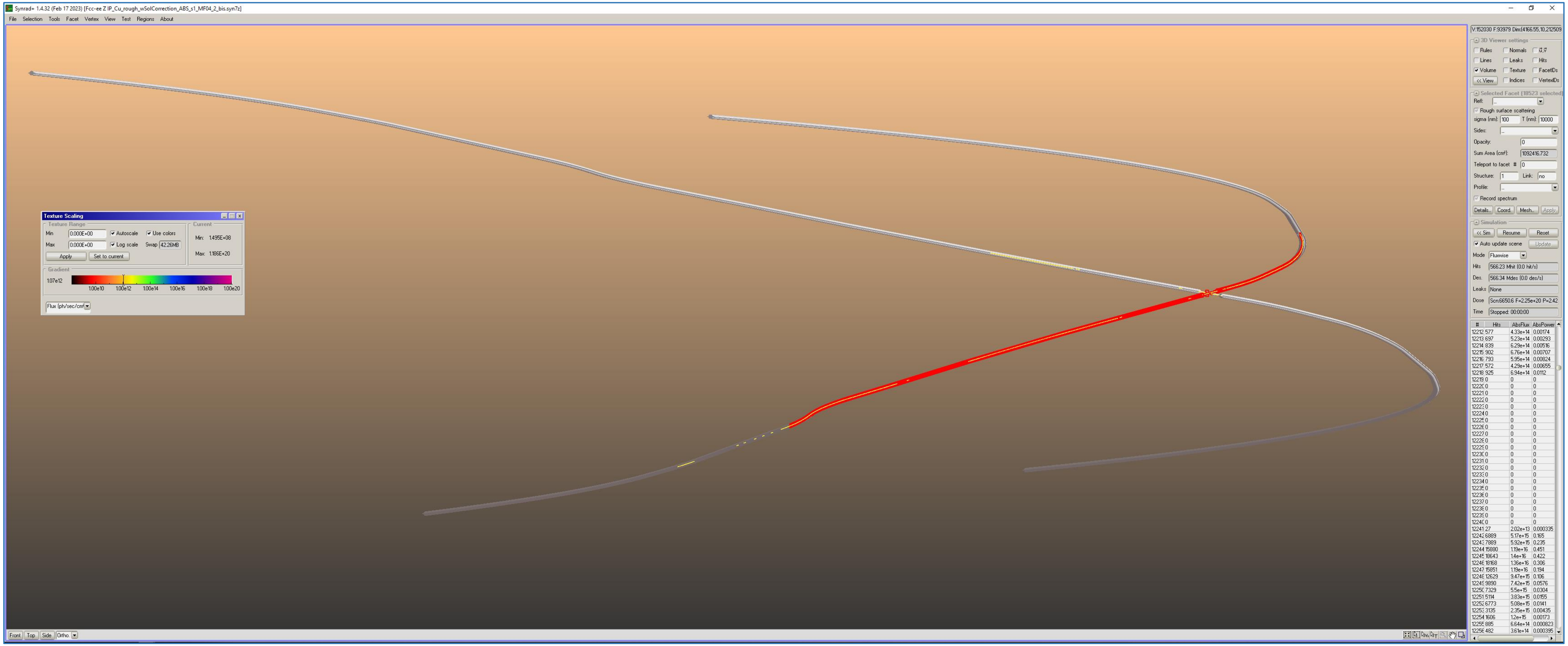

There are a total of 64 magnetic “regions” (in SYNRAD+ parlance) considered, comprising dipoles, quadrupoles, and the solenoid/antisolenoid combination inside the detector (see below)

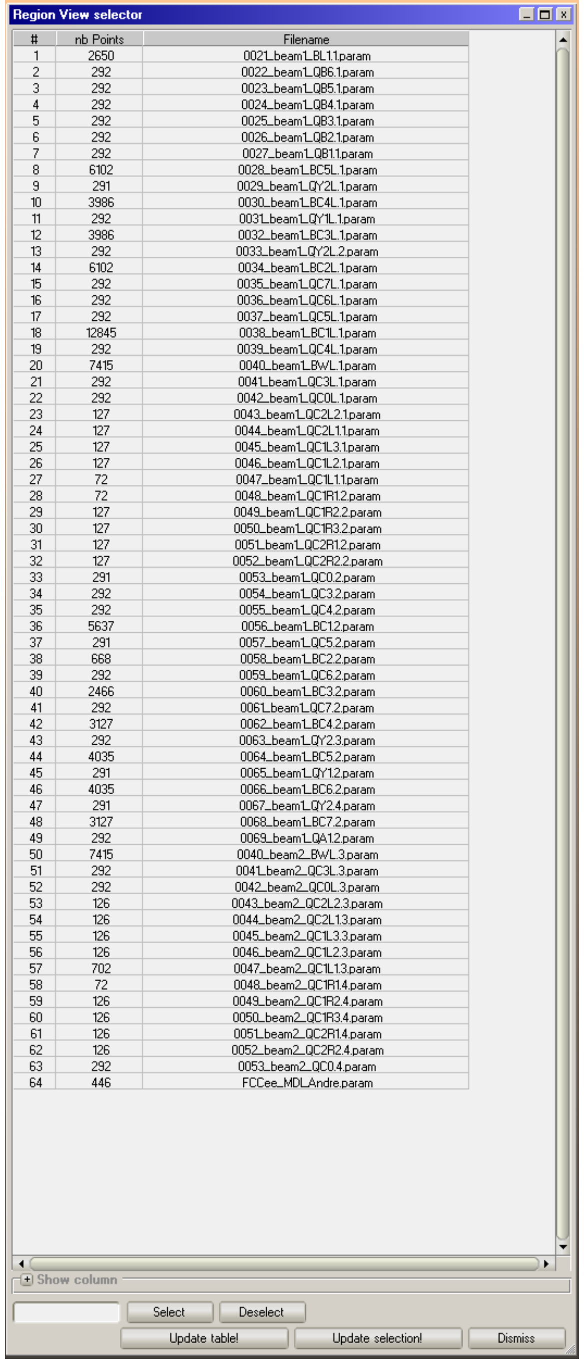

Region View selector

#	nb Points	Filename
1	2650	0021_beam1_BL1.1.param
2	292	0022_beam1_QB6.1.param
3	292	0023_beam1_QB5.1.param
4	292	0024_beam1_QB4.1.param
5	292	0025_beam1_QB3.1.param
6	292	0026_beam1_QB2.1.param
7	292	0027_beam1_QB1.1.param
8	6102	0028_beam1_BC5L.1.param
9	291	0029_beam1_QY2L.1.param
10	3986	0030_beam1_BC4L.1.param
11	292	0031_beam1_QY1L.1.param
12	3986	0032_beam1_BC3L.1.param
13	292	0033_beam1_QY2L.2.param
14	6102	0034_beam1_BC2L.1.param
15	292	0035_beam1_QC7L.1.param
16	292	0036_beam1_QC6L.1.param
17	292	0037_beam1_QC5L.1.param
18	12845	0038_beam1_BC1L.1.param
19	292	0039_beam1_QC4L.1.param
20	7415	0040_beam1_BWL.1.param
21	292	0041_beam1_QC3L.1.param
22	292	0042_beam1_QC0L.1.param
23	127	0043_beam1_QC2L2.1.param
24	127	0044_beam1_QC2L1.1.param
25	127	0045_beam1_QC1L3.1.param
26	127	0046_beam1_QC1L2.1.param
27	72	0047_beam1_QC1L1.1.param
28	72	0048_beam1_QC1R1.2.param
29	127	0049_beam1_QC1R2.2.param
30	127	0050_beam1_QC1R3.2.param
31	127	0051_beam1_QC2R1.2.param
32	127	0052_beam1_QC2R2.2.param
33	291	0053_beam1_QC0.2.param
34	292	0054_beam1_QC3.2.param
35	292	0055_beam1_QC4.2.param
36	5637	0056_beam1_BC1.2.param
37	291	0057_beam1_QC5.2.param
38	668	0058_beam1_BC2.2.param
39	292	0059_beam1_QC6.2.param
40	2466	0060_beam1_BC3.2.param
41	292	0061_beam1_QC7.2.param
42	3127	0062_beam1_BC4.2.param
43	292	0063_beam1_QY2.3.param
44	4035	0064_beam1_BC5.2.param
45	291	0065_beam1_QY1.2.param
46	4035	0066_beam1_BC6.2.param
47	291	0067_beam1_QY2.4.param
48	3127	0068_beam1_BC7.2.param
49	292	0069_beam1_QA1.2.param
50	7415	0040_beam2_BWL.3.param
51	292	0041_beam2_QC3L.3.param
52	292	0042_beam2_QC0L.3.param
53	126	0043_beam2_QC2L2.3.param
54	126	0044_beam2_QC2L1.3.param
55	126	0045_beam2_QC1L3.3.param
56	126	0046_beam2_QC1L2.3.param
57	702	0047_beam2_QC1L1.3.param
58	72	0048_beam2_QC1R1.4.param
59	126	0049_beam2_QC1R2.4.param
60	126	0050_beam2_QC1R3.4.param
61	126	0051_beam2_QC2R1.4.param
62	126	0052_beam2_QC2R2.4.param
63	292	0053_beam2_QC0.4.param
64	446	FCCee_MDI_Andre.param

Show column

Select Deselect

Update table! Update selection! Dismiss

- There are a total of 64 magnetic “regions: 49 for B1, 14 for B2, and 1 for the solenoids
- Total power generated by all is **242 kW**; total photon flux is **$2.25 \cdot 10^{20}$ ph/s**
- This is the ray-tracing for the **ideal case of no photon reflection**

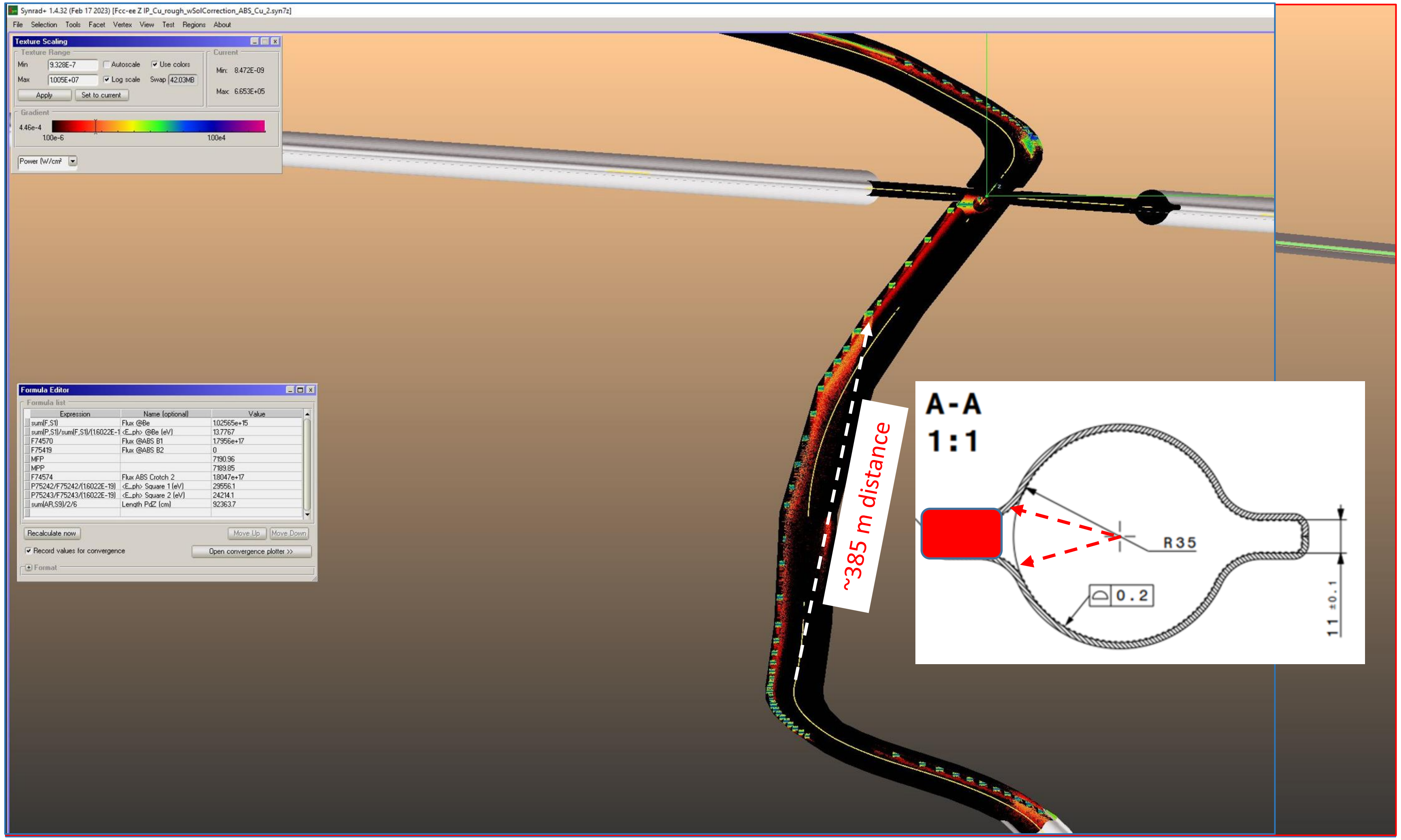

FCC-ee ttbar:

- There are a total of 70 magnetic "regions: 49 for B1, 20 for B2, and 1 for the solenoids
- Total power generated by all is **196 kW**; total photon flux is **$3.99 \cdot 10^{18}$ ph/s**
- This is the ray-tracing for the **ideal case of no photon reflection**
- **High critical energy radiation hitting absorber at ~120 m from IP, Compton secondaries?**

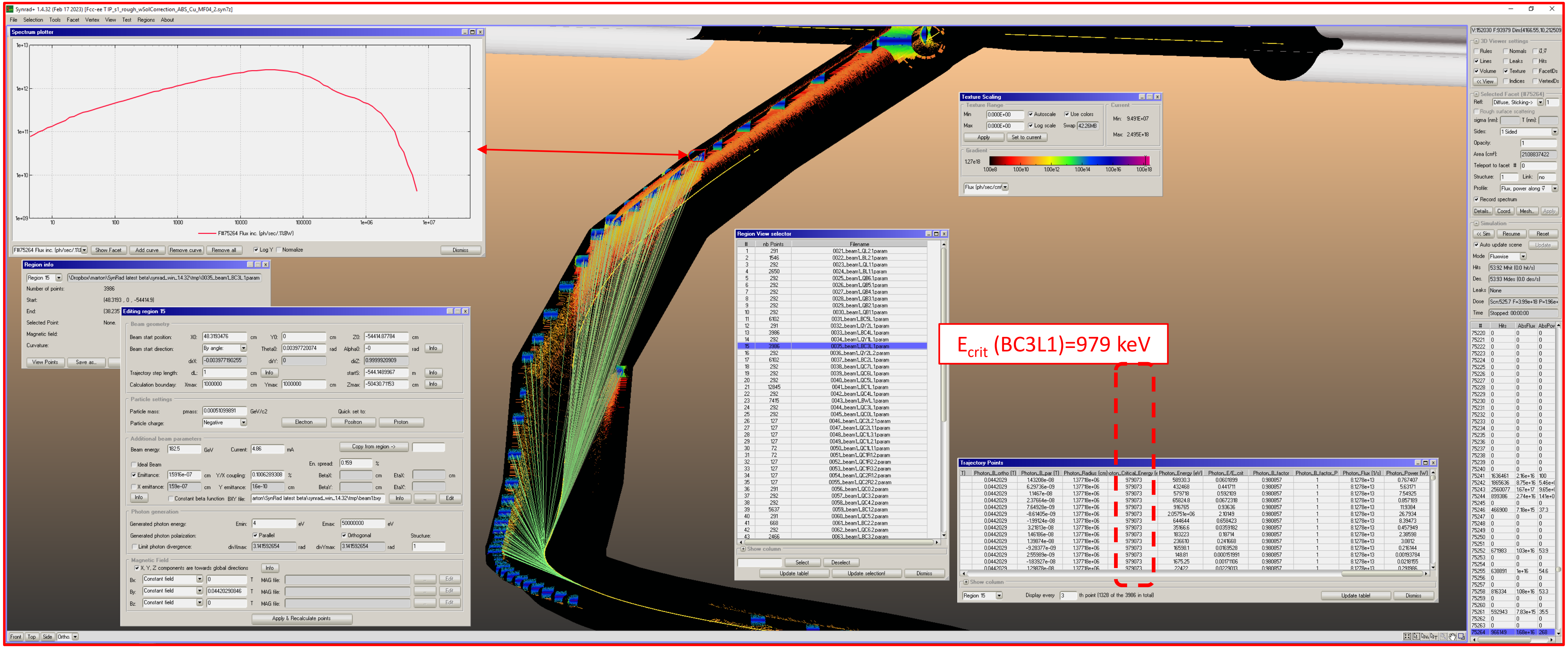

- Here what happens when **angle- and energy-dependent photon reflection** is simulated (with **roughness of the surface taken into account too**)
- **100% of the internal surface of the vacuum chambers is hit by some photons**, whether direct ones or reflected; the consequence is a **SLOWER vacuum conditioning** rate

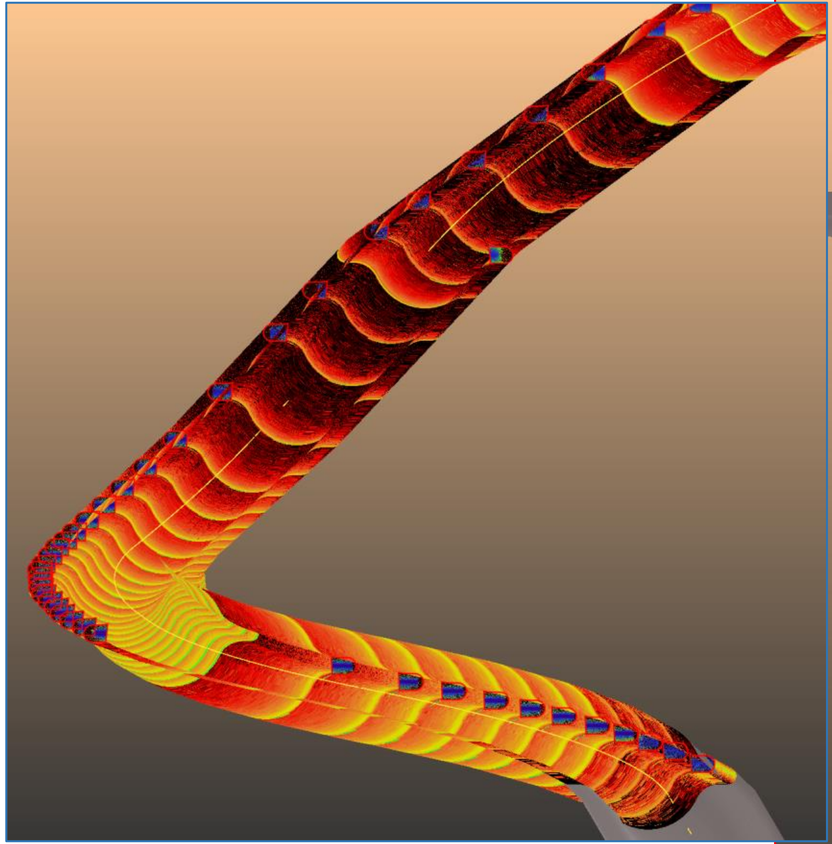

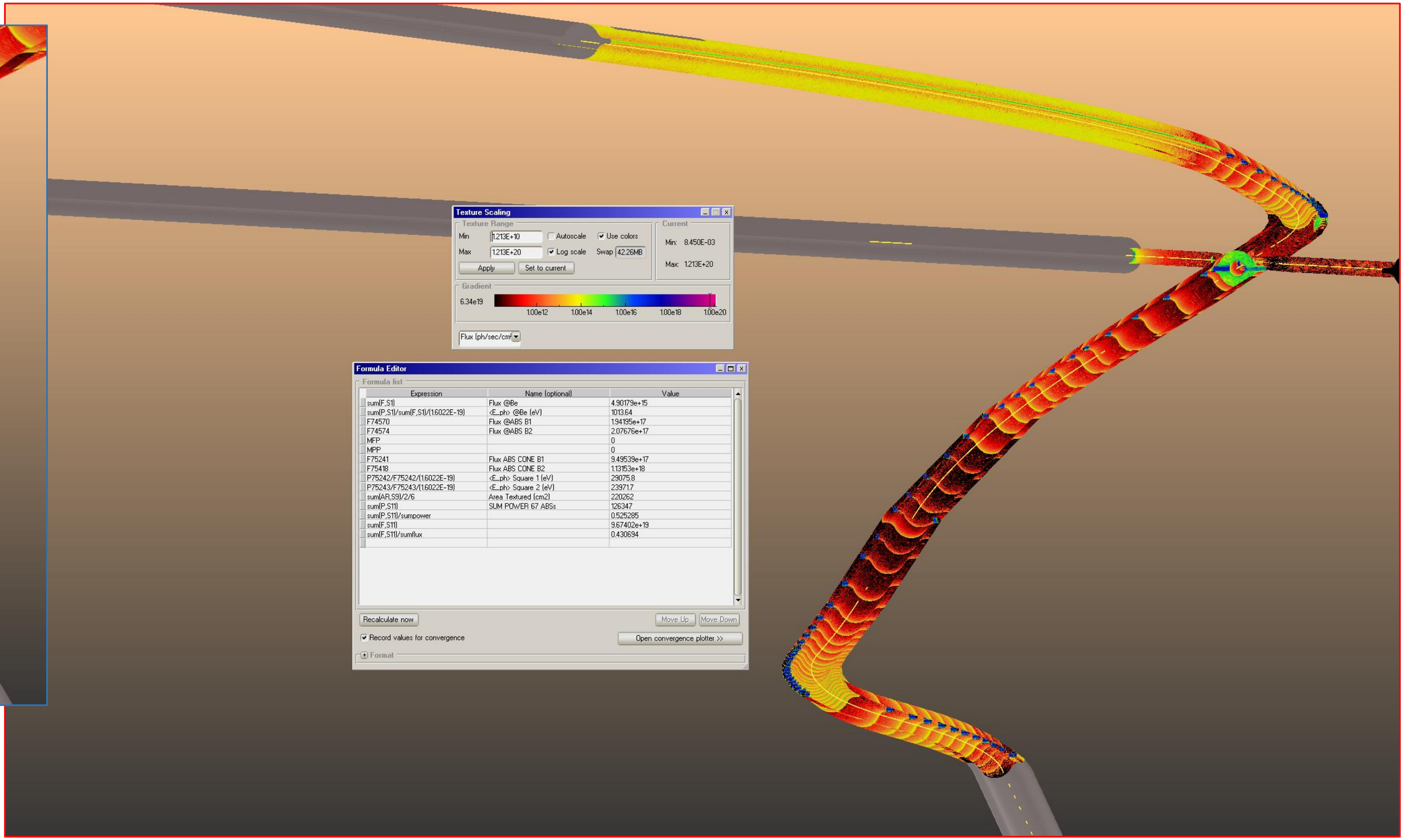

FCC-ee ttbar:

- Here what happens when **angle- and energy-dependent photon reflection** is simulated (with **roughness of the surface taken into account too**)
- **100% of the internal surface of the vacuum chambers is hit by some photons,** whether direct ones or reflected; the consequence is a **SLOWER vacuum conditioning** rate

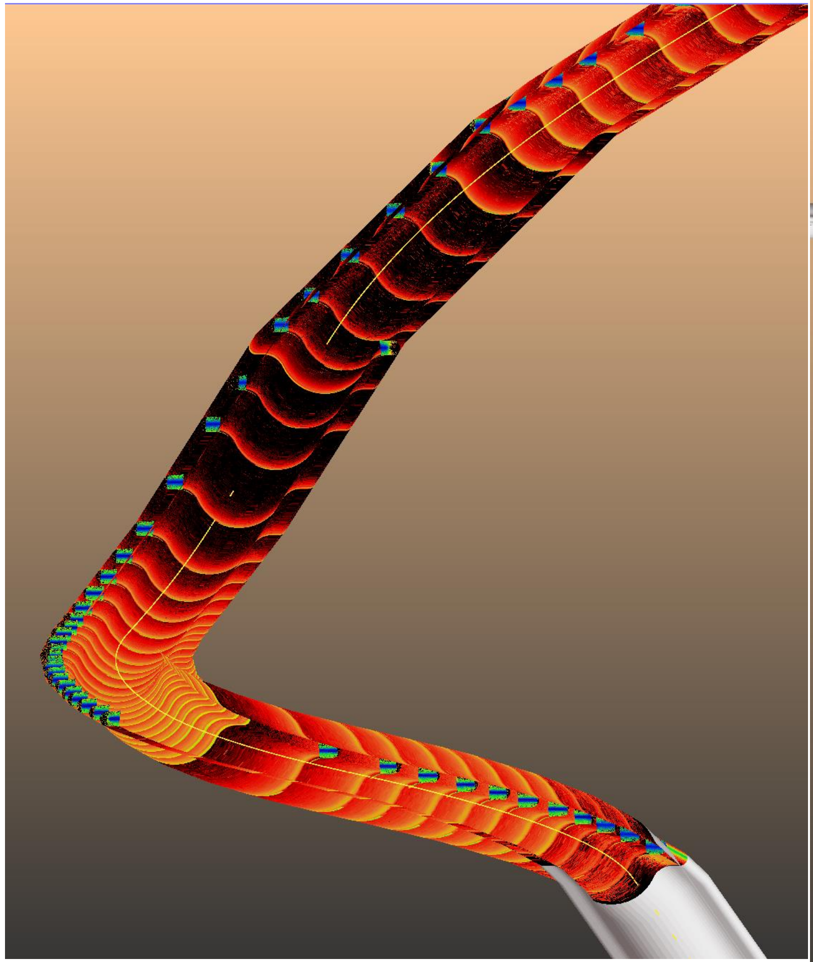

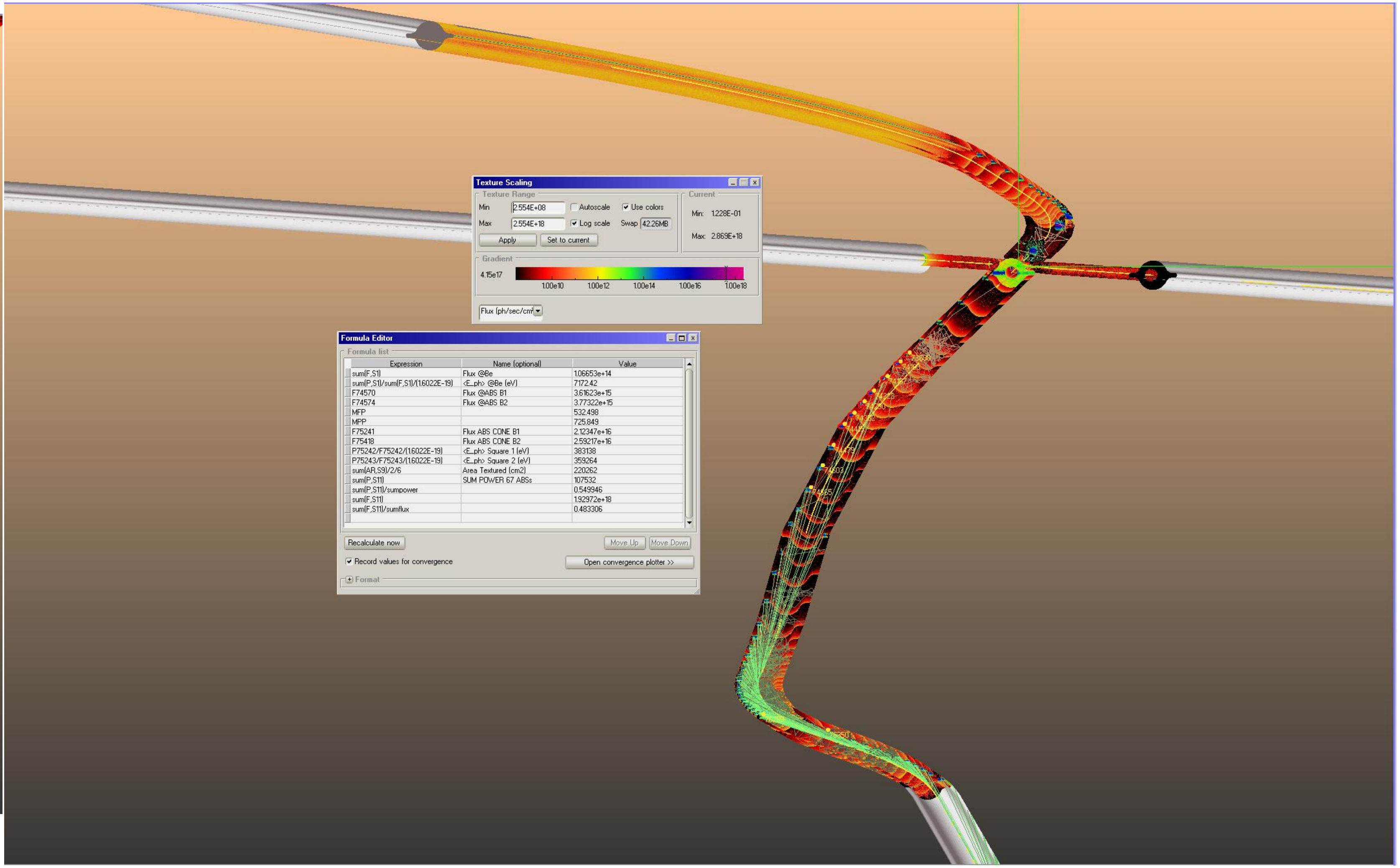

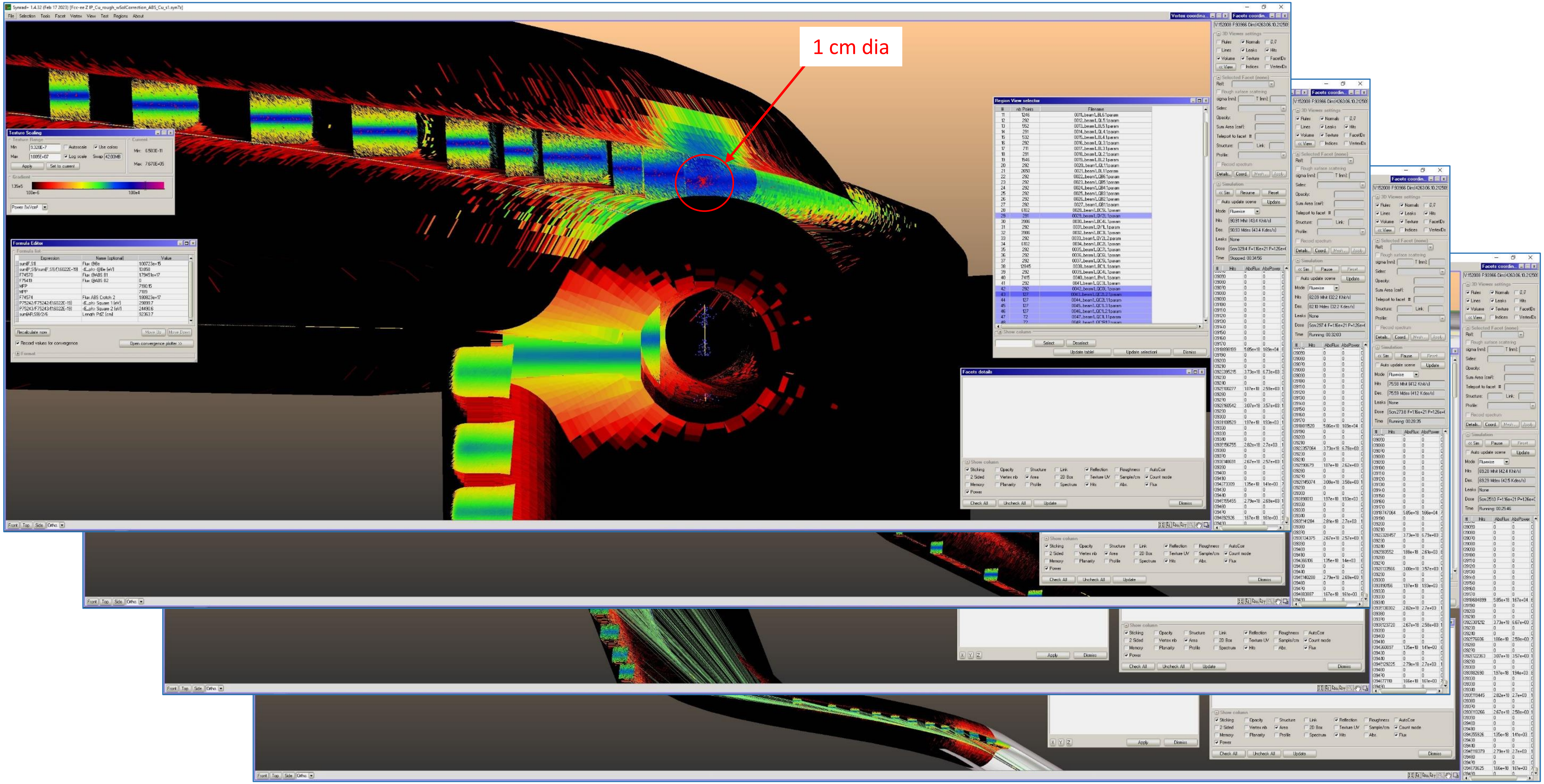

Closing in into the IP region for the no-photon reflection case

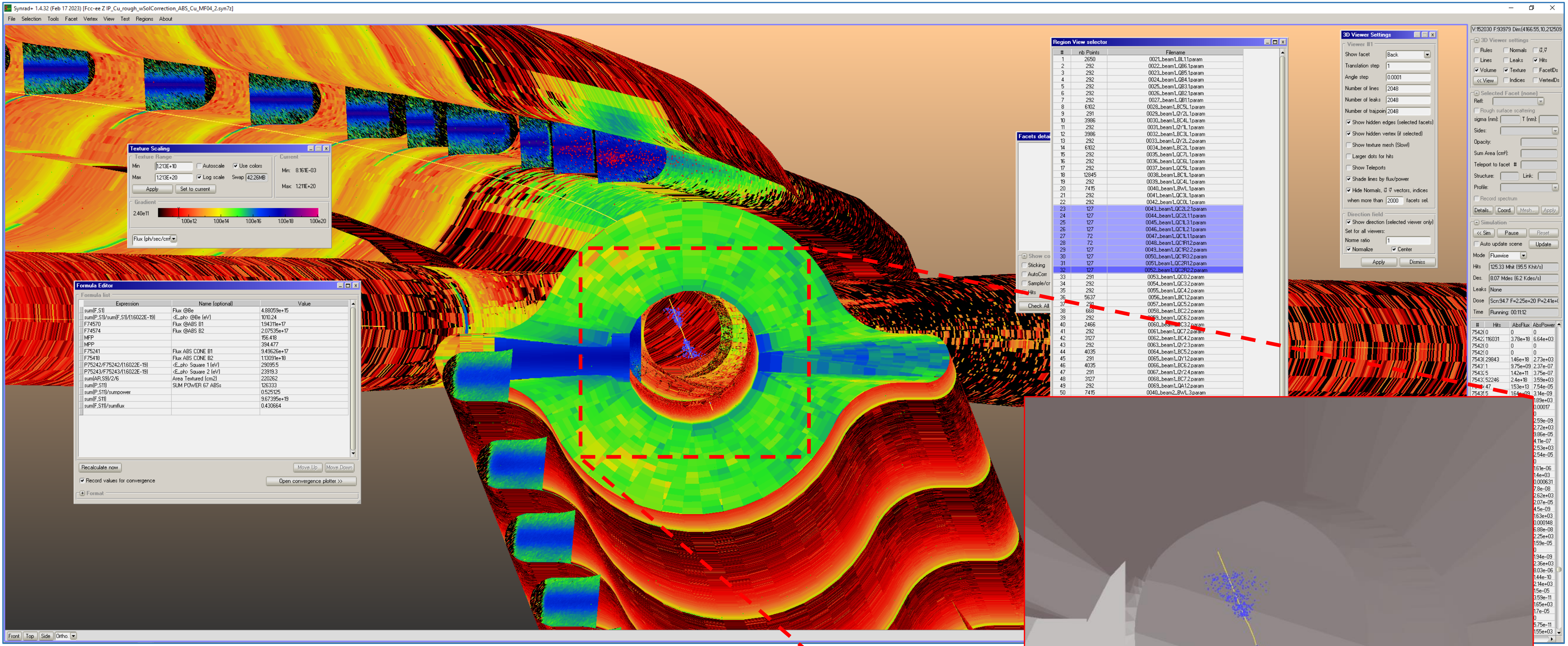

- The horizontally “hourglass” shape of the e- beam is evident →
- The SR along a quadrupole is ZERO when the ideal beam perfectly on-axis and no size, but it grows quickly as the offset from the axis and the bunch size get bigger; **these quadrupoles have very large gradients → large SR emission**!

FCC-ee Z: SR Power from different IP magnet sources, reaching a screen at 60 m (facet 6898):

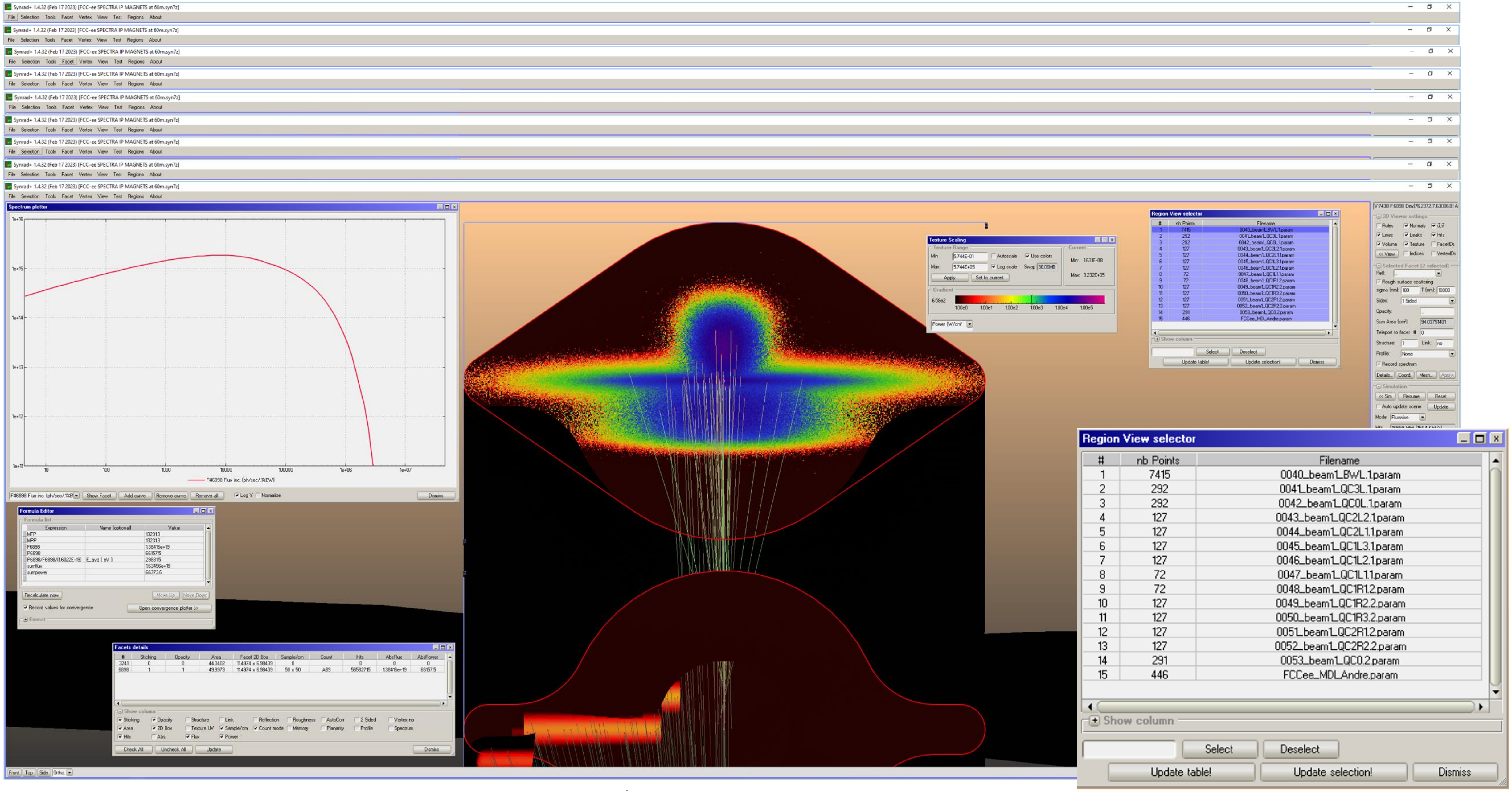

FCC-ee : Comparison of SR Power from different IP magnet sources, reaching a screen at 60 m (facet 6898): Z vs ttbar and ttbar with E_{ph}>150 keV

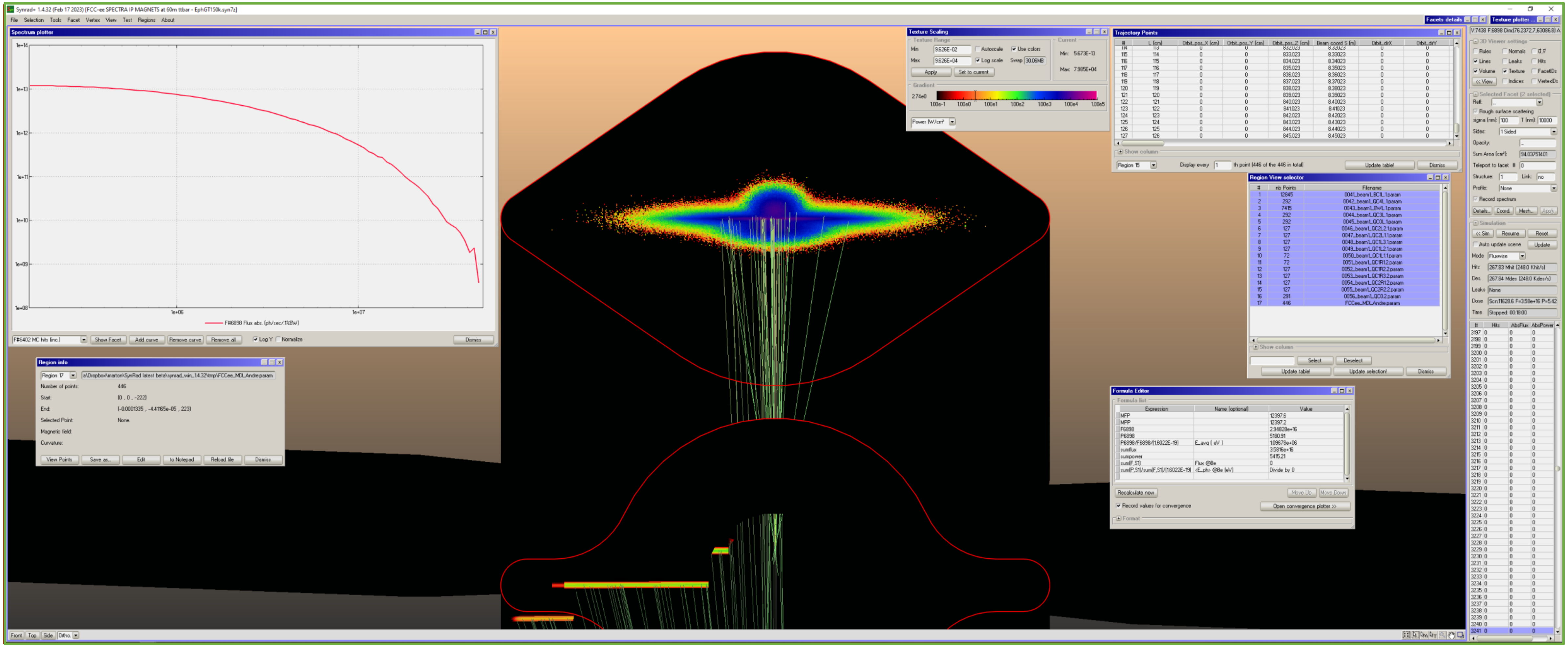

- FCC-ee Z: SR photon **power** distribution **at 100 m** from Z dipole, projected on **10x10 cm²** (**2x2 cm² at center**), for parallel (left) and orthogonal (right) photon polarization; IDEAL BEAM CASE, zero beam size, only natural divergence of the SR fan
- Graphs on the left show the SR spectra (in ph/s/0.1%BW/m) at nominal 1270 mA current (above, RED is parallel pol., BLUE is orthog. polarization), and vertical **power** distribution (+/- 1 cm, smaller square)
- 1 cm corresponds to 0.1 mrad ($1/\gamma$=11.206 μrad);   0.1 mrad = $8.92 \cdot 1/\gamma$

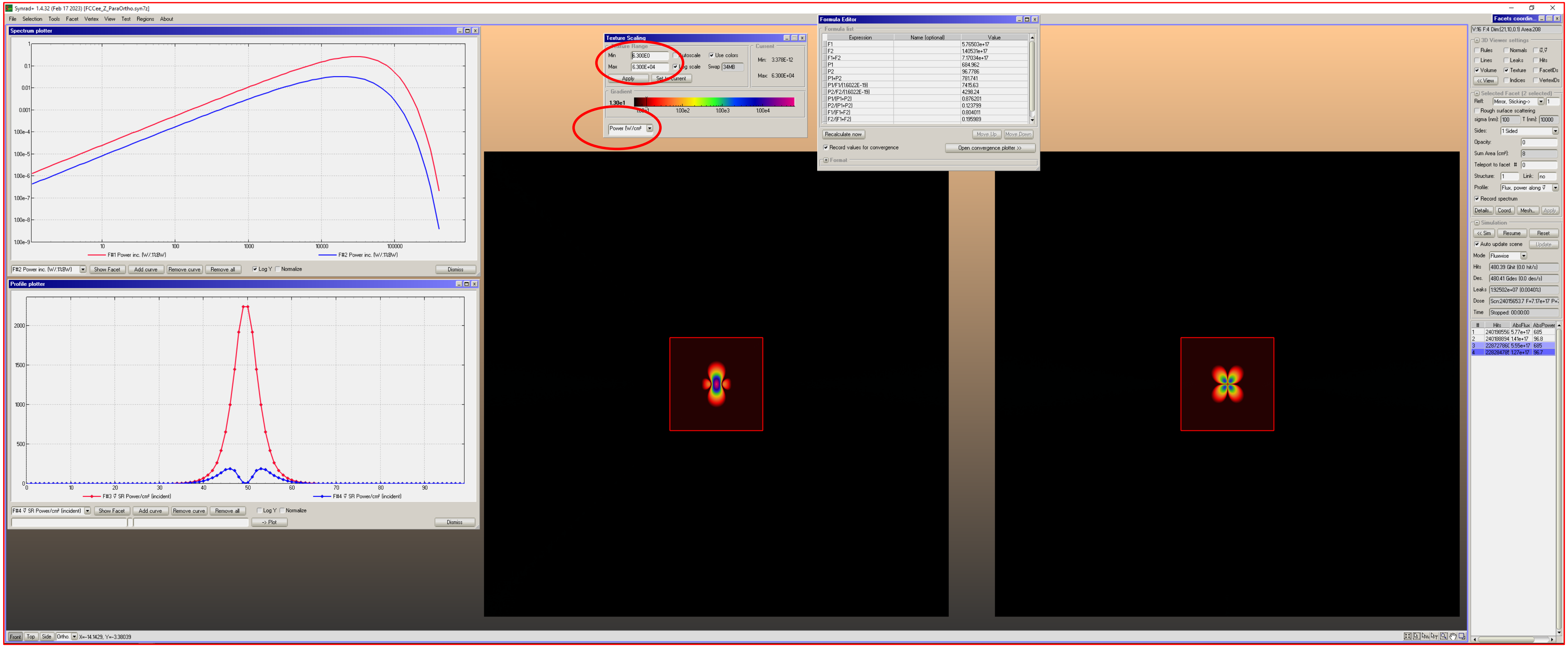

- FCC-ee Z: SR photon **flux** distribution **at 100 m** from Z dipole, projected on **10x10 cm^2 (2x2 cm^2 at center)**, for parallel (left) and orthogonal (right) photon polarization; IDEAL BEAM CASE, zero beam size, only natural divergence of the SR fan
- Graphs on the left show the SR spectra (in ph/s/0.1%BW/m) at nominal 1270 mA current (above, RED is parallel pol., BLUE is orthog. polarization), and vertical **flux** distribution (+/- 1 cm, smaller square)
- 1 cm corresponds to 0.1 mrad ($1/\gamma$=11.206 μrad); 0.1 mrad = $8.92 \cdot 1/\gamma$

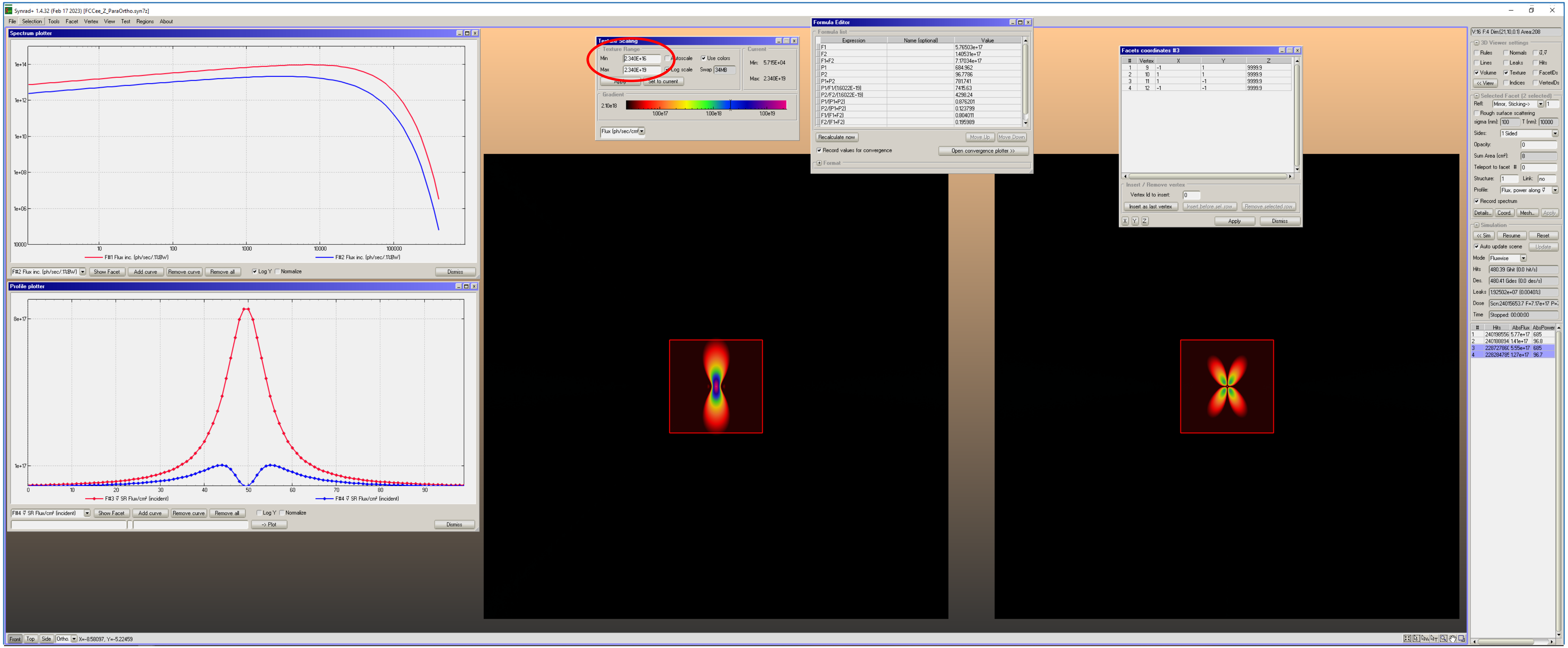

Extremely tight fabrication and alignment tolerances: accurate ray-tracing is a must

Cryostat with integrated anti-solenoid coils

SPACE RESERVATION FOR REMOTE FLANGE CONNECTION (SMA)

Crotch (2 beams→1)

Alignment bellow (ESRF-design)

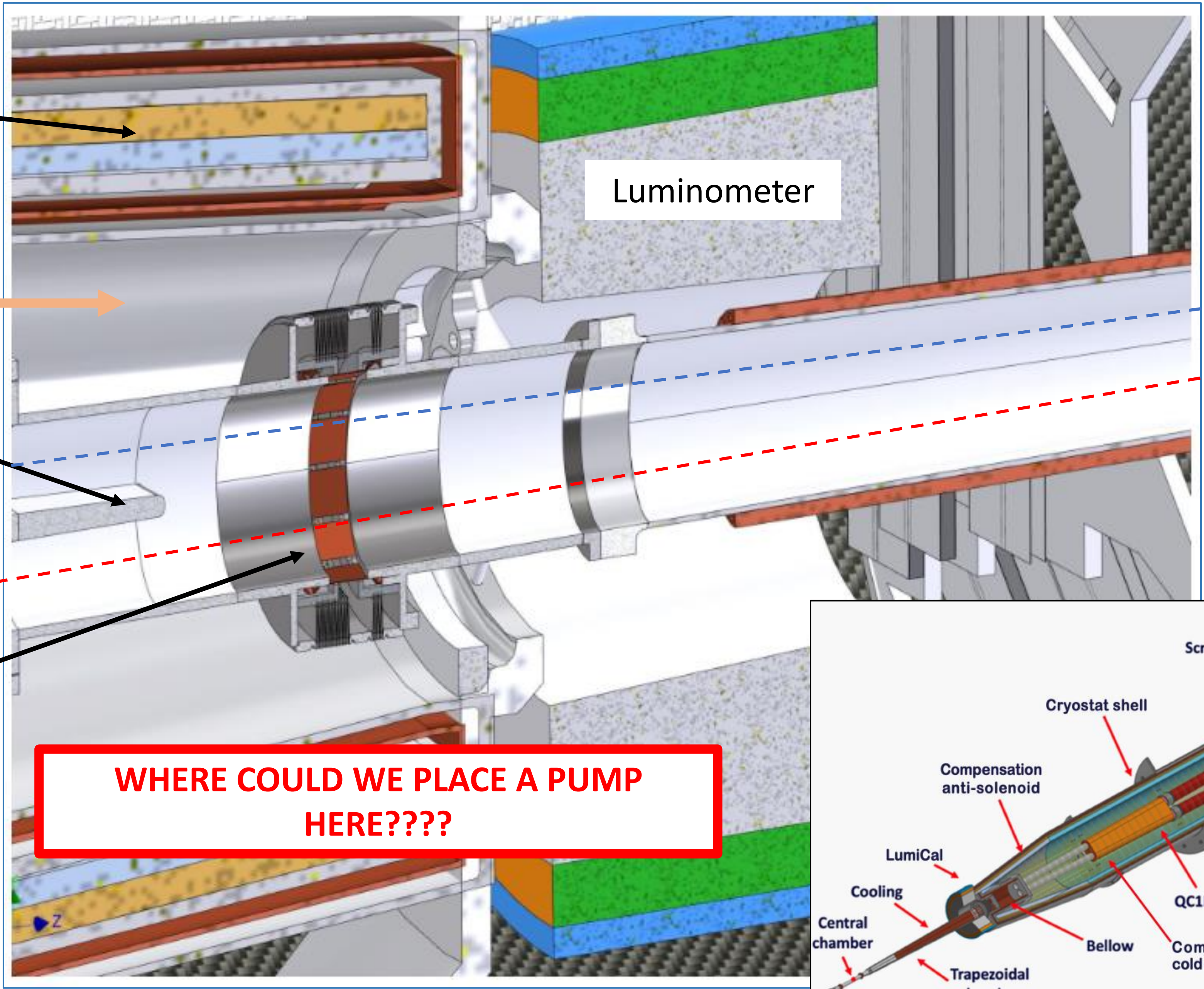

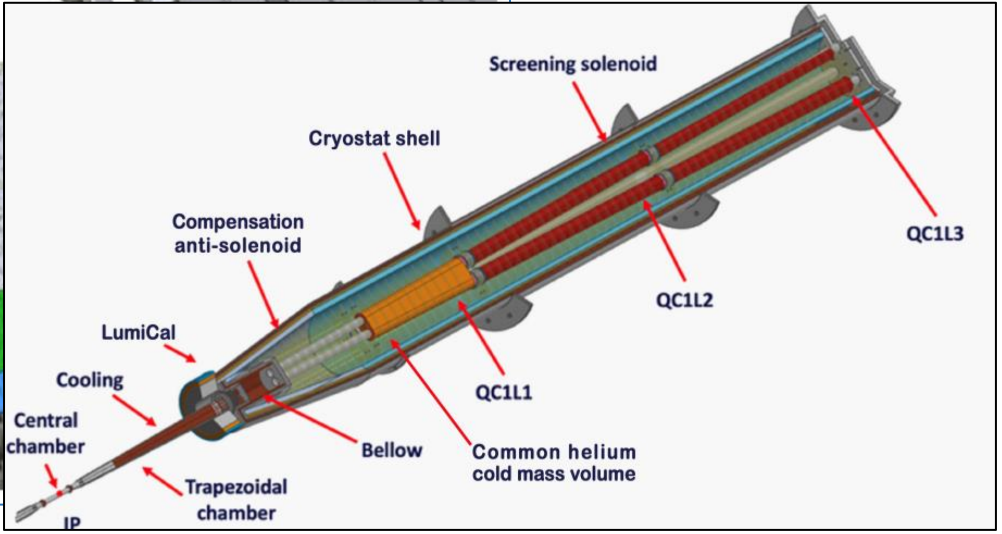

Geometry of the central "X" chamber, as imported from CAD into SYNRAD+ (court. F. Fransesini, INFN/LNF/CERN)

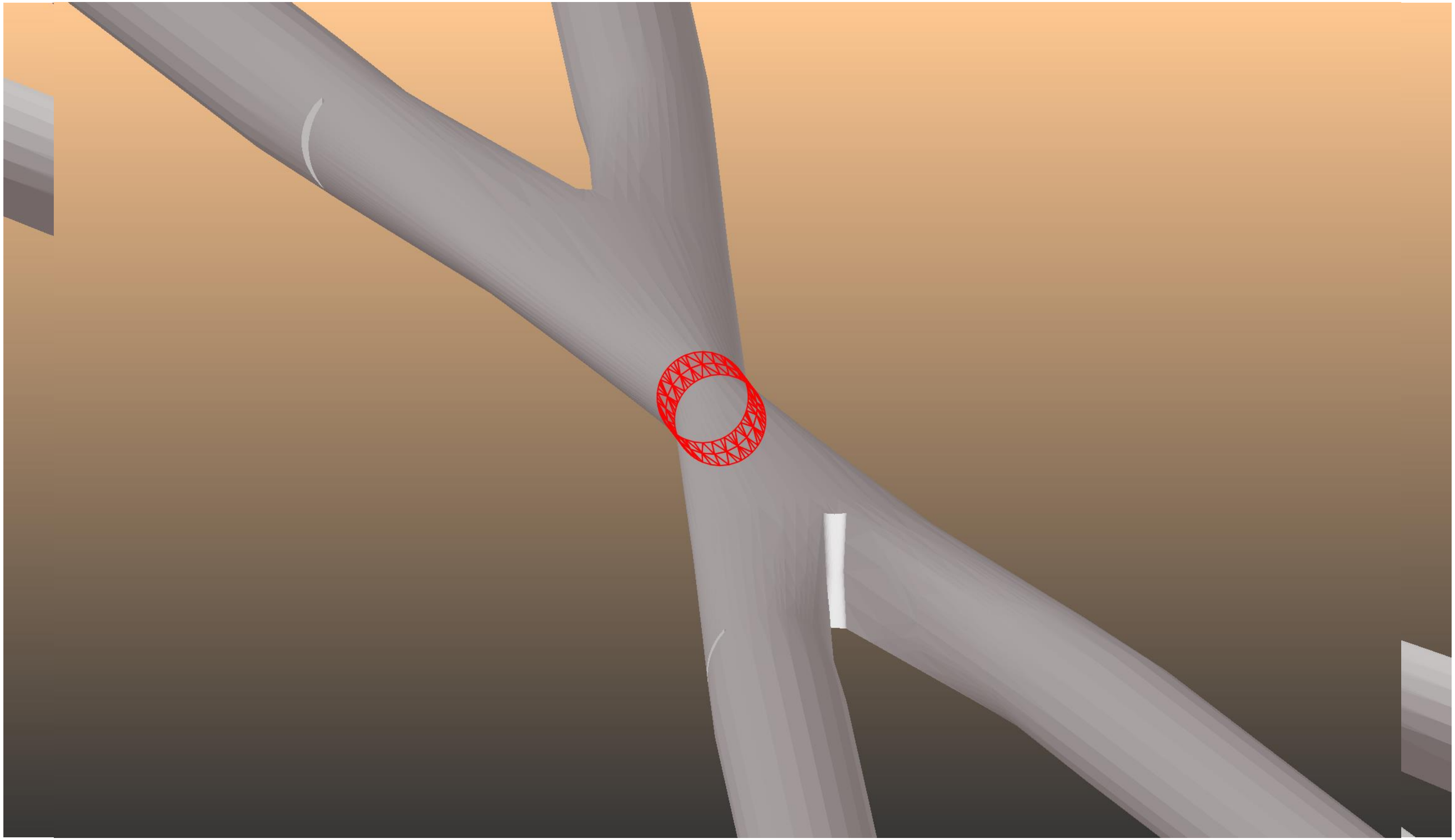

Molflow+ simulation of pressure profiles after 1h (ideal case and Cu reflection) and 100 h (Cu refl.)
Cu-like desorption yield with s=0.008 NEG sticking coeff. and NO NEG before IP; H_2 gas

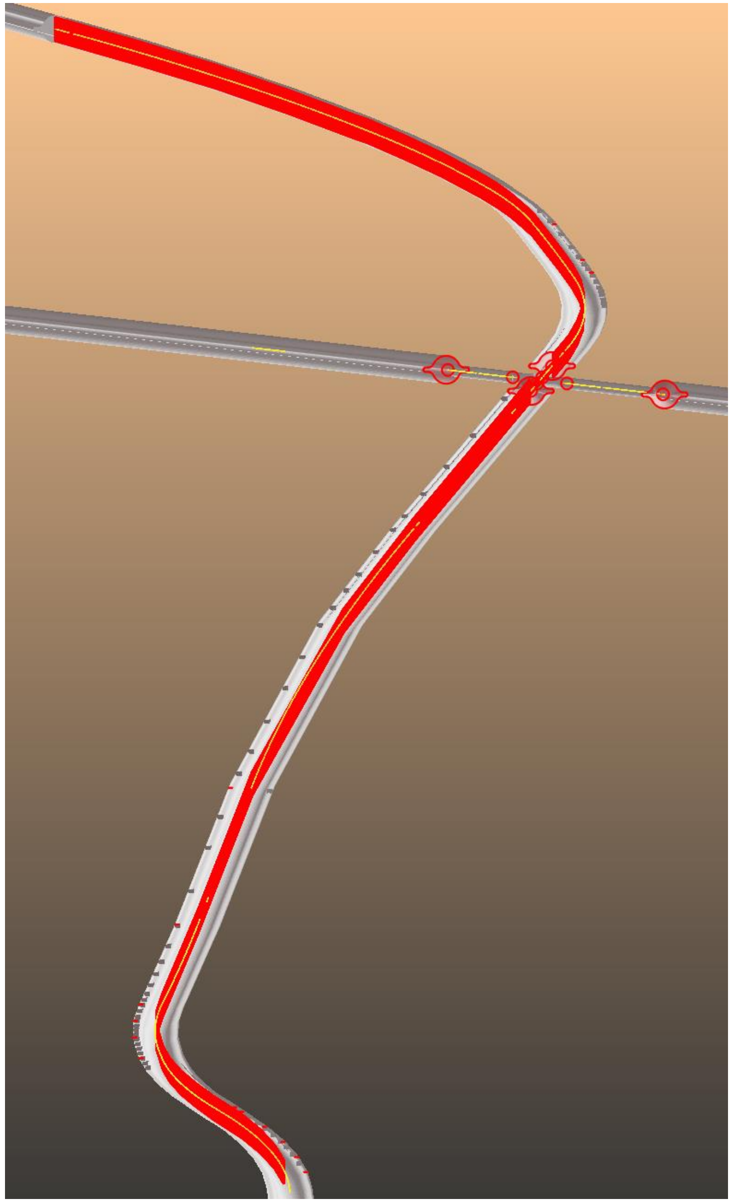

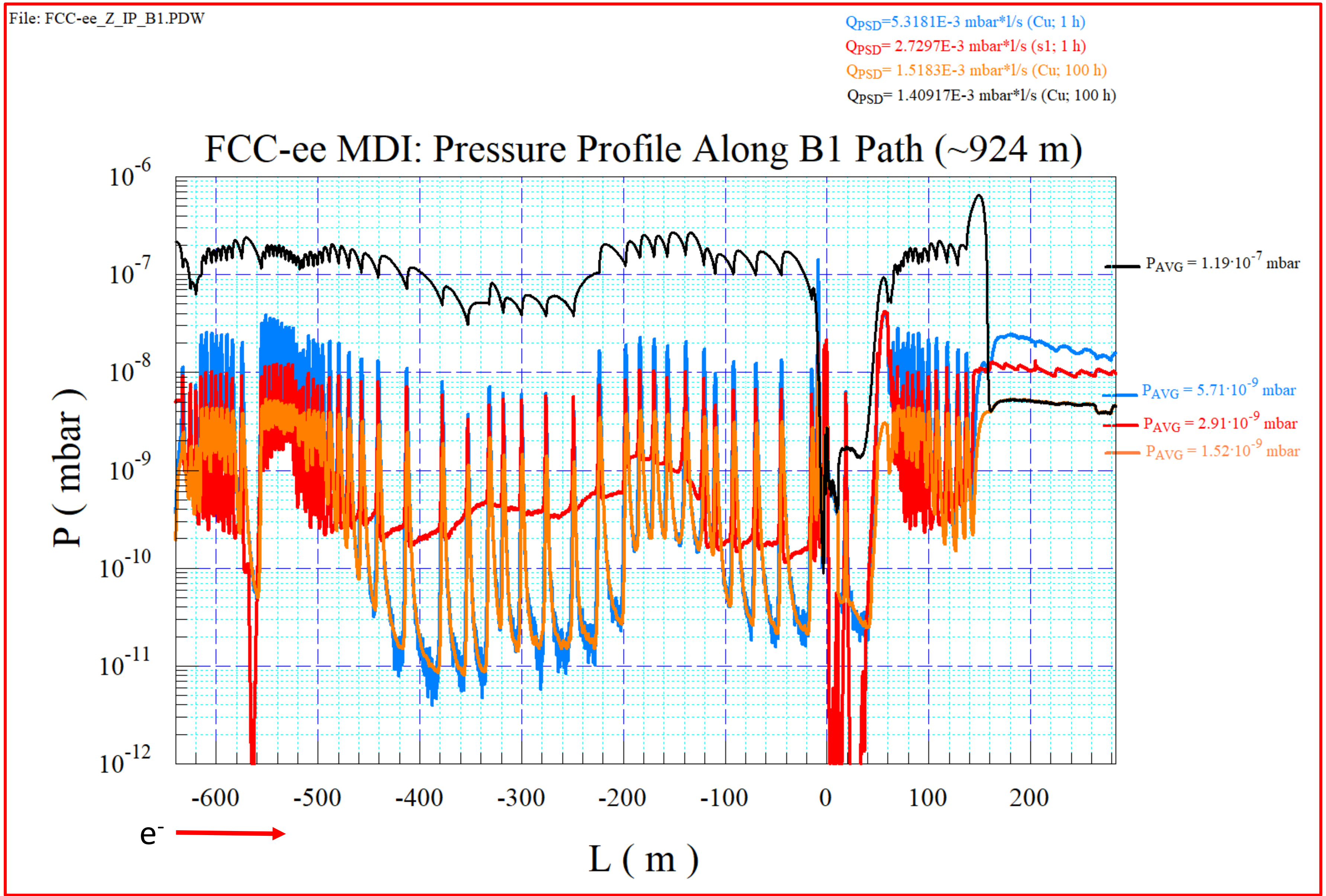

Same as previous one but for the [-200 m; +100 m] around the IP
Cu-like desorption yield with s=0.008 NEG sticking coeff. and NO NEG before IP; H_2 gas

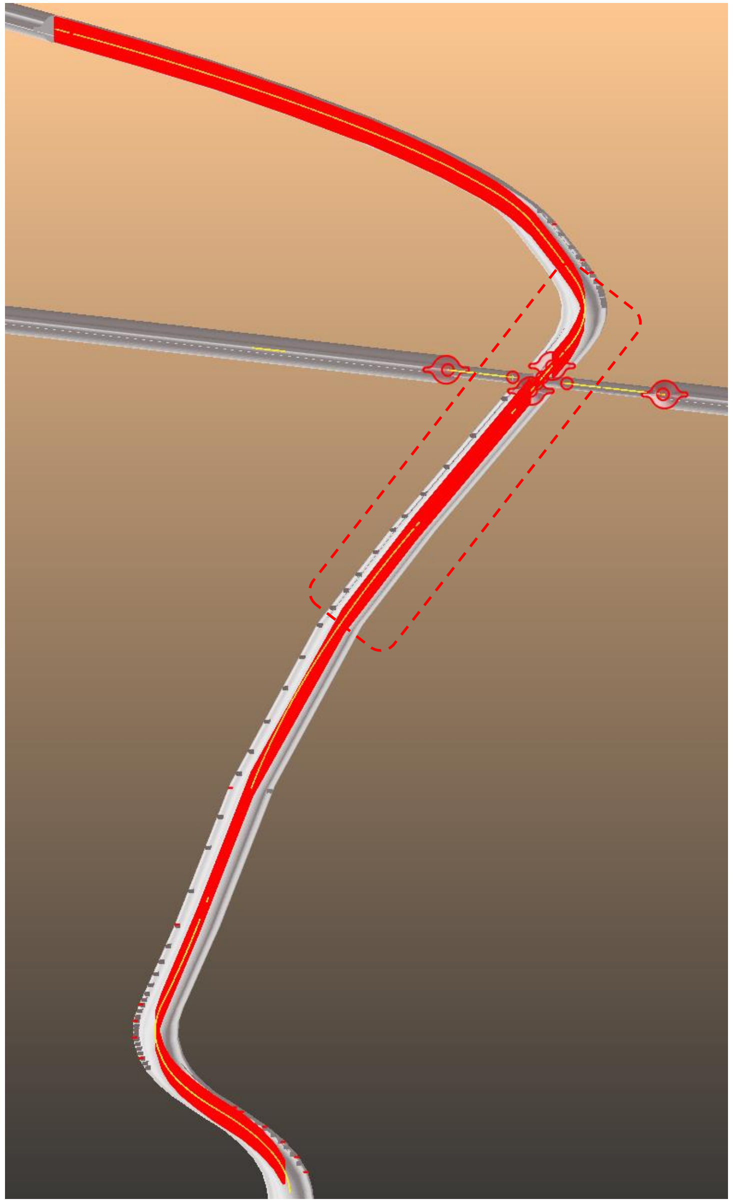

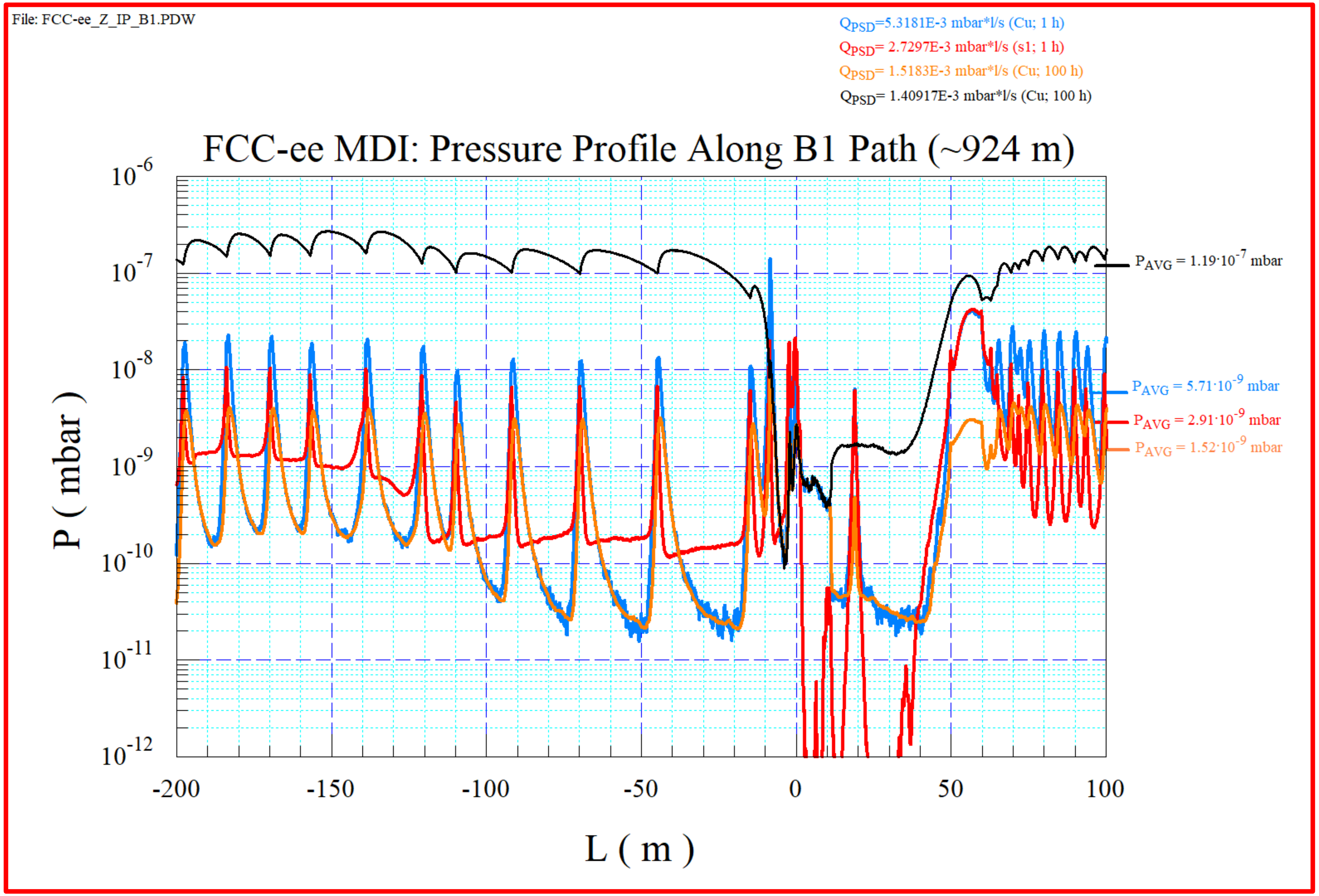

This area needs optimization of pumping and trapping of SR-induced desorption by rectangular absorber: e.g. **sawtooth design**?

Same as previous one but for the +/- 10 m to/from IP
Cu-like desorption yield with s=0.008 NEG sticking coeff. and NO NEG before IP; H_2 gas

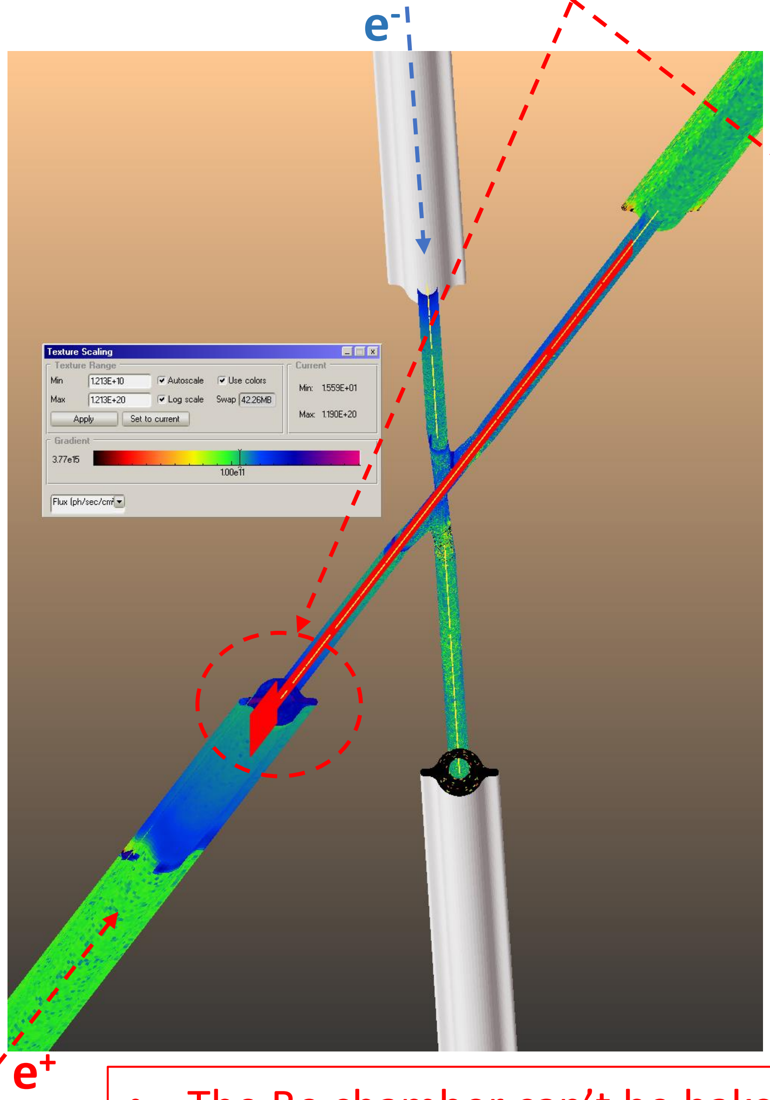

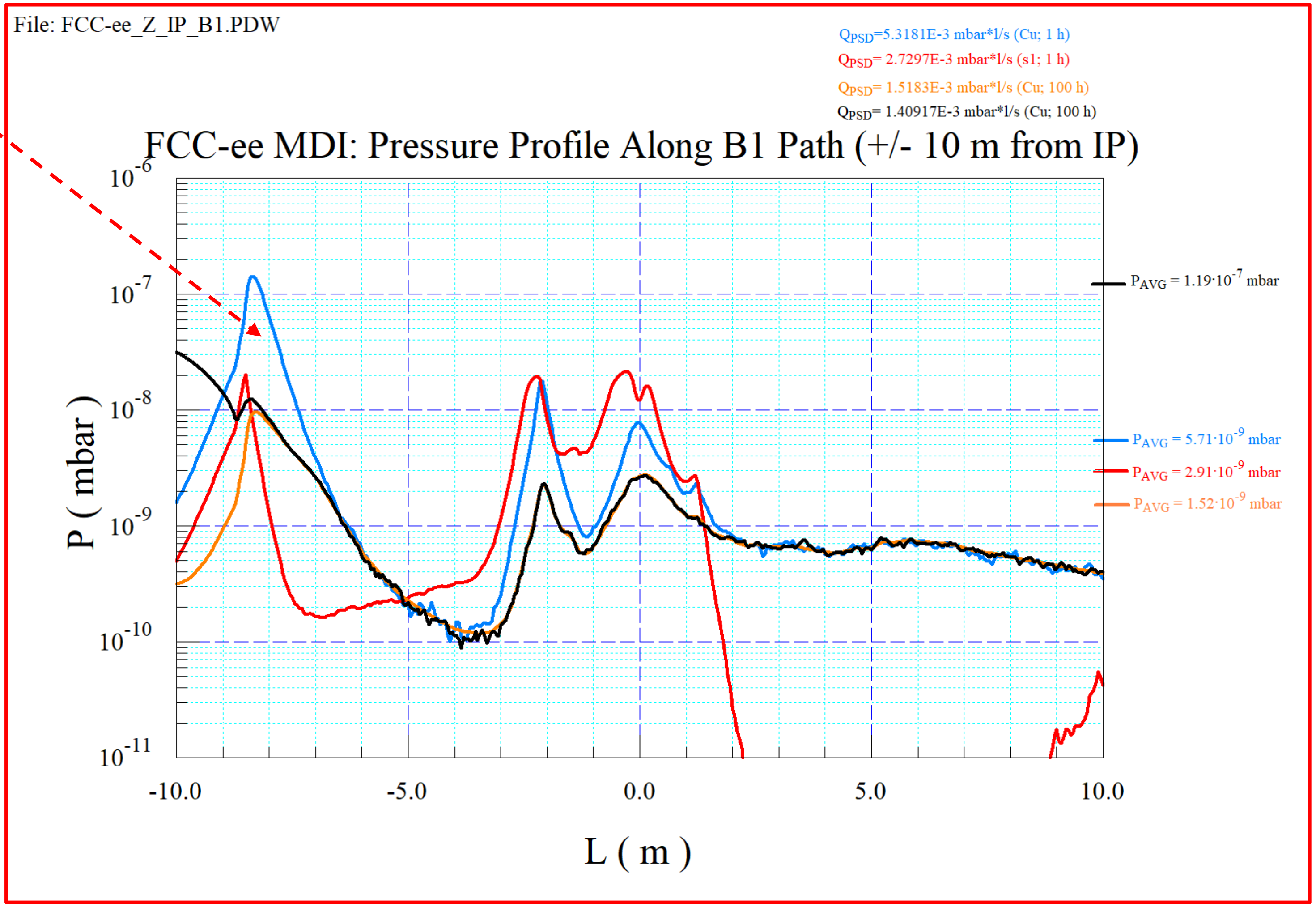

- The Be chamber can't be baked at ~180 C that would be needed for activating the NEG-coating;
- We'd like to find (at least) one place ON EACH SIDE OF THE DETECTOR where a small NEG pump could be located

Conclusions and future work

- The CERN vacuum group has designed and started testing prototype components for the FCC-ee arc vacuum system
- The Mid-Term Cost Estimate exercise has forced us to consider also the possibility to implement a smaller vacuum chamber diameter, from 70 mm to 60 mm
- As a consequence, there is a rather large reduction of the specific conductance and also an increased number of SR absorbers (~12% for the latest lattice version)
- The need for NEG-coated chambers has become even more apparent for the reduced-ID chamber
- Integration in the tunnel is progressing well: 400 m-long vacuum sectors have been identified and taken as reference
- The new design and fabrication technology of the SR absorbers, 3D printing instead of conventional machining or wire erosion, allows us to reduce a bit the amount of the scattered photons along the main circular part of the vacuum chamber
- Design based on these changes of the MDI area is underway (see workshop at LNF later in the week, https://agenda.infn.it/event/37720/timetable/#all.detailed)
- Very time consuming ray-tracing calculations, both for the SR fans and the molecular flow, need to be carried out at each change of the magnetic lattice (which happens quite often): an "automatization" of the generation of the vacuum chamber along the MDI will need to be developed (OpticsBuilder, SYNRAD+, Molflow+) → MANPOWER???
- The collaboration with different groups is progressing well: integration, lattice dynamics, FLUKA, MDI, magnets, etc…
- We are on a reasonable path towards finalizing the design of the FCC-ee vacuum system considering that there are 2 more years prior to the end of this study phase

ACKNOWLEDGMENTS

- The material shown during this presentation has been obtained thanks to a team-work during the last 10 years
- I acknowledge the work of Cedric Garion, Fabrice Santangelo, Christian Duclos, Frederic Luiz, Sam Rorison, Marco Morrone, Fabrizio Niccoli, our machine shop, Marton Ady, Peter Henriksen, Sergio Calatroni, Patrick Krkotic
- Continuous support from FCC and TE management is also acknowledged, never turned down a request
- The collaboration with the FLUKA team (F. Cerutti, B. Humann, A. Lechner et al.) is also acknowledged
- Many thanks to R. Losito for handling our requests for funding for technical development
- Fani Kuncheva-Valchkova, for integration into the tunnel
- Mauro Migliorati and his team at Univ. Rome, for impedance calculations related to chamber components
- Manuela Boscolo and Francesco Fransesini, INFN/LNF/CERN, are acknowledged for coordinating the MDI work and providing information and models for the interaction are vacuum chamber
- Andrea Ciarma, Helmut Burkhardt, for data about radiation issues, beam orbits and related loss mechanisms.